Molecular Modeling of Endogenous and Exogenous Toxins at Phospholipid Interfaces

BY

MANUELA ASEYE AYELE AYEE
B.A., Dordt College, Sioux Center, Iowa, 2006
M.S., Iowa State University, Ames, Iowa, 2008

THESIS

Submitted as partial fulfillment of the requirements
for the degree Doctor of Philosophy in Chemical Engineering
in the Graduate College of the
University of Illinois at Chicago, 2015

Chicago, Illinois

Defense Committee:

Belinda S. Akpa, Chair and Advisor
Ludwig C. Nitsche
Cynthia J. Jameson, Chemistry
Richard D. Minshall, Pharmacology and Anesthesiology
Irena Levitan, Pulmonary, Critical Care, Sleep and Allergy Medicine

I dedicate this Dissertation to my Family – the source of my inspiration.

ACKNOWLEDGEMENTS

I thank my major professor, Dr. Belinda Akpa, for her guidance and support during the course of my doctoral studies. A special thank you goes to Dr. Cynthia Jameson for her encouragement and particularly her assistance with editing and proofreading my manuscripts. I truly appreciate the contributions and suggestions of the other members of my Dissertation committee: Dr. Ludwig Nitsche, Dr. Irena Levitan, and Dr. Richard Minshall. The help and encouragement of the members of my research group, my friends, and all my colleagues, faculty, and staff at the Department of Chemical Engineering is greatly appreciated.

I would also like to acknowledge the sources of my Doctoral funding: the UIC Abraham Lincoln Graduate Fellowship, the UIC Chancellor's Discovery Fund for Multidisciplinary Pilot Research, the National Science Foundation BRIGE Grant #1228035, and the National Institutes of Health CounterACT Program U01-NS083457.

My immediate family members, my parents, Dr. Emmanuel Ayee and Dr. (Mrs.) Alberta Ayee, my sister, Gloria Ayee, and brothers, Joel Ayee and Jonathan Ayee, contributed immensely to my academic journey through the years. The encouragement, prayers, and unending support made this work possible. Thank you all for being there for me.

Finally, and above all, I owe every success to my Heavenly Father.

MAA

TABLE OF CONTENTS

CHAPTER PAGE

1. INTRODUCTION....1
   1.1 Organization of this Thesis....3
2. METHODS....8
   2.1 Computer Simulations of Phospholipid Interfaces....8
   2.2 Overview of The MARTINI Coarse-Grained Force Field....12
      2.2.1 Mapping Coarse-Grained Sites....13
      2.2.2 Nonbonded Interactions....15
      2.2.3 Bonded Interactions....17
      2.2.4 Phospholipid Layer Models in MARTINI....19
   2.3 Simulation Model Systems Used in this Thesis....21
   2.4 Creating Coarse-Grained Topologies and Interaction Parameters for Small Molecules 25
      2.4.1 Structural Mapping....26
      2.4.2 Center-of-Mass Coarse Graining and Parameterization of Bonded interactions....28
      2.4.3 Selection of MARTINI Parameters....30
      2.4.4 Parameterization of Nonbonded Interactions....32
      2.4.5 Model Validation Using Octanol/Water Partitioning....34
   2.5 Molecular Dynamics Simulations of Phospholipid layers....38
      2.5.1 Minimization and Equilibration....39
      2.5.2 Obtaining Phospholipid Layer Properties from Simulations....40
      2.5.3 Obtaining Small Molecule Properties at Phospholipid Interfaces....50
      2.5.4 Obtaining Free Energy Profiles from Steered Molecular Dynamics Simulations....51
3. HYDROXYCOUMARIN TRANSPORT INDICATES A BIOPHYSICAL MECHANISM FOR DIFFERENTIAL TOXICITY....54
   3.1 Introduction....54
   3.2 Bolaamphiphilic Effects on Phospholipid Bilayers....55
   3.3 Creating a Model System....58
      3.3.1 Molecular Dynamics Simulations....58
      3.3.2 Molecule Topologies....58
      3.3.3 Simulation System....60
      3.3.4 Spontaneous Incorporation of Warfarin and Brodifacoum....62
      3.3.5 Constant Velocity Steered Molecular Dynamics Simulations....62
   3.4 Results and Discussion....65
      3.4.1 Spontaneous Retention of Hydroxycoumarins Within the Bilayer....65
      3.4.2 Transfer Free Energy for Bilayer Permeation....67
      3.4.3 Lateral Expansion, Thinning and Curvature of the Bilayer....69
      3.4.4 Changes in the Transmembrane Pressure Distribution....69
      3.4.5 Acyl Chain Packing Order....71

TABLE OF CONTENTS (continued)

CHAPTER PAGE

3.4.6 Amphiphilic Structure and Dynamic Orientation of Interfacial Warfarin and Brodifacoum 73
3.4.7 Transient Pore Formation, Water Permeation and Lipid Flip-Flop 77
3.5 Summary and Conclusion 82

4. CONSCIOUSNESS IMPAIRMENT BY AN ENDOGENOUS METABOLITE 86
4.1 Introduction 86
4.2 Coarse-Graining a Tiny Metabolite 89
4.3 Simulation System 90
4.4 Simulation Results 93
4.4.1 Structural Changes in the Phospholipid Bilayer in the Presence of *Beta*-hydroxybutyric Acid 93
4.4.2 Distribution and Orientation of *Beta*-hydroxybutyric Acid 98
4.4.3 Local Effects of *Beta*-hydroxybutyric Acid in Phospholipid Bilayers 102
4.5 Discussion and Conclusion 106

5. LIPID EMULSIONS FOR THE RAPID REVERSAL OF DRUG TOXICITY 109
5.1 Introduction 109
5.1.1 Reversal of Drug Toxicity by Lipid Emulsions 109
5.1.2 Hypothesized Mechanisms of Action 110
5.2 Creating an Oil Droplet Model 115
5.2.1 Molecular Dynamics Simulations 116
5.2.2 Molecule Topologies 116
5.2.3 Simulation System 120
5.2.4 Constant Velocity Steered Molecular Dynamics Simulations 121
5.3 Results and Discussion 123
5.3.1 Averaging Method Choice for Work Profiles 123
5.3.2 Effects of lipophilicity and charge 125
5.3.3 Effects of structure and size 129
5.3.4 Effects of Prepopulation 133
5.4 Summary and Conclusion 135

6. CONCLUSIONS 137
6.1 Recommendations for Future Work 140

CITED LITERATURE 142

VITA 167

LIST OF TABLES

TABLE PAGE

TABLE 2-1: MARTINI COARSE GRAINING MAIN INTERACTION SITES....14

TABLE 2-2: MARTINI COARSE GRAINING SUBTYPES....14

TABLE 2-3: BUPIVACAINE MAPPING TO MARTINI CG SITES....31

TABLE 2-4: ACETAMINOPHEN MAPPING TO MARTINI CG SITES....31

TABLE 2-5: LENNARD-JONES PAIRWISE COEFFICIENTS FOR CG NEUTRAL BUPIVACAINE....33

TABLE 2-6: LENNARD-JONES PAIRWISE COEFFICIENTS FOR CG NEUTRAL ACETAMINOPHEN....33

TABLE 3-1: EQUILIBRIUM SIMULATION SYSTEM SPECIFICATIONS....61

TABLE 3-2: STEERED SIMULATION SYSTEM SPECIFICATIONS....63

TABLE 4-1: AVERAGE INTERFACIAL CONCENTRATIONS OF BHB....93

TABLE 5-1: TOXIN PROPERTIES....118

TABLE 5-2: ACTIVATION ENERGIES FOR ENTRY INTO OIL FROM WATER....126

TABLE 5-3: ACTIVATION ENERGIES FOR ENTRY INTO DPPC FROM WATER AND INTO OIL FROM DPPC....127

TABLE 5-4: COMPARISON OF POLAR SURFACE AREA AND RELATIVE SIZE OF EACH TOXIN....130

TABLE 5-5: COMPARISON OF ACTIVATION ENERGIES BETWEEN BARE AND PREPOPULATED INTERFACES....133

LIST OF FIGURES

FIGURE PAGE

Figure 2-1: Schematic of a phospholipid bilayer membrane 8

Figure 2-2: Coarse-grained mapping for (a) linear and (b) ring molecules 13

Figure 2-3: Four water molecules (left) mapped to one CG site (right) 15

Figure 2-4: Lennard-Jones potential energy function 16

Figure 2-5: Angle between two bonds sharing a common interaction site 18

Figure 2-6: Dihedral angle between two planes 19

Figure 2-7: Creating a model phospholipid (PL) monolayer at the water/oil interface 21

Figure 2-8: Molecular structures of DPPC (a) and triolein (b) 22

Figure 2-9: Phospholipid monolayers at water/triglyceride interface (left) and bilayer in water (right) 23

Figure 2-10: Chemical structures of neutral bupivacaine (a) and acetaminophen (b) molecules 26

Figure 2-11: Multiple options for coarse-grained structural mapping of bupivacaine 27

Figure 2-12: CG representation of acetaminophen with the selected MARTINI interaction types. 30

Figure 2-13: λ parameter tuning of interaction strength between solute and solvent 36

Figure 2-14: Mass density profile highlighting triglyceride (TG) orientation detail 43

Figure 2-15: Schematic of radial distribution of blue sites around central red site within cutoff distance 46

Figure 2-16: Radial distribution functions of water around phospholipid groups in a DPPC monolayer 47

Figure 3-1: Two-dimensional structure of warfarin (top) and brodifacoum (bottom) overlaid with the coarse-grained representation of each molecule. 59

LIST OF FIGURES (continued)

FIGURE PAGE

Figure 3-2: Snapshots of simulation cells containing fully equilibrated DPPC bilayers in water with warfarin (a) and brodifacoum (b) molecules taken after 320 ns of simulation time. 66

Figure 3-3: Free energy profiles of warfarin (left) and brodifacoum (right) as a function of distance through the bilayer. Statistical error bars are represented as shaded bands around the profiles.....68

Figure 3-4: Lateral pressure profiles from simulations containing brodifacoum and warfarin (curves with square and circle symbols respectively) compared to a bare DPPC bilayer (solid black curve). 70

Figure 3-5: Left: order parameter profiles calculated along the bonds connecting coarse-grained sites in DPPC tails (bond numbering shown on the right). Open symbols represent the sn1 and closed symbols the sn2 tails of DPPC (illustrated on the right). 72

Figure 3-6: Normalized density profiles of the brodifacoum brominated (purple curve with triangle symbols) and hydroxycoumarin (shaded green curve) groups. 75

Figure 3-7: Snapshots of two possible configurations for warfarin (top) and brodifacoum (bottom) located within a DPPC bilayer near the polar choline (white spheres) and phosphate (pink spheres). 76

Figure 3-8: Snapshots of brodifacoum travelling through the DPPC bilayer. 78

Figure 3-9: Radial distribution functions g(r) between the hydroxycoumarins and water in the center of the bilayer. 79

Figure 3-10: Simulation snapshots at four time points as brodifacoum travels through the DPPC bilayer. 81

Figure 4-1: BHB structure (carbon-cyan, oxygen-red, hydrogen-white) overlaid with brown coarse-grained representation 90

Figure 4-2: Snapshot of equilibrated DPPC bilayer in water containing 7 mol% BHB. 91

Figure 4-3: Average cross-sectional area per molecule (top) and water concentration (bottom) in DPPC bilayer as a function of BHB concentration. Error bars are located within each data point. 94

LIST OF FIGURES (continued)

FIGURE PAGE

Figure 4-4: Effect of BHB on mean lateral pressure across DPPC bilayer. Error bars are located within each data point. 96

Figure 4-5: Average angle formed between the P-N (phosphate to choline) vector and the interface normal at different BHB concentrations. 97

Figure 4-6: Coarse-grained order parameter profiles calculated along the bonds (vectors) connecting CG sites constituting DPPC tails for different BHB concentrations. 98

Figure 4-7: Normalized mass density distribution of DPPC bilayer containing 1 mol% BHB. 99

Figure 4-8: Comparison of the distributions of tilt angle between the interface normal and a vector connecting the carboxyl group to the terminal hydroxyl group of BHB embedded in DPPC membrane. 100

Figure 4-9: BHB pair radial distribution functions for various BHB concentrations. 102

Figure 4-10: Random walk trajectories of several BHB molecules in DPPC bilayers at interfacial concentrations of 3 mol% (left) and 7 mol% (right). Each molecule trajectory is shown in a different color. 103

Figure 4-11: Spatially resolved and time averaged 2D order parameter maps for DPPC membranes at BHB concentrations of zero (left), 3 mol% (middle) and 7 mol% (right). 104

Figure 5-1: Schematic of theoretical lipid sink mechanism of toxin sequestration by an oil droplet. 112

Figure 5-2: Two-dimensional structures of toxins overlaid with the coarse-grained representation of each molecule. 119

Figure 5-3: Snapshot of simulation cell containing fully equilibrated DPPC monolayers at the water/triglyceride interface. 120

Figure 5-4: Comparison of work profile (red lines) averaging methods for acetaminophen (top) and bupivacaine (bottom). 124

Figure 5-5: Effect of log*P* on activation energies for neutral toxin molecules 129

LIST OF FIGURES (continued)

FIGURE PAGE

Figure 5-6: Effect of polar surface area on activation energies for neutral (left) and charged (right) toxin species. Values for acetaminophen are not included. 131

Figure 5-7: Effect of radius of gyration on activation energies for neutral (left) and charged (right) toxin species. Solid lines placed to guide the eye. 132

NOMENCLATURE

ACLS	Advanced Cardiovascular Life Support
BAR	Bennett Acceptance Ratio
BDF	Brodifacoum
BHB	*Beta*-hydroxybutyric Acid
CG	Coarse-Grained
DPPC	Dipalmitoylphosphatidylcholine
LJ	Lennard-Jones
MD	Molecular Dynamics
NMR	Nuclear Magnetic Resonance
PMF	Potential of Mean Force
PSA	Polar Surface Area
TG	Triglyceride
WAR	Warfarin

SUMMARY

Potentially harmful drugs, chemicals, and compounds constantly interact with the human body. These substances either enter from the external environment, or are produced internally as waste products of metabolic processes. Studies show that small drug and toxin molecules are able affect the physicochemical properties of physiological membranes, including causing changes to permeability, fluidity, packing, electrostatic potential, and rheology. If these property changes to physiological membranes are sufficiently disruptive, they could also affect the ability of the membranes to function as barriers against unregulated transport of material. The manner in which these changes occur on a molecular level and their possible effects on proteins and other membrane structures is not entirely clear. As such, a molecular-level understanding of alterations they induce in the structure, dynamics, and thermodynamics of phospholipid layers may elucidate the mechanisms by which toxins cause adverse effects in the body.

Toward this end, we undertook molecular dynamics computer simulations to probe the effects of small, potentially toxic molecules on the biomechanical properties of phospholipid layers in an attempt to clarify the mechanisms through which these molecules associate with and alter the properties of these layers. In this thesis, three different applications of our simulation approach are considered: the mechanisms of differential cytotoxicity of exogenous anticoagulant species, the role played by endogenous metabolites in causing consciousness impairment, and the association of potentially toxic drugs with lipid emulsions acting as detoxification agents. Our simulations reveal the nature of the changes in phospholipid layers and the molecular mechanisms by which these changes occur, as well as the free energies

associated with them.

Based on the three example applications we studied, we understand that different molecular properties (size, polar surface area, charge, conformational dynamics) lead to different associations of toxins with phospholipid layers; so that different orientations, different preferred locations of toxin molecules along membrane interfaces, and different degrees of disruption of physical properties of phospholipid layers accompany the interaction of toxin molecules with physiological membranes. Likewise, different molecular properties lead to different free energy profiles for penetration of toxins into membranes. What all three examples show in common is the ability of our coarse-grained molecular dynamics approach to provide molecular-level information on the absorption, transport, and partitioning of toxin molecules into model membranes. We show various ways in which the results of molecular dynamics simulations may be interrogated to find unprecedented levels of detailed information for a given toxin molecule interacting with and possibly penetrating or altering a phospholipid interface. Our computational approach provides useful insight and offers predictions that can be tested experimentally.

1. INTRODUCTION

The human body is constantly inundated by toxic substances. These include potentially harmful drugs and chemicals that enter the body from the external environment (exogenous toxins), as well as compounds produced internally, such as waste products from metabolic processes (endogenous toxins). The kidneys and liver are the main organs tasked with toxin excretion [1-5]; however, to reach these organs, toxins need to travel through the circulatory system. While transported through the bloodstream, these toxic substances interact with proteins, lipoproteins, lipid droplets, cells, and numerous other structures and compounds in the body. Many of these structures encountered by toxic molecules are surrounded by layers composed mainly of phospholipid molecules. These amphiphilic lipid molecules form impervious monolayer and bilayer fluid membranes that enclose and protect the contents within. They form barriers against the unregulated passage of material. Within these semi-permeable phospholipid layers are embedded structures such as proteins, sterols, glycolipids, and glycoproteins [6, 7].

Although it is known that many drugs and toxins bind to specific proteins embedded in phospholipid layers [8-14], the vast diversity of species that have toxic effects on the body indicates that specific binding cannot be the only mechanism by which they act. Even among small molecules (of low molecular weight), there are immense variations in shape, size, charge state and distribution, polarity, conformation, and many other properties. The molecular specificity necessary for direct protein binding cannot be met by all these molecules [15]. It has therefore been proposed that small molecules may affect proteins by an indirect method: changing the biomechanical environment of the protein so as to effect conformational

changes in the protein, thereby compromising its ability to perform its function[16-19]. For membrane-bound proteins, this means that important properties of the fluid membrane would need to be altered in order to propagate changes to the proteins. If the phospholipid layer property changes are sufficiently disruptive, they could also affect the ability of the membrane to function as a barrier against unregulated transport of material.

Studies have shown that small molecules do indeed have an effect on the physicochemical properties of phospholipid layer membranes, including causing changes to permeability, fluidity, packing, lipid orientation, electrostatic potential, and rheology [20-27]. The exact manner in which these property changes occur on a molecular level, and their possible effects on proteins and other structures embedded in the membrane, are not entirely clear. As such, the mechanisms by which toxins cause adverse effects in the body may be elucidated by a molecular-level understanding of alterations in the structure, dynamics, and thermodynamics of phospholipid layers induced by these harmful substances. A molecular-level investigation of specific mechanisms is relatively difficult, if not impossible, to undertake using solely experimental techniques. Therefore, computational methods may provide useful insight and offer predictions that can be tested experimentally.

Toward this end, we undertook molecular dynamics computer simulations to probe the effects of small, potentially toxic molecules on the physical properties of phospholipid layers, in an attempt to clarify the mechanisms through which the small molecules associate with and alter the properties of these layers. This type of computational approach has been shown to provide insight into molecular-level properties of phospholipid layers that are difficult to assess experimentally [26-31]. In this thesis, we consider three different applications of our molecular

simulation approach: the mechanisms of differential cytotoxicity of exogenous anticoagulant species, the role played by an endogenous metabolite in causing consciousness impairment, and the association of potentially toxic drugs with lipid emulsions acting as detoxification agents. Although dealing with vastly different toxic molecules, in all three examples, we hypothesize that small molecules associate non-specifically with and alter the properties of phospholipid layers. More importantly, our simulations reveal the nature of the changes in the phospholipid layers and the molecular mechanisms by which these changes occur, as well as the thermodynamic free energies associated with these processes. Thus, the approach used here, if successful, can be extrapolated to predict mechanisms of action for a vast array of other species in a wide range of associated pathologies (diseases, cytotoxicity, etc.).

1.1 **Organization of this Thesis**

The simulation methodology used is described in detail in Chapter 2, beginning with an overview of general computational methods used to model phospholipid layers. This is followed by a brief overview of the specific interaction scheme we employed – the MARTINI coarse-graining force field and its application to our systems of interest. A detailed description of the techniques we employed to develop coarse-grained topologies for small toxin molecules and the method used to validate these new topologies follows. Chapter 2 is rounded off by specific details relevant to performing the simulations and studies presented in this work as well as descriptions of the methods we used to analyze our results and obtain average properties and detailed quantitative molecular information (conformation, distribution, orientation) as well as free energy profiles from our simulations.

In Chapter 3, the specific problem of cytotoxicity caused by exogenous toxins is considered. This system is an excellent test case of the general approach chosen by us; we were able to demonstrate that the observed differential toxicity of molecules possessing identical chemical moieties attached to different groups may be modulated by their specific interactions with and consequent transformation of a phospholipid bilayer. This investigation was undertaken as part of a larger study to understand the cytotoxic effects of anticoagulants and propose countermeasures against potential chemical warfare agents. The long-acting rodenticide, brodifacoum, is an agent of opportunity – a readily available household or industrial chemical that has the potential to be exploited as a weapon [32]. Brodifacoum was derived from the first-generation anticoagulant warfarin (currently used as a therapeutic) and is a member of a class of second-generation anticoagulants (superwarfarins) designed to overcome rodent resistance to first-generation pesticides. Superwarfarins possess high lipophilicity and are assumed to be more potent than first-generation anticoagulants due to their prolonged residence time in physiological tissues. While warfarin can yield acute tissue damage, conservative dosing and a limited physiological half-life restrict the relevance of this mode of toxicity. Brodifacoum, by contrast, can remain sequestered in organs for up to a year, and malicious release could lead to heavy exposures [33-38]. The mechanisms of brodifacoum toxicity are not well understood. We therefore employed coarse-grained molecular dynamics simulations to explore a potential mechanism for anticoagulant cytotoxicity in general and the heightened toxicity of brodifacoum in particular. Our simulations reveal that permeation of phospholipid bilayers by brodifacoum causes a disruption of membrane barrier function driven by the bolaamphiphilic nature and size of this molecule. We find that brodifacoum partitioning

into bilayers causes membrane thinning, permeabilization, and promotes lipid flip-flop – all phenomena that are suspected to play a role in triggering cell death [39-41]. These phenomena are either absent or less pronounced in the case of the less toxic compound, warfarin.

In Chapter 4, the role of endogenous metabolites in causing consciousness-impairment is examined. Metabolic disorders are among the leading causes of death in the United States every year [42, 43]. One of the most debilitating symptoms of these disorders is their effect on consciousness, with problems ranging from simple memory impairment to coma [44, 45]. The connection between impairments to consciousness and metabolic disorders that affect organs far removed from the brain may be via the elevation of metabolites in the blood stream [46, 47]. When communicated to the brain through the blood stream, these metabolites are thought to operate in a manner similar to anesthetics [46, 48, 49]. Anesthetics are believed to affect consciousness by two distinct mechanisms: (i) direct, site-specific interactions with ion channel proteins in cell membranes [9]; and (ii) indirect effects on ion channels by alteration of membrane structure and dynamics [20, 27, 50]. Metabolites that are thought to impair consciousness differ in shape, size, and protonation state at physiological pH – a feature that is inconsistent with a site-specific mechanism. Thus, non-specific interaction of metabolites with cell membranes is likely. In the case of the metabolite *beta*-hydroxybutyric acid, whose levels are elevated in type I diabetes, experimental evidence suggests that clinically relevant concentrations significantly alter the phase behavior and rheology of phospholipid interfaces [51]. In this chapter, we explore the molecular origins of this phenomenon using coarse-grained molecular dynamics simulations. We demonstrate, by this example, a possibly general mechanism by which small molecules (drugs, metabolites) may change membrane properties.

In turn, the altered membranes may modulate protein receptor or protein channel function. Our simulations demonstrate an important physical phenomenon (a threshold concentration) that may correlate interfacial concentrations of BHB to the occurrence of consciousness-impairment symptoms in patients at threshold metabolite concentrations.

Our third example, in Chapter 5, involves a study of the association of drug molecules with lipid emulsion droplets for biodetoxification. This investigation is a paradigm for discovery of mechanisms of drug sequestration as well other events such as drug penetration into phospholipid membranes. Through clinical reports and *in vivo* experiments [52-56], intravenous delivery of a lipid emulsion has been shown to rapidly reverse the toxic effects of several pharmaceutical agents and restore compromised cardiac function. A key feature of these emulsions is the ability of their particles to act as toxin scavengers. This scavenging action, known as the 'lipid sink' action, is thought to be limited to acting only on highly lipophilic toxins, with hydrophobic partitioning as the primary driving force [56, 57]. However, many of the drug compounds in question exist in a predominantly charged state at physiological pH; electrostatic interactions likely play an important role in driving toxin sequestration. For a rational application of lipid emulsion biodetoxification it is necessary to clarify the key physicochemical characteristics that govern the association of toxin molecules with lipid droplets. To probe the association of toxin molecules with emulsion particulates in this chapter, we employ coarse-grained molecular dynamics simulations to develop molecular topologies for several drug molecules in the multiphase system of interest consisting of a dipalmitoylphosphatidylcholine (DPPC) monolayer at a water/oil interface. Both neutral and ionized coarse-grained topologies are developed for six small drug molecules with varying levels of lipophilicity and differing

degrees of protonation at physiological pH. These topologies are then incorporated into the multiphase droplet system. This scheme is developed to clarify the relative roles of molecular attributes such as lipophilicity, protonation state, size, structure and other factors in mediating toxin sequestration. To the best of our knowledge, this particular approach has not previously been applied to a monolayer system of this type and will allow the study of a sufficiently large system over adequately long timescales to obtain structural, dynamic and thermodynamic information about transport through the phospholipid monolayer. We find some similarities in the association of toxins with the emulsion droplet, even for the cases of lower lipophilicity, where a purely hydrophobic partitioning hypothesis would not predict association with droplets. Furthermore, we explore the potential of toxin partitioning between the aqueous phase, the droplet interface, and the lipid core. In our studies, it appears that lipophilicity alone is not a good predictor of drug association with lipid droplets.

Finally, our overall conclusions and suggestions for future work are in Chapter 6. Here we discuss, on the basis of the findings from the three examples, the extent to which the general computational approach used in this work can be considered a valid general approach to address the nature of the molecular mechanisms by which endogenous and exogenous toxins interact with, partition into, or transit through phospholipid interfaces. Possibilities for extension of this work and further study are also described.

2. METHODS

2.1 Computer Simulations of Phospholipid Interfaces

Phospholipid monolayers and bilayers are pervasive in biological systems. Plasma membranes, for example, enclose and protect cells by providing a physical barrier to the transport of water, ions, and other small molecules into and out of cells. Despite the heterogeneous nature of cell membranes, the basic structure consists of two phospholipid monolayers forming a two-dimensional, fluid (liquid crystalline) phase, a phospholipid bilayer membrane (Figure 2-1), in which are embedded membrane proteins and other structures [58, 59].

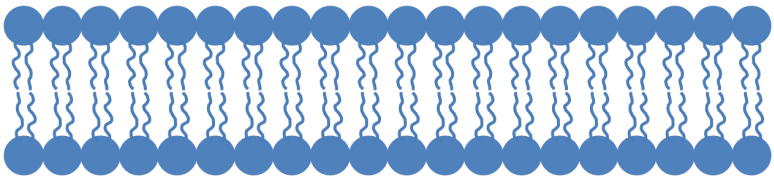

Figure 2-1: Schematic of a phospholipid bilayer membrane

Phospholipid layers can be studied using both experimental and computational means. Experimental techniques for obtaining properties of model membranes include Langmuir monolayer studies, nuclear magnetic resonance, x-ray diffraction, fluorescence, and atomic force microscopy experiments [60-63]. Relatively long characteristic time scales (10^{-7} – 10^{-1} s) and system size requirements limit most of these techniques.

Computational modeling of phospholipid layers can be accomplished with varying levels of detail. At one end of the spectrum, continuum mechanics can be used to study phospholipid membranes as a continuous mass or a thin elastic sheet rather than discrete entities (such as atoms or molecules) [64-67]. These models are useful for studies of macroscopic systems that can be described using properties such as spontaneous curvature, bending rigidity, and surface tension [68-70]. Continuum models, however, cannot probe phenomena that occur at an intermediate (mesoscopic) or molecular length scale, nor can they adequately describe membranes made up of many different components. Particulate models are therefore better suited to model the heterogeneous nature of cell membranes. Using a top-down approach, particle-based models, some with implicit solvent, may be used to study mesoscopic as well as macroscopic properties. Phenomena such as membrane undulations, shape deformations, diffusion, thickness fluctuations and other properties that are evident at intermediate length and time scales can be studied [71-73]. By not explicitly representing the solvent, length and time scales that may not be conveniently probed at atomistic levels become accessible.

On the opposite end of the spectrum, atomistic models explicitly represent the individual atoms of each molecule as interacting particles [59, 74-78] so that the specific interactions within and between molecules can be studied. However, atomistic models tend to be computationally demanding, thus imposing limits on both the time and length scales that can be examined [69]. Systematic studies exploring multiple conditions and parameters become prohibitive. In coarse graining molecules using a bottom-up approach, several atoms are grouped into one interaction site, thus reducing the total number of particles in the simulation so that larger length and time scales can be probed [58, 79, 80]. Systems can be increasingly

coarse-grained by grouping just a few or relatively large numbers of atoms into one interaction site. For example, Noguchi and Takasu [81] describe a solvent-free system of self-assembled lipid bilayer vesicles. This type of system differs from other coarse-grained models in that each molecule is not represented by several particles; rather, the amphiphilic lipid molecules are each modeled as one rigid rod with hydrophilic and hydrophobic sections. This type of method suffices for studies in which the individual molecular interactions are not as important as the overall behavior of the membrane.

For systems where the interactions within and between molecules are important and an understanding of molecular conformational changes is desired, it is necessary to use a technique that preserves the general shape and structure of each molecule. In order to elucidate the mechanisms by which toxins alter the structure and dynamics of phospholipid layers, we choose a coarse graining approach that groups several atoms into discrete sites in each molecule. These sites are parameterized such that they interact with each other to reproduce the measured physicochemical properties of the molecules they represent. Using coarse-grained molecular dynamics simulations, it is feasible to probe the time-dependent evolution of variations in structure, dynamics, and thermodynamics of multi-component model systems.

In order to simulate phospholipid layer systems, it is necessary to design models for the molecules representing the various components in the system. The manner in which each of the interaction sites or particles that represent the molecule interacts with all the other particles in the system can be described using a set of mathematical functions. The form of the functions and the parameters used in the equations are collectively referred to as a force field.

The classical force fields most commonly used in molecular dynamics simulations include the following:

i) GROMOS (GROningen MOlecular Simulation), which employs a united atoms approach where CH, CH_2 and CH_3 groups are modeled as single particles [82-85],

ii) CHARMM (Chemistry at HARvard Macromolecular Mechanics), which explicitly describes all hydrogen atoms in the system and expresses intramolecular interactions in a detailed manner [86, 87], and

iii) AMBER (Assisted Model Building with Energy Refinement), like CHARMM, was initially developed to use explicit hydrogen atoms and is generally used for biomolecular simulations of proteins primarily [88], but has also been extended to lipids [89].

These three force fields are generally used to model atomic scale systems using classical dynamics. For example, Henneré et al. [90, 91] demonstrated the development of all-atom model systems to mimic the surfaces of lipid emulsion droplets with the aid of GROMOS force field parameters. These model systems included only the phospholipid monolayer interfacial region without representing a majority of the oil core. The physical and chemical properties of their model systems were in good agreement with experimental data.

We desire to overcome the temporal and spatial limitations imposed by atomistic simulations in order to probe longer times and larger system sizes. In order to achieve this, the overall number of degrees of freedom in our systems is reduced by grouping sets of atoms together into single interaction sites (coarse graining) and determining the interaction parameters systematically. Several different coarse graining schemes exist for modeling lipids, including schemes that either implicitly or explicitly represent the solvent [72, 81, 92-96]. One

coarse graining scheme using explicit solvent is based on the MARTINI force field [79, 80], which has been shown to reproduce the essential structural, dynamic, and thermodynamic properties of phospholipid layers in a semi-quantitative manner. In this thesis, we employ coarse-grained molecular dynamics computer simulations using the MARTINI scheme to elucidate the molecular-scale mechanisms underlying the absorption, transport, and partitioning of endogenous and exogenous toxins as they encounter a phospholipid layer. Molecular dynamics simulations can provide details of the molecular-scale interactions at phospholipid interfaces that are necessary for interpretation of experimental studies on model physical systems [90, 91, 97, 98]. Furthermore, once validated against measurements on model physical systems, molecular dynamics studies can be used to predict behavior of similar or more complex physical systems.

2.2 **Overview of The MARTINI Coarse-Grained Force Field**

The MARTINI coarse-grained force field proposed by Marrink et al. [79, 80] was initially developed and parameterized for lipid and surfactant systems, for which it was found to reproduce thermodynamic data well. For example, partitioning free energies between polar and nonpolar phases for various chemical species were replicated. Interaction potentials from this scheme have been extended to biomacromolecules including carbohydrates [99], proteins [100], and polymers [101]. A comprehensive guide to the various applications and further development of MARTINI may be found at http://md.chem.rug.nl/cgmartini/ and the review article by Marrink and Tieleman [102].

2.2.1 Mapping Coarse-Grained Sites

The standard MARTINI coarse-grained force field employs a four-to-one mapping that replaces approximately four heavy atoms (such as carbon, nitrogen, phosphorus, oxygen, etc.) with one coarse-grained interaction site, as shown with the hexadecane molecule in Figure 2-2(a). For small ring structures such as the benzene ring in Figure 2-2(b), the mapping is changed to a two- or three-to-one scheme so as to increase the resolution and preserve the overall geometry of the ring.

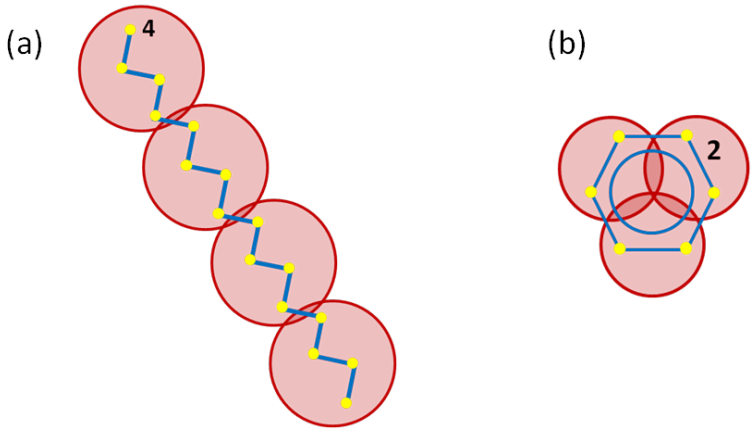

Figure 2-2: Coarse-grained mapping for (a) linear and (b) ring molecules

In the MARTINI force field, four main interaction sites are defined (Table 2-1): polar (P), nonpolar (N), apolar (C), and charged (Q).

TABLE 2-1: MARTINI COARSE GRAINING MAIN INTERACTION SITES

Symbol	Meaning	Description
P	Polar	Groups of neutral atoms that are easily soluble into water
N	Nonpolar	Groups that are partly polar and partly apolar
C	Apolar	Groups that are hydrophobic
Q	Charged	Groups that are ionized
S		Special particles used to model ring structures

Each main interaction site has several subtypes that are distinguished either by their hydrogen-bonding capabilities (for nonpolar or charged groups) or their degree of polarity (for polar and apolar groups) (Table 2-2).

TABLE 2-2: MARTINI COARSE GRAINING SUBTYPES

Hydrogen-bonding Capabilities		**Degree of Polarity**
Symbol	**Meaning**	**1** (low polarity)
d	donor	**2**
a	acceptor	**3**
da	both	**4**
0	none	**5** (high polarity)

For example, one P_4 type coarse-grained site is used to represent four water molecules, as illustrated in Figure 2-3. Here, P describes the polar nature of the water molecules and the number 4 means the degree of polarity is relatively high.

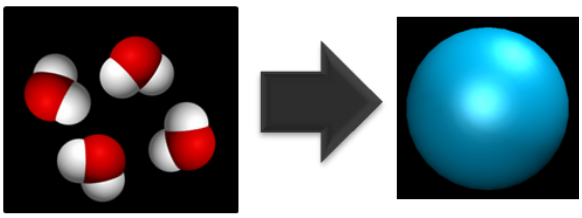

Figure 2-3: Four water molecules (left) mapped to one CG site (right)

2.2.2 Nonbonded Interactions

Non-bonded interactions are cut off at 1.2 nm. Van der Waals interactions between neutral, nonbonded particle pairs in the MARTINI force field are described using a shifted Lennard-Jones (LJ) 12-6 potential energy function, $\mathrm{U_{LJ}}(\mathbf{r})$ (see Figure 2-4).

$$\mathrm{U_{LJ}}(\mathbf{r}) = 4\varepsilon_{ij}\left[\left(\frac{\sigma_{ij}}{\mathbf{r}}\right)^{12} - \left(\frac{\sigma_{ij}}{\mathbf{r}}\right)^{6}\right] + \mathrm{S_{LJ}}(\mathbf{r}) \qquad \mathbf{r} < \mathbf{r_c}$$

(2-1)

$$\mathrm{S}(\mathbf{r}) = 0 \qquad \mathbf{r} < \mathbf{r_1}$$

(2-2)

$$\mathrm{S}(\mathbf{r}) = \mathrm{A}(\mathbf{r} - \mathbf{r_1})^2 + \mathrm{B}(\mathbf{r} - \mathbf{r_1})^3 \qquad \mathbf{r_1} < \mathbf{r} < \mathbf{r_c}$$

(2-3)

Here, for any two particles *i* and *j*, $\mathbf{r}$ is the vector representing the distance between them, σ_{ij} represents the distance of closest approach, and ε_{ij} is the depth of the potential well which describes the strength of their interaction. The function $\mathrm{S}(\mathbf{r})$ smoothly shifts the potential

function to zero between the inner ($\mathbf{r}_1 = 0.9\ \mathrm{nm}$) and outer ($\mathbf{r}_c = 1.2\ \mathrm{nm}$) cutoff distances to avoid discontinuity in the potential at the cutoff. This equation describes the repulsion and long-range attraction interactions of particles that are not connected by chemical bonds.

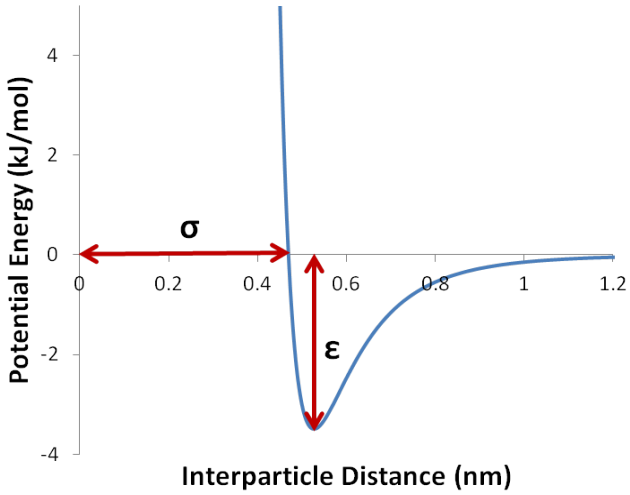

Figure 2-4: Lennard-Jones potential energy function

Electrostatic interactions between charged groups (represented by the MARTINI 'Q' main interaction site) that are not bonded to each other are described by a shifted Coulombic potential energy function, $\mathrm{U_C(r)}$:

$$\mathrm{U_C}(\mathbf{r}) = \frac{\mathrm{q}_i \mathrm{q}_j}{4\pi\varepsilon_0 \varepsilon_r \mathbf{r}} + \mathrm{S_C}(\mathbf{r}) \qquad \mathbf{r} < \mathbf{r}_c$$

(2-4)

where $q_{i,j}$ are the charges on each particle, $\varepsilon_r = 15$ is the relative dielectric screening constant, and ε_0 is the dielectric permittivity of free space. This potential acts along the line connecting two charged particles separated by a distance $\mathbf{r}$. Once again, the potential is smoothly shifted to zero between the two cutoff values (0.0 nm to 1.2 nm) by the function $S_C(\mathbf{r})$. Long-range electrostatic interactions were neglected since pairwise interactions beyond 1.2 nm were not considered.

2.2.3 **Bonded Interactions**

Between covalently bonded CG sites, a harmonic potential is used to describe the bond stretching interactions, $U_{bond}(r)$:

$$U_{bond}(\mathbf{r}) = \frac{1}{2} K_{bond}(\mathbf{r} - \mathbf{r}_{bond})^2$$

(2-5)

where r_{bond} represents the equilibrium bond length with a force constant of K_{bond} that describes the stiffness of the bond. LJ interactions are not included between directly bonded particles, but they are for second nearest neighbors.

A harmonic cosine potential is used to represent chain stiffness for the angles between three consecutive bonded particles (Figure 2-5):

$$U_{angle}(\theta) = \frac{1}{2} K_{angle}[\cos(\theta) - \cos(\theta_0)]^2$$

(2-6)

with K_{angle} being the force constant and $\theta_0$the equilibrium bond angle. For ring structures, the equilibrium bond lengths and angles are selected to preserve the underlying geometry. A set of constraints can also be used to replace bonds or angles to maintain the ring rigidity. Within a ring system, intramolecular LJ interactions are generally excluded.

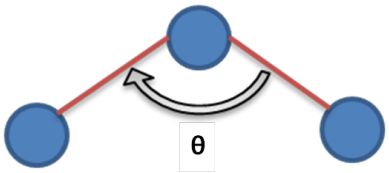

Figure 2-5: Angle between two bonds sharing a common interaction site

Out-of-plane distortions can be prevented by using a dihedral angle potential (Figure 2-6) for more complicated geometries, $U_d(\varphi)$:

$$U_d(\varphi) = K_d(\varphi - \varphi_d)^2$$

(2-7)

where φ represents the angle between the plane comprised of particles i, j, k and that made up of particles j, k, l, with φ_d being the equilibrium angle and K_d the force constant.

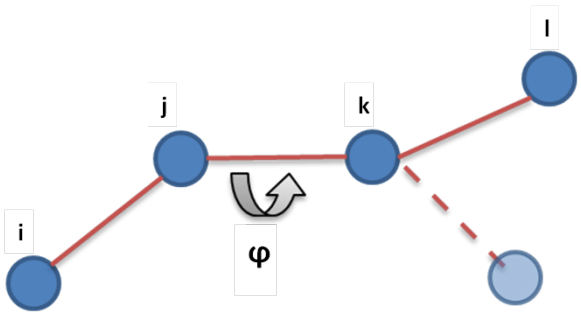

Figure 2-6: Dihedral angle between two planes

The MARTINI force field and coarse graining scheme has been used as an important building block in our studies of molecular-scale toxin interactions with phospholipid interfaces. We have extended the standard interaction parameters to create representations of all our small molecules of interest, as will be described in the upcoming section.

2.2.4 **Phospholipid Layer Models in MARTINI**

Experimental and computational phospholipid bilayer studies, interactions of species with, and permeability across these membranes are pervasive in scientific literature due to their biological significance as cell membrane models [79, 80, 103-108]. For phospholipid monolayers, however, two main types of systems are usually studied experimentally and computationally:

(i) lipid monolayers on solid supports, and

(ii) Langmuir films at the interface of air and water [109-113].

These monolayer systems have generally been studied to better understand biological processes which contain lipid monolayer structures, e.g., lung surfactant prevents lung collapse

by changing the surface tension on alveoli surfaces [114]. Studies of phospholipid monolayers adsorbed at the oil/water interface are quite rare and interaction studies of small molecules at these interfaces are even less common. To understand the interactions of toxins with phospholipid layers and the consequences manifested as changes in the structure and dynamics of these layers, it is essential to develop and validate models, not only of phospholipid bilayers in water, but good representations of monolayers adsorbed at aqueous/triglyceride and aqueous/air interfaces as well. These types of monolayers would represent systems of biological relevance such as our model of lipid droplets (Figure 2-7), which shall be discussed further in Chapter 4. For this system, different small toxin molecules will be included in the model to study their specific interactions with lipid droplet interfaces.

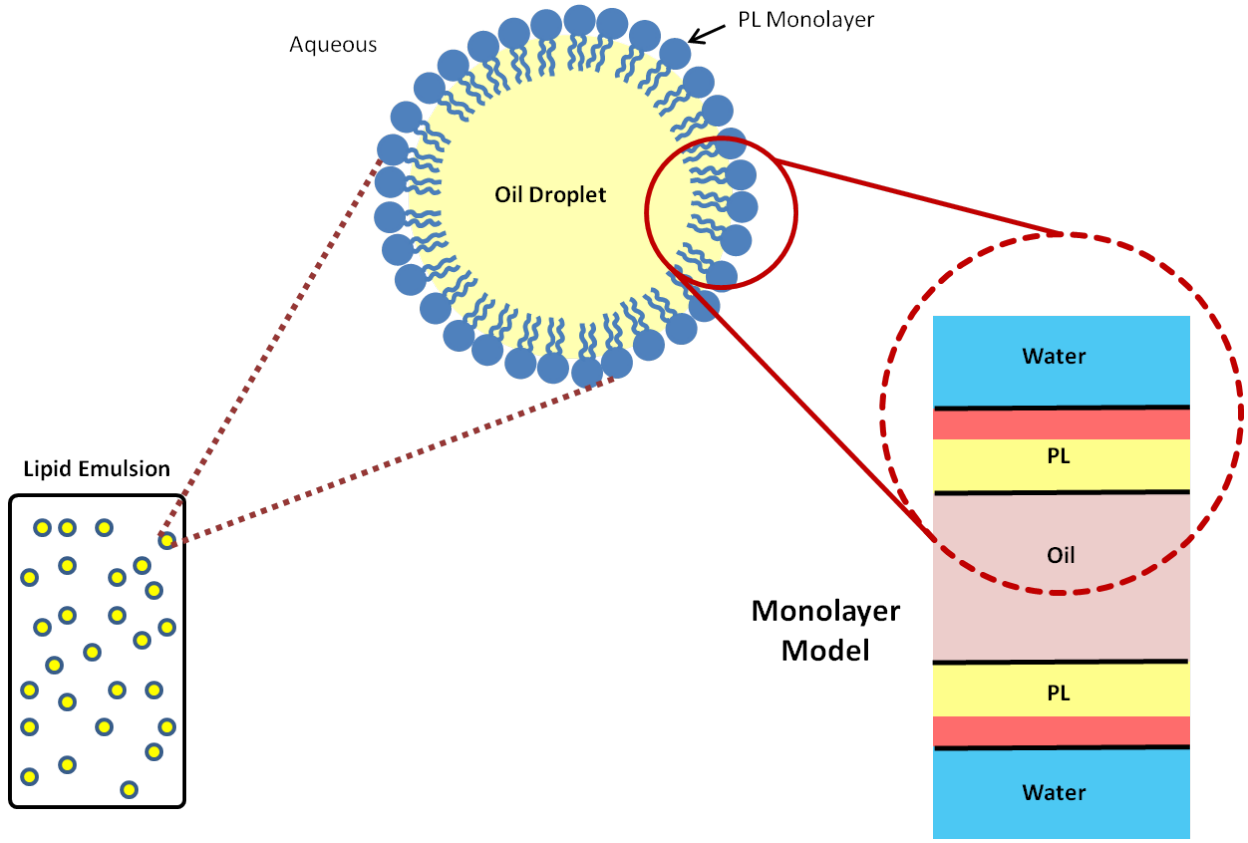

Figure 2-7: Creating a model phospholipid (PL) monolayer at the water/oil interface

2.3 Simulation Model Systems Used in this Thesis

To this end, we have developed several simulation systems consisting of phospholipid layers either presented as bilayers solvated in water or monolayers at the water/triglyceride interface (Figure 2-9). Dipalmitoylphosphatidylcholine (DPPC) (Figure 2-8 (a)) was chosen as the representative phospholipid molecule, while glycerine trioleate (triolein) (Figure 2-8 (b)) was used as the representative triglyceride molecule for the lipid phase. DPPC is an amphiphilic molecule composed of a hydrophilic head group and hydrophobic fatty acid tails. The head group contains a positively charged choline group and a negatively charged phosphate moiety.

A glycerol backbone, to which the two saturated palmitic fatty acid tails are connected, is attached to the head group. Triolein is a triglyceride composed of a glycerol backbone and three monounsaturated oleic fatty acid tails.

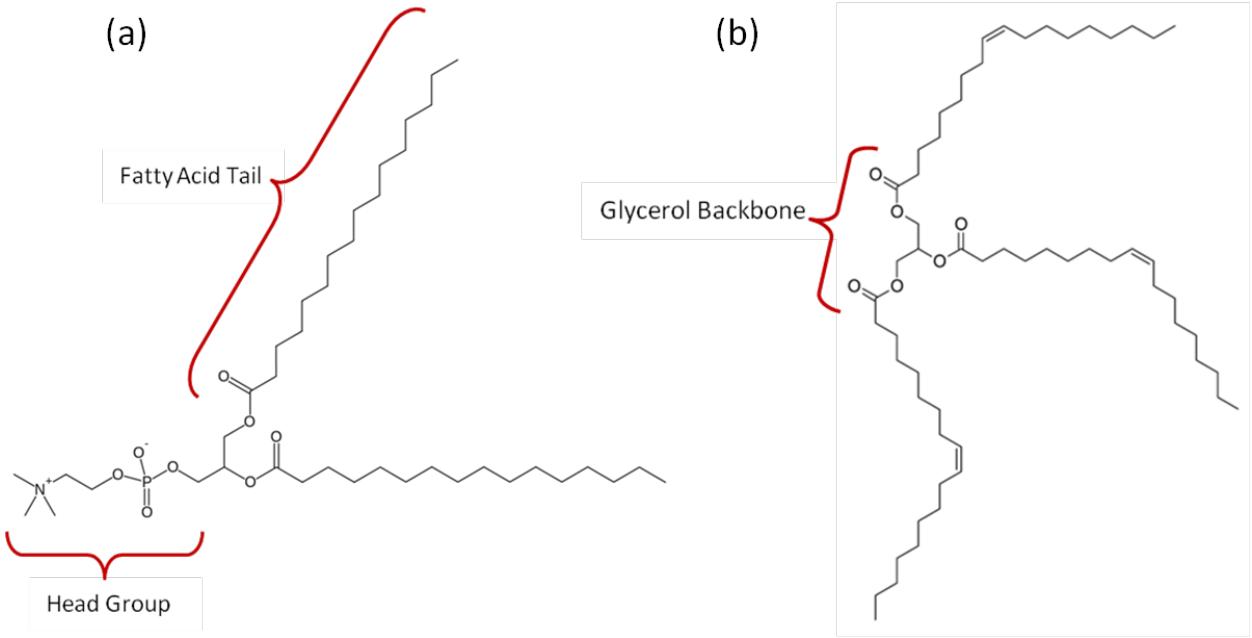

Figure 2-8: Molecular structures of DPPC (a) and triolein (b)

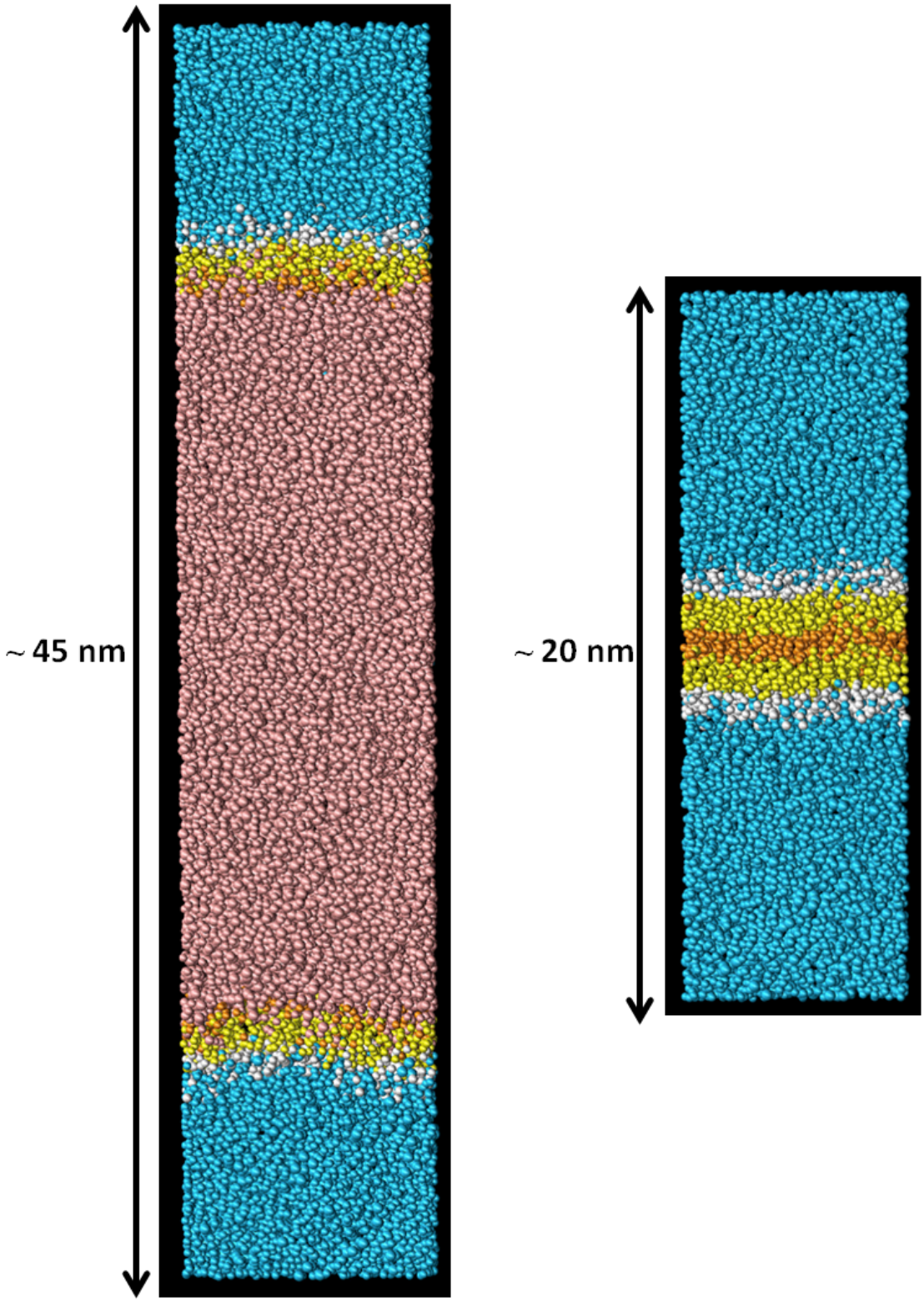

Figure 2-9: Phospholipid monolayers at water/triglyceride interface (left) and bilayer in water (right)

Coarse-grained topologies for DPPC, triolein, and water were downloaded from the MARTINI website (http://md.chem.rug.nl/cgmartini/). As illustrated in Figure 2-9, the DPPC fatty acid tails were each represented by four coarse-grained interaction sites (three shown as yellow spheres with the terminal site represented by an orange sphere), connected to the glycerol backbone (two white spheres). The glycerol backbone was bonded to white spheres representing the negatively charged phosphate group and the positively charged choline group. Thus, a DPPC molecule containing 130 atoms was conveniently represented by just 12 CG interaction sites. A similar mapping protocol was applied to the triolein molecule, rendering a 167-atom molecule using only 16 interaction sites (shown as pink spheres in Figure 2-9 (a)).

The CG topologies for triolein and water (Figure 2-3) were replicated to produce slabs of each component. DPPC was replicated to produce two monolayers. In the case of the water/triglyceride interface (Figure 2-9 (a)), each DPPC monolayer was placed on either end of the triolein slab with water on the outer hydrophilic ends of the phospholipids. For bilayers, the DPPC monolayers were joined with their tails in contact with each other and water was placed on either end (Figure 2-9 (b)). Water was placed on the top and bottom of the simulation boxes to prevent interactions of dissimilar species across the box boundaries, as each simulation box was set up with periodic boundary conditions in all three Cartesian directions. Each system consisted of 200 coarse-grained DPPC molecules with 100 phospholipid molecules in each monolayer. For the water/triglyceride interface systems, 1000 coarse-grained triolein molecules, and 8000 coarse-grained water particles (i.e.: 32,000 real water molecules) were included.

2.4 Creating Coarse-Grained Topologies and Interaction Parameters for Small Molecules

Because the MARTINI force field was created and parameterized for biomacromolecules, very few topologies currently exist for small molecules such as the toxins of interest in our studies. Therefore, we implemented a center-of-mass approach to map MARTINI coarse-grained interactions sites onto chemical structures for the compounds of interest. This approach utilized the standard MARTINI particle definitions but was optimized to preserve the shapes and sizes of the small molecules. Our optimized approach often meant using less than a 4-to-1 mapping scheme, even for molecules without rings. In addition, different bond lengths and angles than those prescribed by the standard MARTINI scheme were used to ensure faithful coarse-grained representations of our small molecules. We were able to make the toxin molecules, even those with multiple rings, stable by methodically specifying bond and angle constraints from the underlying chemical structure of each molecule. We were also able to reproduce the octanol/water partitioning behavior for each toxin compound studied.

The procedure we employed to create coarse-grained representations of small molecules followed five main steps, which were repeated until a suitable configuration was obtained:

i) Map groups of atoms into coarse-grained interaction sites to preserve molecular structure.

ii) Determine coarse-grained coordinates, bonds, and angles from atomic structure.

iii) Based on the chemical moiety characteristics, determine which MARTINI particle types to use.

iv) Parameterize all the non-bonded interactions between coarse-grained sites.

v) Validate the coarse-grained representation of the molecule by calculating octanol/water partitioning through simulation.

2.4.1 **Structural Mapping**

To demonstrate how we mapped coarse-grained particles onto the chemical structure of small toxin molecules, let us first consider two of our toxins of interest: bupivacaine and acetaminophen (Figure 2-10). Bupivacaine is a local anesthetic drug associated with marked cardiotoxic effects in hypersensitive patients or if administered incorrectly [53, 55, 115-117]. Acetaminophen is a hepatotoxic pain and fever-reducing drug [118-120].

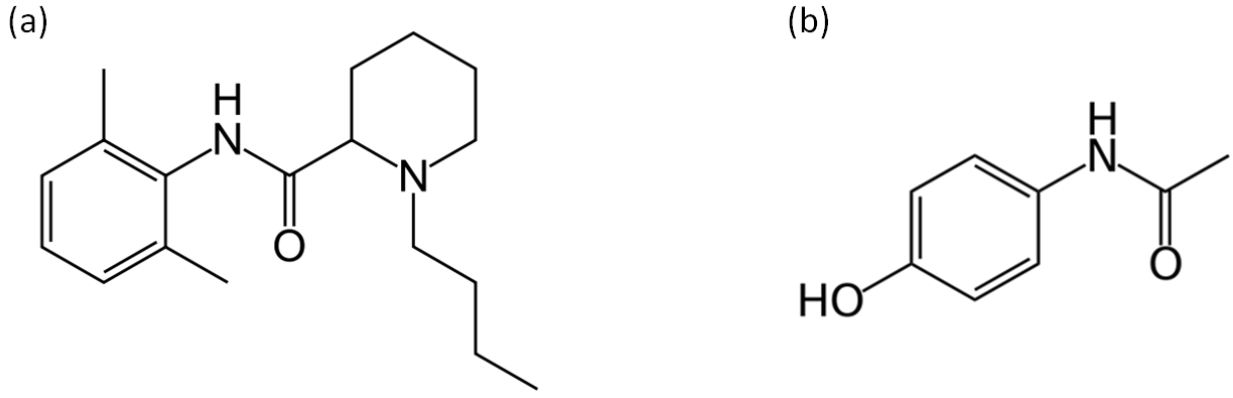

Figure 2-10: Chemical structures of neutral bupivacaine (a) and acetaminophen (b) molecules

There are multiple options for mapping coarse-grained particles to the structure of such molecules. As demonstrated in Figure 2-11, a first attempt at coarse graining the bupivacaine

molecule involves visual inspection to determine which atoms can be grouped together while maintaining the molecular structure.

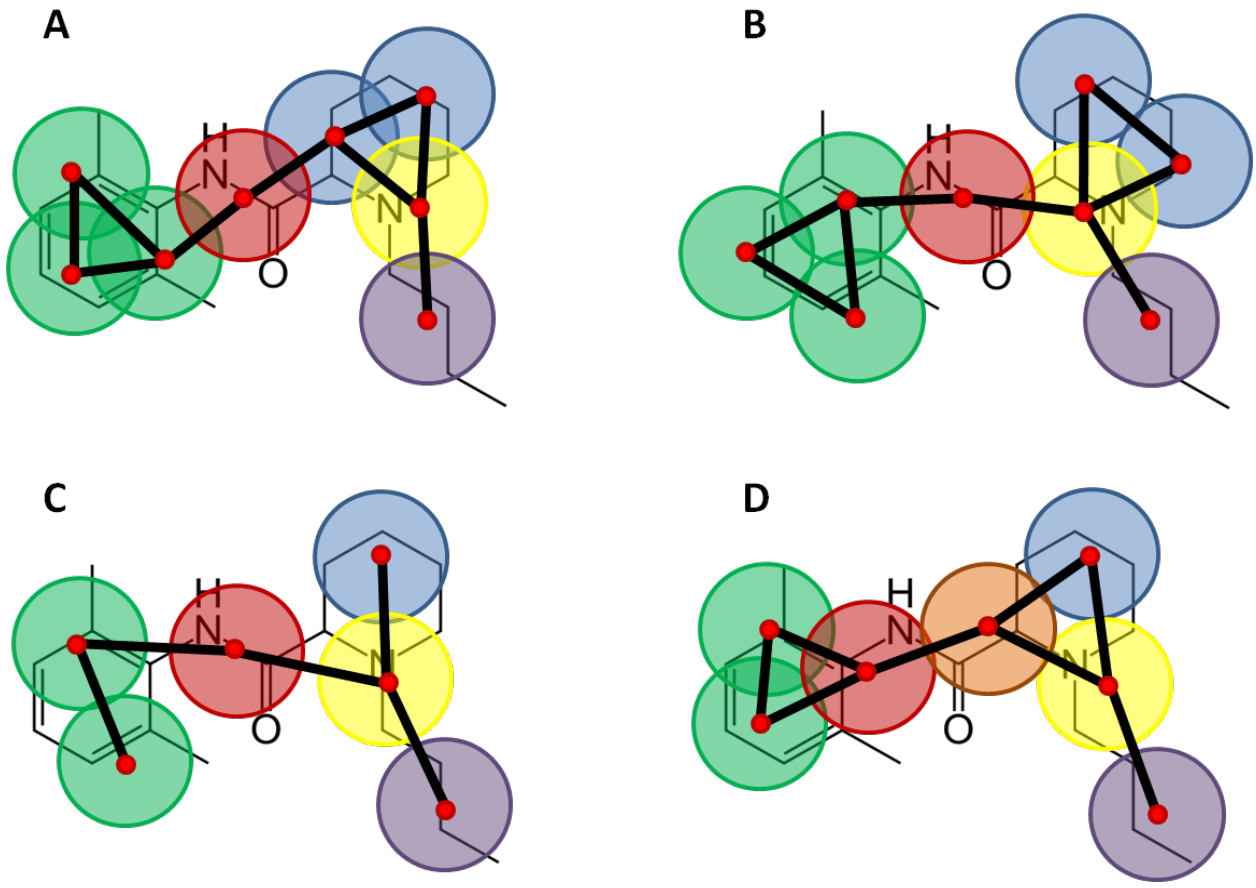

Figure 2-11: Multiple options for coarse-grained structural mapping of bupivacaine

This inspection results in a mapping that converts the molecule consisting of 49 atoms into coarse-grained representations made up of only 6 - 8 interaction sites. In the case of acetaminophen, the 20 atoms composing the molecule were mapped to 4 CG interaction sites

(Figure 2-12). The particular configuration chosen needed to be tuned by observing the molecule during simulation to determine if it is able to maintain a three-dimensional structure similar to that expected for a molecule of its shape and size.

2.4.2 **Center-of-Mass Coarse Graining and Parameterization of Bonded interactions**

After determining which atoms to map into each coarse-grained site, the next step was to calculate the particle positions, equilibrium bond lengths, bond angles, and possible dihedral angles. The atomistic three-dimensional structure of most molecules can be obtained from chemical structure databases. These provide information on atom positions in relation to each other, which we then used to calculate the coarse-grained particle coordinates as well as bond lengths and angle sizes through a center-of-mass approach.

For bupivacaine and acetaminophen in particular, this center-of-mass scheme used atom coordinates obtained from 3D structure-data files (SDF) from the PubChem Compound database. The unique chemical structure identifier for bupivacaine is CID 2474 [121] and that of acetaminophen is CID 1983 [122]. Using atom groupings as shown in Figure 2-11 for bupivacaine and Figure 2-12 for acetaminophen, the location of the center-of-mass of each group of atoms was determined from atomic positions weighted by atomic masses. Equation (2-8) was used to obtain the initial positions ($\mathbf{r}_{\mathrm{CG}}$) of coarse-grained sites for all our small toxin molecules from the center-of-mass of the constituent heavy atoms:

$$\mathbf{r}_{CG} = \frac{\sum_{i=1}^{n}(\mathrm{m}_i \mathbf{r}_i)}{\sum_{i=1}^{n} \mathrm{m}_i}$$

(2-8)

The number of heavy atoms mapped to each CG site is represented by n, with $\mathbf{r}_i$ being the coordinates of a heavy atom i, and m_i being its mass. A similar center-of-mass method was determined to be the most robust approach for coarse graining and obtaining bonds, angles, and dihedrals for proteins [100].

Equilibrium bond lengths are calculated from the initial coarse-grained positions using the length of the vector between two bonded CG sites. Finally, equilibrium bond angles are obtained using trigonometric ratios as the angle formed between two bond vectors. These equilibrium bond and angle values were used by the force field with Equations (2-5) and (2-6) to obtain weak harmonic bond and angle potentials that describe the bond stretching and chain stiffness interactions respectively. Due to the size of the small molecules and rings causing planarity, there was no need for dihedral angle calculations as long as all angles were well specified. By employing this center-of-mass coarse graining scheme for acetaminophen and bupivacaine molecules, reasonable coarse-grained positions, bonds and angles were obtained. For the four possible configurations attempted for bupivacaine illustrated in Figure 2-11, options (A) and (B) with 8 coarse-grained sites each produced coarse-grained particles that were too close together. Thus the short bond lengths produced large repulsive Van der Waals forces between particles, resulting in unstable simulations. The configuration shown in Figure 2-11 (C) attempted to space out the CG particles by increasing the number of atoms included in each site. This configuration did not explicitly represent the two rings of bupivacaine and was

subsequently rejected in favor of the model in Figure 2-11 (D) that faithfully represented the rings and contained only 7 CG sites. This configuration also predominantly utilized ring type (S) particles with parameters of reduced interaction strength. We found this configuration for bupivacaine to be the most stable during simulation.

2.4.3 **Selection of MARTINI Parameters**

Each small molecule needed to be parameterized based on the standard MARTINI [79] interaction types (described in Section 2.2.1) in order to utilize the force field. Table 2-3and Table 2-4 list the MARTINI interaction sites chosen to represent each of the building blocks for bupivacaine and acetaminophen. The respective masses calculated based on the atoms constituting each CG particle are also listed.

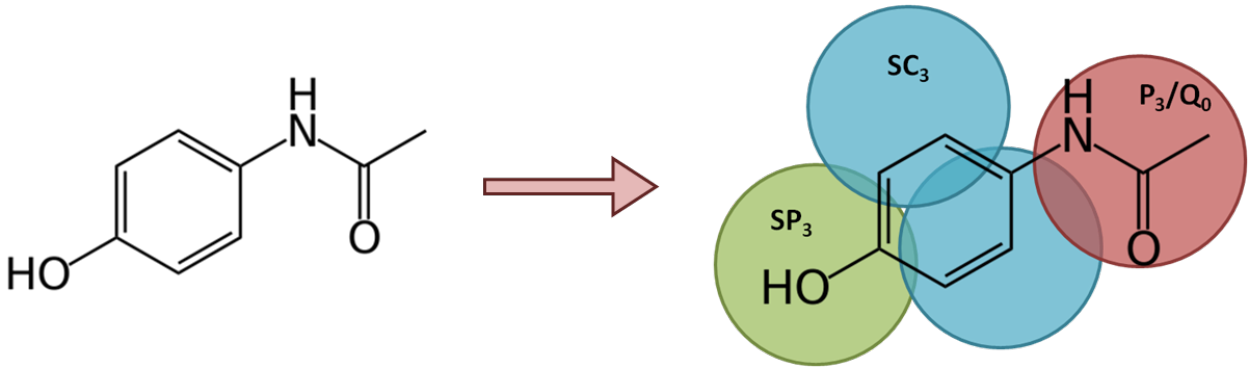

Figure 2-12: CG representation of acetaminophen with the selected MARTINI interaction types.

Although the neutral forms of bupivacaine and acetaminophen are illustrated in Figure 2-11 and Figure 2-12, both molecules can be found predominantly in the protonated state at physiological conditions. Therefore, we assigned particular CG particles the ability to exist in either neutral or charged states, as shown in Table 2-3and Table 2-4. For bupivacaine, the piperidine nitrogen group can be represented as either a neutral SP_2 group or a charged SQ_0 group. Similarly, for acetaminophen, the terminal acetamide group can be modeled as a P_3 polar group or a charged Q_0 site.

TABLE 2-3: BUPIVACAINE MAPPING TO MARTINI CG SITES

Chemical Building Block	**MARTINI Type**	**Particle Type**	**Color in Figure 2-11**D	**Mass (amu)**
2,6-Dimethylphenyl	SC_4/SC_5	Apolar Ring	Green	54/36
Carboxamide	SP_2/SP_3	Polar Ring	Red/Orange	72/54
Piperidine Methylene	SC_2	Apolar Ring	Blue	54
Piperidine Nitrogen	SP_2/SQ_0	Polar Ring/Charged	Yellow	54
Butyl	C_2	Apolar	Purple	54

TABLE 2-4: ACETAMINOPHEN MAPPING TO MARTINI CG SITES

Chemical Building Block	**MARTINI Type**	**Particle Type**	**Color in Figure 2-12**	**Mass (amu)**
R=COH	SP_3	Polar Ring	Green	36
-C=C-	SC_3	Apolar Ring	Blue	45/45
Acetamide	P_3/Q_0	Polar/Charged	Red	72

2.4.4 **Parameterization of Nonbonded Interactions**

The MARTINI force field defines Lennard-Jones parameters (ε and σ) to represent the van der Waals interactions between neutral, nonbonded particle pairs. These parameters are used with Equations (2-1), (2-2), and (2-3) to determine the strength and nature of the interactions between every pair of CG particles. Using the particle type definitions in the tables above, we determined the pairwise interaction coefficients for bupivacaine and acetaminophen (Table 2-5 and Table 2-6 respectively).

For ring-ring interactions, there is a 75% reduction in the ε-value, effectively reducing the strength of interaction between particles in rings and conferring greater stability on the molecule. The σ-value for ringed interactions is also reduced from 4.7 Å to 4.3 Å due to the closer packing of particles that small rings experience [79]. It is important to note that all the MARTINI force field parameters, topological files and particle definitions were created to be directly used with the Gromacs molecular dynamics package. Therefore, it is necessary to convert all the information into input that is meaningful to our molecular dynamics simulator of choice – LAMMPS (Large-Scale Atomic/Molecular Massively Parallel Simulator) [123].

These and several other coarse-grained toxin models we developed were validated by determining their simulated partitioning free energies between polar (water) and nonpolar (water-saturated octanol) solvents, and comparing these results to experimental values. Following validation, they were added to phospholipid layer models to study the nature of their interactions with these structures and consequently, the changes that each of these toxins induced on the layer structure and dynamics.

TABLE 2-5: LENNARD-JONES PAIRWISE COEFFICIENTS FOR CG NEUTRAL BUPIVACAINE

MARTINI Type		Interactions	ε (Kcal/mol)	σ (Å)
SC_4	SC_4	intermediate	0.627	4.3
SC_4	SC_5	intermediate	0.627	4.3
SC_4	SP_2	intermediate	0.627	4.3
SC_4	SP_3	almost intermediate	0.556	4.3
SC_4	SC_2	almost intermediate	0.556	4.3
SC_4	C_2	almost intermediate	0.741	4.7
SC_5	SC_5	intermediate	0.627	4.3
SC_5	SP_2	intermediate	0.627	4.3
SC_5	SP_3	intermediate	0.627	4.3
SC_5	SC_2	almost intermediate	0.556	4.3
SC_5	C_2	almost intermediate	0.741	4.7
SP_2	SP_2	almost attractive	0.807	4.3
SP_2	SP_3	almost attractive	0.807	4.3
SP_2	SC_2	semi repulsive	0.484	4.3
SP_2	C_2	semi repulsive	0.645	4.7
SP_3	SP_3	attractive	0.896	4.3
SP_3	SC_2	semi repulsive	0.484	4.3
SP_3	SP_2	almost attractive	0.807	4.3
SP_3	C_2	semi repulsive	0.645	4.7
SC_2	SC_2	intermediate	0.627	4.3
SC_2	SP_2	semi repulsive	0.484	4.3
SC_2	C_2	intermediate	0.837	4.7
C_2	C_2	intermediate	0.837	4.7

TABLE 2-6: LENNARD-JONES PAIRWISE COEFFICIENTS FOR CG NEUTRAL ACETAMINOPHEN

MARTINI Type		Interactions	ε (Kcal/mol)	σ (Å)
SP_3	SP_3	attractive	0.896	4.3
SP_3	SC_3	almost intermediate	0.556	4.3
SP_3	P_3	attractive	1.195	4.7
SC_3	SC_3	intermediate	0.627	4.3
SC_3	P_3	almost intermediate	0.741	4.7
P_3	P_3	attractive	1.195	4.7

2.4.5 **Model Validation Using Octanol/Water Partitioning**

The free energy change associated with partitioning from an aqueous to an organic environment is an important thermodynamic property of liquid and solid phase systems [124]. The basis of the MARTINI force field is reproduction of partitioning free energies of chemical building blocks between water and organic solvents. This free energy is obtained from the difference between the hydration (in water) and solvation (in organic solvent) free energies of a particular species.

$$\Delta G_{octanol/water} = \Delta G_{hydration} - \Delta G_{solvation}$$

(2-9)

The free energy can be obtained from direct partitioning of a species between a water and an octanol phase [79, 80]. At equilibrium, densities of drug molecules in each phase can be used to calculate a simulated partitioning free energy.

$$\Delta G_{octanol/water} = kT \ln\left(\frac{\rho_{octanol}}{\rho_{water}}\right)$$

(2-10)

The MARTINI force field initially parameterized numerous chemical species by reproducing their hydration free energies by direct partitioning of solute particles between phases. These values were later found to differ slightly from free energies obtained by calculation using a thermodynamic integration method [124] due to finite concentration

effects. Thermodynamic integration results represent an infinitely dilute system and are therefore more accurate.

We performed coarse-grained simulations to calculate the partitioning free energy of each of our small molecules between octanol and water using Gromacs software package (version 4.6.3) [125]. Gromacs was used to take advantage of the Bennett Acceptance Ratio (BAR) [126] implementation to perform free energy difference calculations. Each simulation consisted of an individual drug molecule in water or in water-saturated octanol. The interaction strength between the small molecule of interest and the solvent was coupled to a variable λ. This variable was slowly tuned from 1 (solvated, full interaction strength) to 0 (molecule in a vacuum, no interaction with solvent). The free energy of solvation or hydration of the small molecule was then calculated using the free energy perturbation method known as the Bennett Acceptance Ratio.

Specifically, two sets of simulations were performed consisting of 26 separate simulations each:

i. one to calculate the desolvation free energy (molecule going from octanol to vacuum, λ = 1 to 0);
ii. the other to calculate the hydration free energy (molecule going from vacuum to water, λ = 0 to 1).

To change from one state to another, λ was slowly incremented or decreased by taking several discrete steps. The free energy difference between states at successive values of λ could be calculated directly because the difference between the states was relatively small [126]. A soft-

core Lennard-Jones potential (Equation (2-11)) was used for nonbonded interactions to ensure there was no overlap between particles at small λ values.

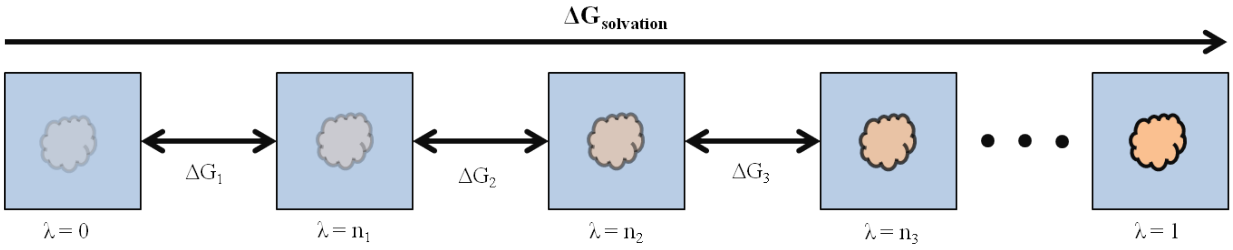

Figure 2-13: λ parameter tuning of interaction strength between solute and solvent

In Gromacs, using the genbox tool, each small molecule was solvated in a periodic box with 2000 CG water particles or 911 CG octanol molecules (saturated with 88 CG water particles). The system was then subjected to energy minimization using a steepest-descent algorithm for 10,000 steps or until forces reached 10 kJ/mol/nm with a timestep of 0.01 ps (for a total of 100 ps). Van der Waals Lennard-Jones interactions were shifted from 0.9 nm to a 1.2 nm cutoff. Electrostatics interactions were calculated using a shifted (0.0 nm to 1.2 nm) Coulombic potential. The system was then equilibrated by integrating Newton's equations of motion using a leapfrog algorithm with a timestep of 0.005 ps (simulation time of 5 ns). An isothermal-isobaric (NPT constant) ensemble was used with isotropic pressure and temperature maintained at 1 bar and 298.15 K respectively using Berendsen coupling protocols [127]. The whole system was coupled together for temperature and pressure because of its relatively

small size. The parameter λ was coupled to the small molecule interactions (0 meant the molecule was decoupled; 1 meant the molecule interactions were fully coupled).

After equilibration, several simulations at 26 different λ values between 0 and 1 were run using a leapfrog stochastic dynamics integrator for 50,000 steps with timestep of 0.02 ps (simulation time of 1 ns) each. Soft-core parameters prevented overlapping of particles when λ went to 0 (or as the molecule was decoupled):

$$V_{sc}(\mathbf{r}) = (1-\lambda)V^A(r_A) + \lambda V^B(r_B)$$

(2-11)

$$r_A = (\alpha\sigma_A^6\lambda^2 + r^6)^{\frac{1}{6}}$$

(2-12)

$$r_B = (\alpha\sigma_B^6(1-\lambda)^2 + r^6)^{\frac{1}{6}}$$

(2-13)

V^A and V^B represent the normal van der Waals potentials when λ = 0 (state A) and 1 (state B), respectively. The soft-core parameter α = 1.3 and the distance of closest approach σ = 0.47 nm.

The Gromacs BAR tool (g_bar) was then used to combine the individual energy differences obtained from each λ simulation into a free energy difference, which is the free energy of solvation/hydration for the solute of interest. The derivative of the free energy as a function of λ, $\left(\frac{\partial G}{\partial \lambda}\right)$ was integrated using a trapezoid method. Specific octanol/water

partitioning values for each toxin molecule are presented in subsequent chapters and compared to experimental or computed literature values.

2.5 **Molecular Dynamics Simulations of Phospholipid layers**

Once the coarse-grained small molecule model was validated, we performed molecular dynamics simulations based on integrating Newton's equations of motion using the classical molecular dynamics code LAMMPS (Large-Scale Atomic/Molecular Massively Parallel Simulator) (http://lammps.sandia.gov.; version: 5 Sep. 2014) [123], distributed by Sandia National Laboratories. In general, two types of simulation were performed in our studies (which will be described in more detail in subsequent chapters): equilibrium and/or steered molecular dynamics. The starting configuration for each simulation system was generated using the packing optimization program Packmol [128]. All simulations were performed at 323 K, which is above the main phase transition temperature of DPPC. Periodic boundary conditions were used in all three Cartesian directions.

Van der Waals interactions between neutral, nonbonded particle pairs were described using a shifted Lennard-Jones 12-6 potential energy function. Between covalently bonded CG sites, a weak harmonic potential was used to describe the bond stretching interactions and a weak harmonic cosine potential was used to represent chain stiffness for the angles between three consecutive bonded particles. Non-bonded interactions were cut off at 1.2 nm and the Lennard-Jones potential was shifted from 0.9 nm to the cutoff. The electrostatic potential was shifted from 0.0 nm to the cutoff distance of 1.2 nm. Long-range electrostatic interactions were neglected since pairwise interactions beyond 1.2 nm were not considered.

A velocity Verlet [129] method was used to integrate the equations of motion [130-132] which generated particle positions and velocities. An isothermal-isobaric (NPT) ensemble was maintained which allowed the volume (and hence the cross sectional area) of the phospholipid layer systems to fluctuate freely. Semi-isotropic pressure coupling was used to maintain tensionless layers. Every 10 time steps, a center-of-mass velocity was removed before calculating the temperature of each component to prevent the systems from freezing and translating through space as an artifact of the accumulation of round-off errors by the numerical integration method [133]. Graphics were rendered using the Visual Molecular Dynamics (VMD) program, a molecular visualization tool developed by the Theoretical and Computational Biophysics Group at the University of Illinois at Urbana-Champaign [134]. Specific details pertaining to each phospholipid layer system studied and the consequences of the presence of toxin molecules on the layers are provided in the subsequent chapters.

2.5.1 **Minimization and Equilibration**

For each simulation, an energy minimization and equilibration phase was necessary to relax the initial preassembled configuration before commencing the simulation. The energy minimization is used to remove any bad contacts caused by particles overlapping and is performed using an iterative conjugate gradient algorithm. The gradient of the force at every step is combined with the step taken beforehand in order to find a direction perpendicular to the previous one in which to search next. The system needed to be in a local potential energy minimum once the stopping criterion was satisfied.

Following energy minimization, each system is run through an equilibration period (typically for at least 200 ns). Temperature and pressure were held constant at 323 K (50 °C) and 1 atm, respectively, using an isothermal-isobaric (NPT) ensemble. This allowed the volume (and hence the cross sectional area) of the system to fluctuate freely and to self-adjust to an equilibrium value. For the equilibration phase of all simulations, each component of the system was coupled separately to a temperature bath using a Berendsen thermostat [127] with a coupling constant of 1 ps. A separate isotropic Berendsen barostat was applied to each component to maintain the system pressure at 1 atm with a coupling constant of 1 ps. Berendsen coupling protocols are used for equilibration due to their efficiency in relaxing the system to the target temperature and pressure values. Fully equilibrated phospholipid monolayer and bilayer systems can be seen in Figure 2-9. Thermodynamic properties such as temperature, pressure, volume, and energy reached equilibrium values long before the end of the equilibration period. Following equilibration, a production run was performed for every simulation system using either equilibrium or steered molecular dynamics techniques.

2.5.2 **Obtaining Phospholipid Layer Properties from Simulations**

Structural, dynamical and thermodynamic properties of phospholipid layers can be extracted from coarse-grained molecular dynamics simulations. Especially in the case of pristine interfaces that do not contain toxin molecules, these properties can be directly compared to experimental data as well as results from atomistic simulations, thus verifying the capacity of the MARTINI coarse-grained force field to accurately reproduce the properties of phospholipid interfaces. Once the simulation system for the phospholipid layer has been verified, changes to

the properties caused by the addition of toxin molecules can be determined. (Some representative properties are discussed below.) These changes in properties reveal the ways in which toxin molecules specifically affect the integrity of phospholipid interfaces. They provide clues as to the molecular mechanism of action of toxins in disrupting normal functions of membranes as well as information on the ability of phospholipid interfaces to sequester and control the crossing of small molecules.

2.5.2.1 **Area per Lipid**

The validity of a computational representation of a phospholipid layer can first be tested by the average area per lipid at constant temperature and pressure. If this structural parameter is stable, the system has reached equilibrium and other properties can be measured as well[58, 90, 91, 135]. Area per lipid is also used to determine if the simulated phospholipid layer is in the correct physical phase at a particular temperature and pressure. The geometric area per lipid value is calculated as the product of average box lengths in the plane of the phospholipid layer divided by the number of phospholipids in each layer.

After equilibration of DPPC bilayers and monolayers, we obtained area per lipid values of 58.6 Å and 61.5 Å respectively. These values are consistent with atomistic bilayer simulation values of 61.0 – 66.0 Å and experimental values of 57.0 – 71.7 Å [136-138]. Attractive van der Waals forces are known to control area per lipid in saturated phosphatidylcholine layers [139]. Therefore, toxin molecules interacting with a phospholipid like DPPC would need to overcome an energy barrier to disrupt this attractive force. An increase in area would indicate that toxin molecules have inserted themselves between phospholipid molecules resulting in disruption in

the structure of the layer [140]. A large increase in area per lipid in the presence of a toxin molecule c ould indicate a pronounced thinning of the phospholipid interface, which ultimately may lead to irreversible membrane collapse.

2.5.2.2 **Mass/Electron Density Profile**

Mass or electron density profiles can be obtained from simulations by binning the simulation box in the direction normal to the phospholipid surface and averaging the total mass or electrons in each bin over the duration of the simulation. These values are obtained by using information about the mass of or number of electrons contained within each coarse-grained interaction site. The mass density of water obtained from our simulations was approximately 980 kg/m^3, which was consistent with the literature water density value of 988 kg/m^3 at 50°C [141]. We found that the density profiles of the particles representing the choline and phosphate groups of DPPC molecules overlapped. This indicated that the phospholipid polar head groups were oriented mostly parallel to the plane of the monolayers or bilayers and perpendicular to the direction of the normal to these layers, resulting in a P-N angle of approximately 90° relative to the interface normal. These results are in good agreement with atomistic simulation studies of monolayers and bilayers [91, 142].

For simulations of monolayers at the aqueous/triglyceride interface (further described in Chapter 4), ordering appeared in the triglyceride (TG) phase density profiles near the interface for small systems due to interactions between the fatty acid tails of triolein and DPPC molecules. This resulted in increased densities of the triolein tails around 5.5 nm and 10.5 nm

near the phospholipid tails and increased densities of triolein polar glycerol backbones around 6 nm and 10 nm in Figure 2-14 (trimodal TG Tail and bimodal TG Head profiles respectively).

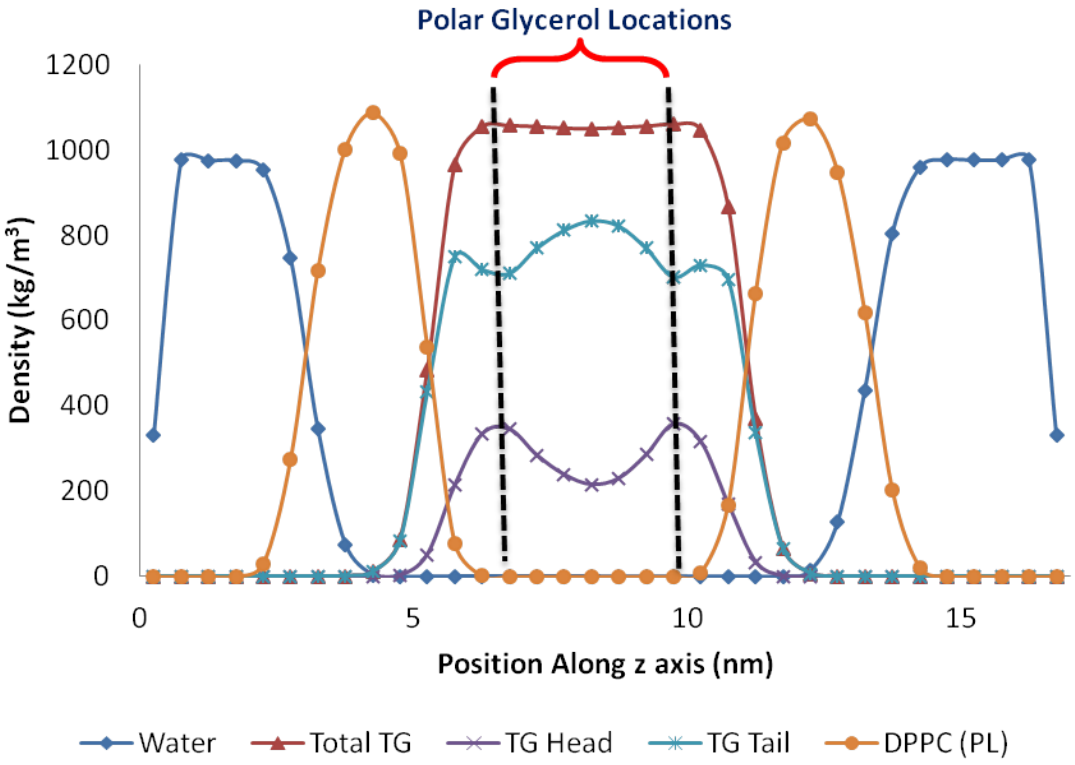

Figure 2-14: Mass density profile highlighting triglyceride (TG) orientation detail

The ordering caused the small triolein phase to have an increased density of 1050 kgm^{-3} at 50°C, whereas its experimental density at 40°C is reported to be 899 kgm^{-3} [141, 143]. The triglyceride ordering close to phospholipid monolayers that we observed is consistent with an atomistic aqueous/lipid simulation by Henneré et al. [90] in which they observed an increase in

the density of their oil layer due to the ordered arrangement of the triglycerides at the phospholipid interface. This is most likely a finite system size effect because our initial model represents only a small section of the interfacial region of an oil droplet. Droplets of this type in physiological conditions tend to have diameters of approximately 200 – 500 nm, whereas our simulation box was only 16 nm in this specific case. Therefore, in our simulations of aqueous/triglyceride systems that will be presented in Chapter 4, we have used a larger triolein section. Our simulations indicate that the ordering of triolein disappears farther away from the phospholipid interface. Running simulation of these larger systems is much more tractable due to the coarse graining technique employed.

Electron density profiles can be compared directly with those obtained from small-angle x-ray and neutron diffraction experiments [144-147]. Our results can therefore be used as predictions with which new x-ray and neutron diffraction experiments may be compared, especially for the cases of phospholipid layers affected by toxin molecules.

2.5.2.3 **Phospholipid Hydration**

To quantify the hydration of phospholipid molecules, a radial distribution function, $g(r)$, is computed between each phospholipid interaction site and water. This function is a time-averaged representation of the change in water density with radial distance from the particular site in question (i.e. choline, phosphate, glycerol backbone, tail). The radial distribution function is defined as:

$$g(r) = \frac{N(r)}{4\pi r^2 \rho dr}$$

(2-14)

where $N(r)$ represents the number of particles in a spherical shell of thickness dr at a distance r from a reference particle (Figure 2-15). The number density, ρ, is the ratio of the number of particles to the total volume. This function is plotted against distance from the reference site (Figure 2-16). The heights and widths of the peaks indicate that the phospholipid head group particles (choline - blue and phosphate - red) are much more hydrated than the backbone - green or tail groups - purple. This is evident from coarse-grained simulations although specific interactions pertaining to hydration that are usually calculated in atomistic studies cannot be determined in a CG system. Such atomic scale interactions include hydrogen bonding across oxygen atoms in water and oxygen atoms in the DPPC phosphate group. The coarse-grained scheme cannot access the length of hydrogen bonds (1.5 – 2.5 Å) [148] because of the relatively large Lennard-Jones σ parameter (4.7 Å) that limits how close any two interaction sites can get to one another.

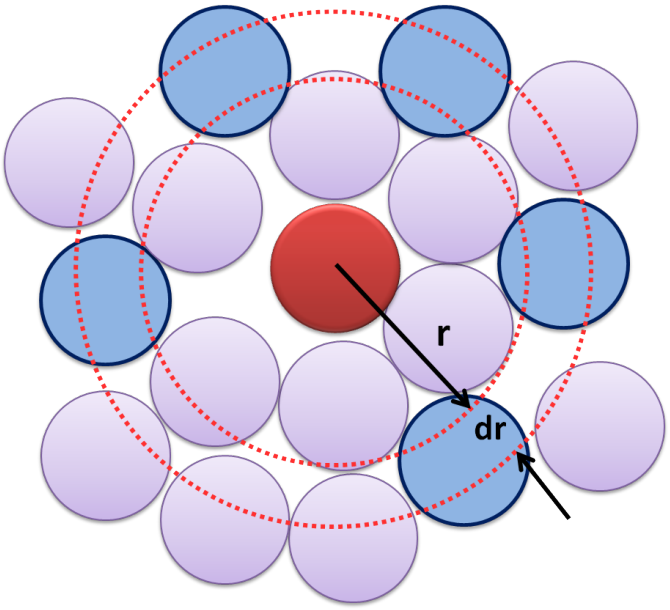

Figure 2-15: Schematic of radial distribution of blue sites around central red site within cutoff distance

By integrating the first maximum peaks located at approximately 0.5 nm for the choline and phosphate groups in Figure 2-16, a number of 5.3 and 4.1 coarse-grained water particles were calculated to be located around each choline and phosphate group respectively. This is equivalent to 21.2 and 16.4 real water molecules respectively. Much fewer water molecules were located near the glycerol backbone and even fewer near the tails. The hydration of the phosphate and choline groups was similar and can be attributed to the fact that the two groups were oriented parallel to the interface, allowing them both direct access to the water phase.

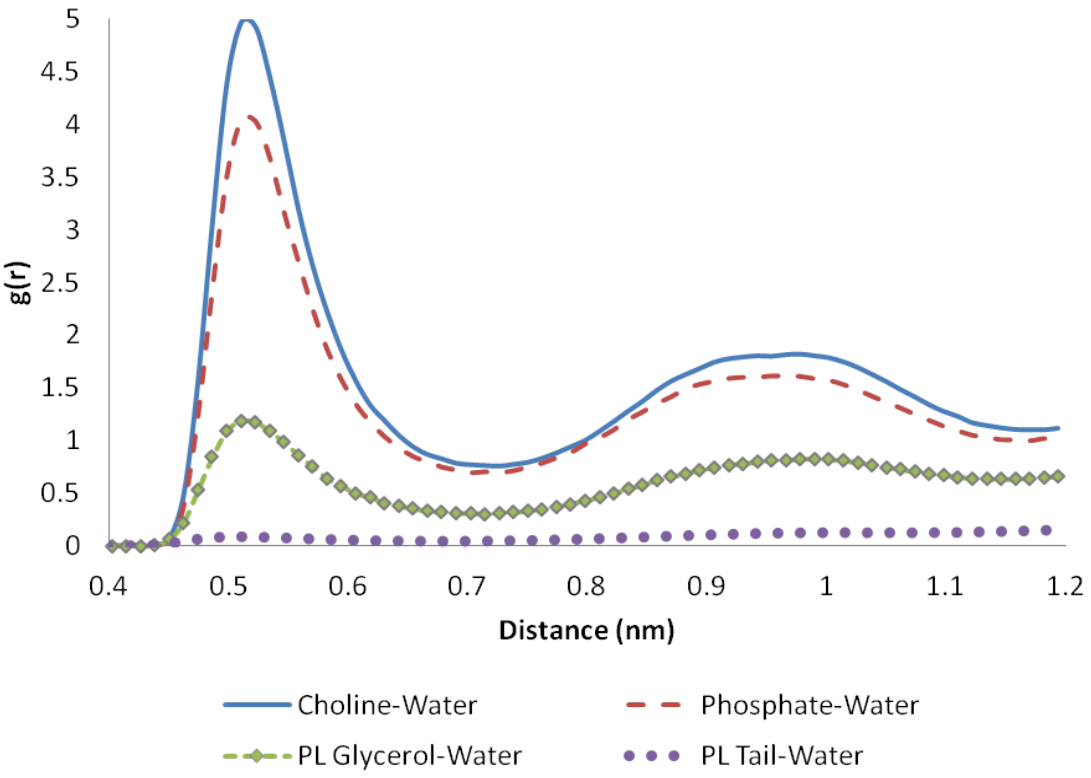

Figure 2-16: Radial distribution functions of water around phospholipid groups in a DPPC monolayer

An atomistic DPPC bilayer study by Pandey and Roy [149] found somewhat similar results for the radial distribution of water oxygen atoms around the nitrogen of the choline group. They observed that the clustering of oxygen atoms around the DPPC molecules resulted in a first hydration shell located at approximately 0.5 nm from the nitrogen atom, the same value we got in our coarse-grained study. From integration of this peak they obtained an average value of 13.64 water molecules clustered in the first hydration shell of the nitrogen atom. This value is smaller than the value of 21.2 we obtained from our coarse-grained simulations. For the phosphorus group in the Pandey study that corresponds roughly to our

phosphate coarse-grained site, they found the first radial distribution peak at approximately 0.4 nm; lower than that observed in our study. This discrepancy arises from the closest distance of approach of two coarse-grained particles being always greater than 0.4 nm in our work. Pandey and Roy also calculated that only 3.27 water molecules were clustered in the first hydration shell around phosphorus, whereas in the CG system, we calculated a value of 16.4 water molecules. A possible explanation for this apparent discrepancy is that in the atomistic scheme, the nitrogen and phosphorus atoms are surrounded by several other moieties (methyl and oxygen), which may cause steric hindrance and prevent water molecules from getting closer to these atoms. In the coarse-grained scheme, such interactions may be minimal. Changes in phospholipid hydration in the presence of small molecules can indicate one of the ways in which toxins can disrupt lipid membranes by causing large amounts of water to enter the hydrophobic region.

2.5.2.4 **Order Parameter**

Phospholipid layers are dynamic two-dimensional fluids. The lipid molecules have the ability to diffuse within the layer and even flip-flop into opposing layers, in the case of bilayers. This dynamic environment allows the phospholipid tails to assume varied orientations during simulations. The bond order parameters of the tail are a measure of this disorder in orientation. The order parameter has been measured experimentally for phospholipids from the orientation of carbon-deuterium bonds in the tails using ^{2}H NMR techniques [150]. The ensemble and time-averaged angle between the carbon-carbon bonds in the tail and the layer normal was used to

calculate the order parameter from atomistic simulations [28] for comparison with values obtained from NMR experiments.

For coarse-grained particles, although there are no explicit carbon atoms, a similar approach can be taken, where vectors between coarse-grained particles have angles relative to the layer normal [80]. Using Equation (2-15) to compute order parameters for consecutive particles in the phospholipid tail yields values that are averages over those found for consecutive carbon-carbon bonds in atomistic simulations.

$$P_2 = \frac{1}{2}\langle 3\cos^2\theta - 1\rangle$$

(2-15)

The angle between coarse-grained tail bonds and the normal is represented by θ. A P_2 value of 1 indicates perfect alignment and -0.5 corresponds to complete anti-alignment. Random orientations of the tail bonds correspond to a P_2 value of 0.

Phospholipid tail order parameters show a broad plateau at the beginning of the tails near the glycerol backbone because the tails are tethered and more aligned in that region. The order decreases towards the ends because the end sections are not tethered and move around more freely [91]. The presence of a foreign group such as a toxin intercalating in the tail region can induce more ordering of these bonds by reducing the free volume available for phospholipid tails, if the area per lipid remains unchanged and thickness increases [91]. Conversely, the presence of a foreign group in the tail region may induce disordering of these

bonds by increasing the overall area per lipid [90]. Changes in phospholipid order parameters can suggest ways in which toxin molecules may disrupt lipid interfaces.

2.5.2.5 **Lateral Pressure Distribution**

The lateral pressure profile is a distribution of the inhomogeneous pressure across a bilayer in the direction normal to the interface. The components of pressure resulting from repulsive interactions between the phospholipid molecules appear as positive contributions, whereas the cohesive tensions that tend to exclude water from the hydrophobic parts of the phospholipid emerge as negative values in the pressure profile. Changes in the lateral pressure profile serve as indicators of structural changes within the bilayer [151, 152]. In a simulated tensionless lipid bilayer, the net repulsive and cohesive pressure components cancel each other out. Therefore, decreases in repulsive interactions at certain locations along the bilayer normal caused by penetrating foreign species will lead to decreases in cohesion in other parts of the bilayer and vice versa.

2.5.3 **Obtaining Small Molecule Properties at Phospholipid Interfaces**

While it is important to understand changes to the properties of phospholipid layers in the presence of small toxin molecules, it is also informative to study the orientation, conformation, distribution, and preferred location of these small molecules along the various component functional groups of the lipid molecule.

In a manner similar to that described in Section 2.5.2.2, density profiles can be obtained, indicating the average distribution and preferred locations of small molecules in a simulation.

These profiles also provide insight into the average orientations assumed by small molecules with respect to phospholipid layers when the densities of individual particles or groups of particles that constitute these molecules are plotted separately. Orientation can be probed further by defining vectors between particles or groups of particles. Using trigonometric ratios, the angles between these vectors and some reference vector of interest (such as the normal to the interface) can be determined.

Radial distribution functions (discussed in Section 2.5.2.3) can be used to determine the probability of finding a particular group or molecule at a distance r from another group or molecule. This is useful for identifying aggregation of like or unlike groups and quantifies average distance of closest approach between any two groups. The orientation and location of a small molecule inside a phospholipid layer will depend on the chemical moieties that constitute the small molecule in question. Changes in conformation of the small molecule can also be informative to its molecular mechanism of action. These properties can be observed through simulation snapshots and quantified using some of the methods described above.

2.5.4 **Obtaining Free Energy Profiles from Steered Molecular Dynamics Simulations**

Free energy profiles are obtained from steered molecular dynamics simulations. These profiles represent the thermodynamic barriers to transport across a phospholipid layer, as well as energetically favored locations in the layer. It has been shown through experimental evidence that retention of small molecules in bilayers depends on molecular size [153]. A linear relationship between the size of extraneous molecules (in terms of chain length) and their free energy of partitioning into lipid membranes has been observed. Larger molecules partitioned

more readily into lipid membranes. Therefore, free energy profiles can provide important insight into the thermodynamic driving force associated with small molecule interactions with phospholipid layers.

Our steered MD simulations start with the center-of-mass of a target molecule tethered to a moving point. As the tether point is moved at a constant velocity from the water phase into the phospholipid layer, the total restoring force exerted by the spring to keep the toxin molecule tethered is recorded. The molecule is, however, allowed to move freely in the xy-plane.

According to the isobaric-isothermal Jarzynski equality (Equation (2-16)), for a system coupled to a constant temperature and pressure bath that is going through a nonequilibrium transition between two equilibrium states, the change in Gibbs free energy (ΔG) between the two states is directly related to the work done (W) on the system as the transition occurs [154-156]:

$$\langle e^{-W/k_BT} \rangle = e^{-\Delta G/k_BT} \quad \textbf{(2-16)}$$

The exponential average $\langle e^{-W/k_BT} \rangle$ can be difficult to estimate, therefore a cumulant expansion has been proposed [155, 156]. For a very slow transition and if the process is reversible (when a small pulling velocity is used), one can neglect all but the first term of the cumulant expansion to obtain an estimate of the Gibbs free energy change:

$$\langle W \rangle = \Delta G$$

(2-17)

A running integral of the restoring force over the distance covered by the solute molecule yields the potential of mean force (PMF) [157-159] for transit from the aqueous phase into the phospholipid layer. This is then equivalent to the work done by the solute molecule during permeation. In the limiting case of a large spring constant (stiff spring approximation), the potential of mean force has been shown to be approximately equal to the change in free energy [155]. The absolute height of free energy barriers obtained from coarse-grained molecular dynamics simulations are known to be typically higher than those from atomistic simulations [79]. But the existence and location of such barriers are nonetheless informative in understanding the absorption, transport, or partitioning of a foreign molecule into a phospholipid layer.

3. HYDROXYCOUMARIN TRANSPORT INDICATES A BIOPHYSICAL MECHANISM FOR DIFFERENTIAL TOXICITY

3.1 Introduction

Agents of opportunity are commercially available chemicals that have the potential to be weaponized [32]. One such chemical threat is the anticoagulant rodenticide brodifacoum. Following oral or transdermal exposure, this compound interferes with blood clotting which leads to potentially fatal hemorrhaging [33, 34, 36-38, 160, 161]. Brodifacoum inhibits coagulation by indirectly depleting the active form of vitamin K, a cofactor necessary for synthesis of clotting proteins [33-37, 160, 162-167]. Thus, bleeding caused by brodifacoum exposure can be treated by supplementing vitamin K. However, study of warfarin, the clot preventing therapeutic from which brodifacoum is derived, indicates a potential for anticoagulant-induced cytotoxicity [168-171] – a pathological event that is not addressed by vitamin K therapy. While warfarin can yield acute tissue damage, conservative dosing and a limited physiological half-life restrict the clinical relevance of this mode of toxicity. In contrast, brodifacoum can remain sequestered in organs for up to a year [33-38], and malicious or accidental release could lead to large exposures. Like many agents of opportunity, the mechanisms of toxicity and acute and chronic consequences of brodifacoum exposure are not well understood. Appreciation of these mechanisms will be necessary in order to design strategies for the treatment of exposure to this chemical threat and the development of defenses against it.

In this chapter, we employ molecular dynamics (MD) simulations to explore a potential membrane-mediated mechanism for anticoagulant cytotoxicity in general and the heightened

toxicity of brodifacoum in particular. Vitamin K epoxide reductase, the enzymatic target for both warfarin and brodifacoum, is responsible for post-translational modification of a number of clotting proteins [172-174]. As the enzyme is an integral membrane protein that resides at the endoplasmic reticulum, the anticoagulants must cross the plasma membrane to reach this intracellular site of action. The size and lipophilicity of these anticoagulant species suggests transmembrane flux by passive permeation is possible [175-177]. During their transit, we posit that the class of anticoagulants to which both brodifacoum and warfarin belong (i.e., hydroxycoumarins) may disrupt membrane barrier function by accumulation within – and transit through – the lipid bilayer. The molecular simulations described herein reveal the detailed mechanisms by which warfarin and brodifacoum disrupt a lipid membrane and, hence, the molecular phenomena that may underlie their differential cytotoxicity. The simulations reveal differences in mode of entry, molecular orientation and retention within the bilayer, as well as consequent changes in structure of the model membrane. Bilayer thinning and permeabilization due to incorporation of these extraneous species permits water permeation. This, if accompanied by uncontrolled flux of ions and other small molecules, would indicate a dysregulation of the delicate homeostatic balance necessary to maintain cell health. Further, we identify a potential for brodifacoum-driven flip-flop of membrane phospholipids.

3.2 **Bolaamphiphilic Effects on Phospholipid Bilayers**

Brodifacoum is an amphiphilic molecule with polar groups on two ends separated by a lipophilic central region. Bolaform amphiphilic molecules (bolaamphiphiles) are molecules composed of two polar moieties separated by a lipophilic spacer, in contrast to traditional

amphiphilic molecules which have only one polar section connected to a lipophilic one. Like traditional amphiphiles, however, bolaamphiphiles are surface-active agents and form nanostructures in aqueous solution such as micelles, ribbons, and fibers [178-180]. In nature, they occur as a major constituent of the cell membranes of archaebacteria, affording these organisms properties that enable them to survive in extreme conditions such as high temperatures and low pH. These properties include superior stability of cell membranes composed mostly of bolaamphiphiles [181].

Due to their membrane stabilizing and self-aggregation properties, bolaamphiphiles have been studied extensively in order to create nanostructures for applications such as targeted drug delivery [178]. Their polar head groups can be functionalized to interact directly with specific biomolecules like nucleic acids and phospholipids. Also, by tuning the groups making up the lipophilic spacer, bolaamphiphiles can be made more or less membrane stabilizing [182, 183]. The overall length of bolaamphiphile molecules is an important parameter as well. Membrane-spanning molecules in which the lipophilic spacer length matches the thickness of the aliphatic tail region of phospholipid bilayers have been found to be particularly membrane stabilizing. This stabilizing effect changes based on the composition of the lipophilic spacer, with e.g. rigid aromatic rings lending more stability to the membrane than unbranched saturated aliphatic chains [179, 183]. Rates of lipid flip-flop have been observed to increase in the presence of membrane-spanning bolaamphiphiles, but tend to decrease as the stiffness of the aliphatic linker is increased [181, 183]. The conformation adopted by bolaamphiphiles in phospholipid membranes is also important. Molecules with lipophilic spacers made up of flexible moieties are able to adopt U-shaped or hairpin conformations in lipid bilayers [182,

183]. The incidence of this folded conformation as opposed to the membrane spanning one depends on both the flexibility of the lipophilic linker as well as the bolaamphiphile concentration.

Since most applications focus on the membrane stabilizing properties and nanostructure formation of bolaamphiphiles, few studies have probed the properties of bolaamphiphiles with lipophilic linkers that are shorter than the hydrophobic thickness of phospholipid membranes. Even fewer studies focus on these shorter bolaamphiphiles, which have asymmetric polar head groups. One study suggests that bolaamphiphiles that are shorter than the bilayer thickness have a destabilizing effect and consequently cause phase separation between monopolar lipids and bolaamphiphiles [182]. This destabilization is due to the hydrophobic mismatch between the thickness of the aliphatic tail region of the bilayer and the shorter lipophilic spacer of the bolaamphiphiles.

Our molecule of interest, brodifacoum, is similar in structure to an asymmetrical bolaamphiphile due to the polar hydroxycoumarin moiety on one end and the induced heightened polar nature of the bromine group on the other end of the molecule, separated by several aromatic groups. Although brodifacoum has a bolaamphiphilic structure, its length is on the order of that of a phospholipid; therefore it cannot span the membrane. Due to this mismatch in length of the hydrophobic region of brodifacoum and phospholipid bilayers, we observe that brodifacoum adopts dynamically varying configurations in the bilayer, and hence has a destabilizing effect.

3.3 Creating a Model System

3.3.1 Molecular Dynamics Simulations

Coarse-grained molecular dynamics simulations of dipalmitoylphosphatidylcholine (DPPC) bilayers in water were employed to study the consequences of warfarin and brodifacoum incorporation in model phospholipid membranes. Details of the software used for equilibrium and steered MD simulations are provided in Section 2.5.

3.3.2 Molecule Topologies

The MARTINI coarse-graining approach and force field [79, 80] were employed to create molecule topologies for systems incorporating warfarin, brodifacoum and a DPPC bilayer fully solvated in water. The MARTINI approach creates coarse-grained representations of each molecule by replacing the constituent atoms with interaction sites consisting of 2-4 heavy atoms. These sites, and their non-bonded interaction properties, are chosen so as to preserve the underlying geometric structure and physicochemical properties of the molecule. The structure of DPPC was taken from an existing topology (http://md.chem.rug.nl/cgmartini/), as was the coarse-grained representation for water. Our coarse-grained representations of the hydroxycoumarin molecules were created by grouping atoms into interaction sites located at the corresponding centers of mass. Warfarin (23 heavy atoms) and brodifacoum (35 heavy atoms) were represented by 8 and 14 coarse-grained particles respectively (Figure 3-1). Standard MARTINI interaction types were then assigned to each coarse-grained particle and equilibrium bond lengths and angles were determined based on particle connectivity.

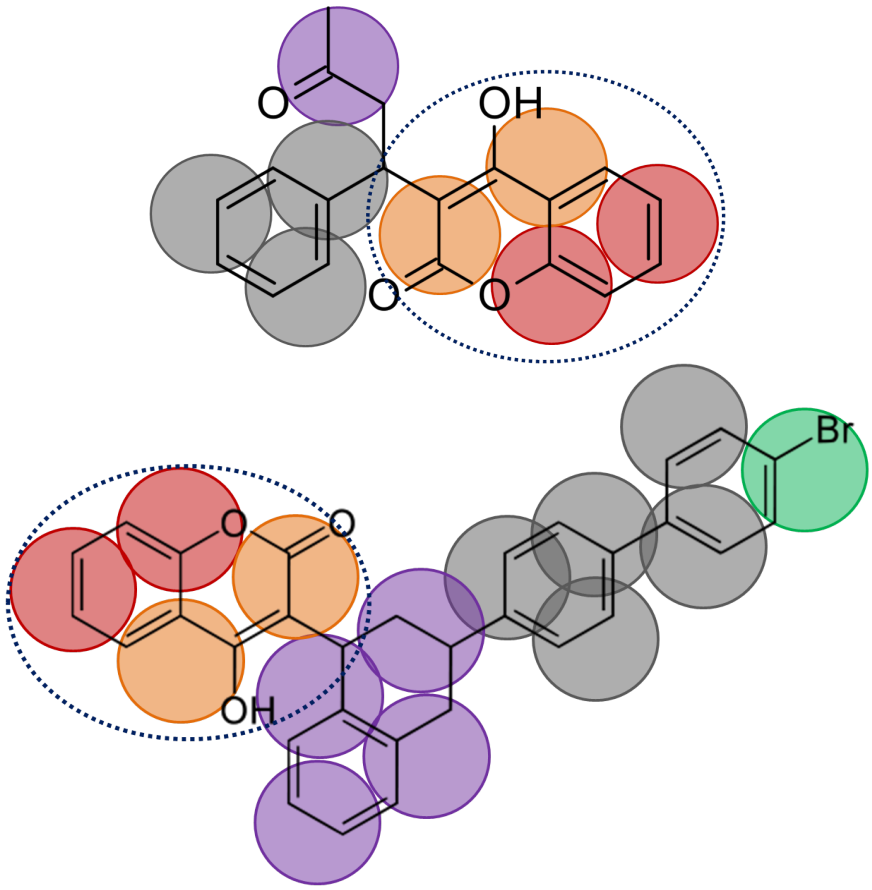

Figure 3-1: Two-dimensional structure of warfarin (top) and brodifacoum (bottom) overlaid with the coarse-grained representation of each molecule.
The hydroxycoumarin ring moiety common to both molecules is colored in red/orange and circled (a negative charge is distributed between the orange particles for deprotonated species). In the case of warfarin, the phenyl ring is colored grey and the carbonyl group is purple. For brodifacoum, the tetralin ring is colored purple, the biphenyl group grey and the brominated moiety is green. This color scheme is used in all subsequent images of the two molecules, except when indicated otherwise.

Van der Waals interactions between neutral, non-bonded particle pairs were described using a shifted Lennard-Jones 12-6 potential energy function. Non-bonded interactions were cut off at 1.2 nm and the Lennard-Jones potential was shifted from 0.9 nm to the cutoff. For charged non-bonded interactions, the Coulombic electrostatic potential was shifted from

0.0 nm to the cutoff distance of 1.2 nm. Hence, long-range electrostatic interactions were neglected, as pairwise interactions beyond 1.2 nm were not considered. A weak harmonic potential was used to describe interactions between covalently bonded sites, and a weak harmonic cosine potential was used to represent chain stiffness for the angles between three consecutive bonded particles.

The selected particle types for CG models of warfarin and brodifacoum were validated by reproducing the octanol/water partition coefficient using the BAR free energy difference method as implemented in Gromacs. Partition coefficients of 3.1 and 8.65 for warfarin and brodifacoum respectively were estimated by the free energy difference between solvation in water and water-saturated octanol. These values compare well with the experimentally determined octanol/water partition coefficients of 2.7 for warfarin and 8.5 for brodifacoum[173].

As brodifacoum and warfarin exist as acid-base pairs and are predominantly found in their charged states at physiological pH, we considered both neutral and deprotonated forms of these species in our simulations. Representation of the deprotonated (ionized) species was achieved by replacing two CG interactions sites (colored orange in Figure 3-1) in the hydroxycoumarin ring with charge-bearing particle types of charge magnitude -0.5 each.

3.3.3 **Simulation System**

Each simulation system consisted of a central phospholipid bilayer containing 100 DPPC molecules in each leaflet and surrounded on both sides by water slabs containing 4000 coarse-grained water particles each (Figure 3-2). The polar head groups of DPPC were fully solvated in

the aqueous phase, with the hydrophobic tails forming the center of the bilayer. In most cases, either the neutral or deprotonated form of the hydroxycoumarin species of interest was initially incorporated within the aqueous phase. In the case of brodifacoum, the poor aqueous solubility of the molecule led to rapid aggregation in the aqueous phase. Thus, simulations incorporating multiple brodifacoum molecules at various concentrations were initiated with the hydroxycoumarin intercalated amongst DPPC molecules in the bilayer. For simulations containing deprotonated warfarin and brodifacoum, an equal number of Na^+ counterions was added to maintain charge neutrality. System specifications for all simulations are summarized in Table 3-1. This set includes a reference system containing a fully solvated phospholipid bilayer without hydroxycoumarin molecules.

TABLE 3-1: EQUILIBRIUM SIMULATION SYSTEM SPECIFICATIONS

Hydroxycoumarin species	Number of hydroxycoumarins	Charge
Warfarin	50	Neutral
Warfarin	50	-1
Brodifacoum	20	Neutral
Brodifacoum	10	-1
Brodifacoum	20	-1
Brodifacoum	30	-1
Brodifacoum	40	-1

The general methods used in the simulations are described in Section 2.5. Simulation production runs lasted 320 ns and were used for data analysis. An integration time step of 20 fs was used to integrate the equations of motion [130-132]. An isothermal-isobaric (NPT)

ensemble was maintained; volume (and hence the cross sectional area) of each system was allowed to fluctuate freely. Each component of the simulation system was coupled separately to a temperature bath using Nosé-Hoover protocols [184-186] with a coupling constant of 1.5 ps. Pressure coupling at 1 atm was achieved using a Parrinello-Rahman scheme [132] with a coupling constant of 5 ps. To maintain a tensionless bilayer, pressure coupling was implemented as semi-isotropic.

3.3.4 **Spontaneous Incorporation of Warfarin and Brodifacoum**

Using a system with hydroxycoumarin molecules initially distributed in the aqueous phase, spontaneous membrane incorporation of each hydroxycoumarin was simulated. Initial aqueous-phase concentrations of warfarin and brodifacoum were 85.7 mM and 34.3 mM respectively. In the case of brodifacoum, for which aqueous solubility is very poor (0.46 μM) [168], this initial concentration led to spontaneous aggregation. The aggregate rapidly associated with the phospholipid bilayer, with subsequent dissociation of the molecules due to favorable interactions with the hydrophobic region of the lipid bilayer.

3.3.5 **Constant Velocity Steered Molecular Dynamics Simulations**

Steered molecular dynamics simulations were employed to estimate the thermodynamic landscape for transit through the bilayer. In each case, one molecule of either warfarin or brodifacoum was steered at a constant velocity through (i) a 'bare' DPPC bilayer or (ii) a bilayer already populated with additional warfarin or brodifacoum molecules (at 11 mol% and 13 mol% respectively). Steered simulation specifications are listed in Table 3-2. Each

simulation was run for 400 ns and consisted of a 200 ns equilibration phase during which the motion of a target warfarin or brodifacoum molecule was constrained in the z-dimension. This was achieved by tethering the molecule to a fixed point in the aqueous phase using a harmonic spring potential. The constraint prevented spontaneous entry into the bilayer during equilibration. A further 10 ns post-equilibration simulation was performed to obtain multiple initial configurations for constant velocity simulations.

TABLE 3-2: STEERED SIMULATION SYSTEM SPECIFICATIONS

Hydroxycoumarin species	Number of hydroxycoumarins	Charge
Warfarin	1	Neutral
Warfarin	50	Neutral
Warfarin	1	-1
Warfarin	50	-1
Brodifacoum	1	Neutral
Brodifacoum	20	Neutral
Brodifacoum	1	-1
Brodifacoum	20	-1

The center-of-mass of the target molecule was then tethered to a moving point. As the tether point was moved at a constant velocity along the z-coordinate from the aqueous phase into the bilayer, the force required was recorded. While traversing this path, the molecule was allowed to move freely in the xy-plane. The harmonic spring constant and velocity of the tether point were 40 Kcal/mol/ $Å^2$ and 1 Å/ns respectively. The tether point velocity was chosen to cause a rate of transit orders of magnitude smaller than the root mean square thermal velocity

of ~1050 Å/ns for DPPC, thereby ensuring that the bilayer was not needlessly perturbed by solute permeation [157, 159, 187]. Each steered simulation was run for 200 ns and replicated 10 times using the different initial configurations obtained from the prior z-constrained simulations in order to reduce systematic errors [154, 158, 159, 187, 188]. The isobaric-isothermal Jarzynski equality (Equation (2-16) in Section 2.5.4) was used to estimate free energy profiles from the work done during transit from water to bilayer. All other simulation conditions for steered simulations were identical to those used for the unconstrained simulations.

3.4 Results and Discussion

Both neutral and charged forms of the hydroxycoumarin molecules spontaneously accumulated within DPPC bilayers, with a consequent change in structure and dynamics of the membrane. In all cases, incorporation of the deprotonated (ionized) form yielded a similar, but more pronounced effect. As >99% of brodifacoum and warfarin molecules are expected to be deprotonated at physiological pH (pKa ~5 at pH 7.4), we present here the results for the charged form of each hydroxycoumarin, except where stated otherwise. Although the simulations all contained the same number of phospholipids, at equilibrium, all the brodifacoum molecules were sequestered within the bilayers, while a large fraction of warfarin remained in the water phase. Therefore, results are compared on the basis of similar interfacial concentrations of the two hydroxycoumarin compounds.

3.4.1 Spontaneous Retention of Hydroxycoumarins Within the Bilayer

Figure 3-2 presents snapshots taken from simulations of spontaneous hydroxycoumarin uptake in the presence of a DPPC bilayer. The interfacial concentrations of warfarin (Figure 3-2 (a)) and brodifacoum (Figure 3-2 (b)) are similar at 11 mol% and 13 mol% respectively. At these and higher interfacial concentrations (not shown), brodifacoum is not observed to leave the bilayer within the 320 ns duration of the simulation. Warfarin, in contrast, diffuses freely in and out of the DPPC interface. Neither species exhibits phase segregation or other aggregation within the bilayer.

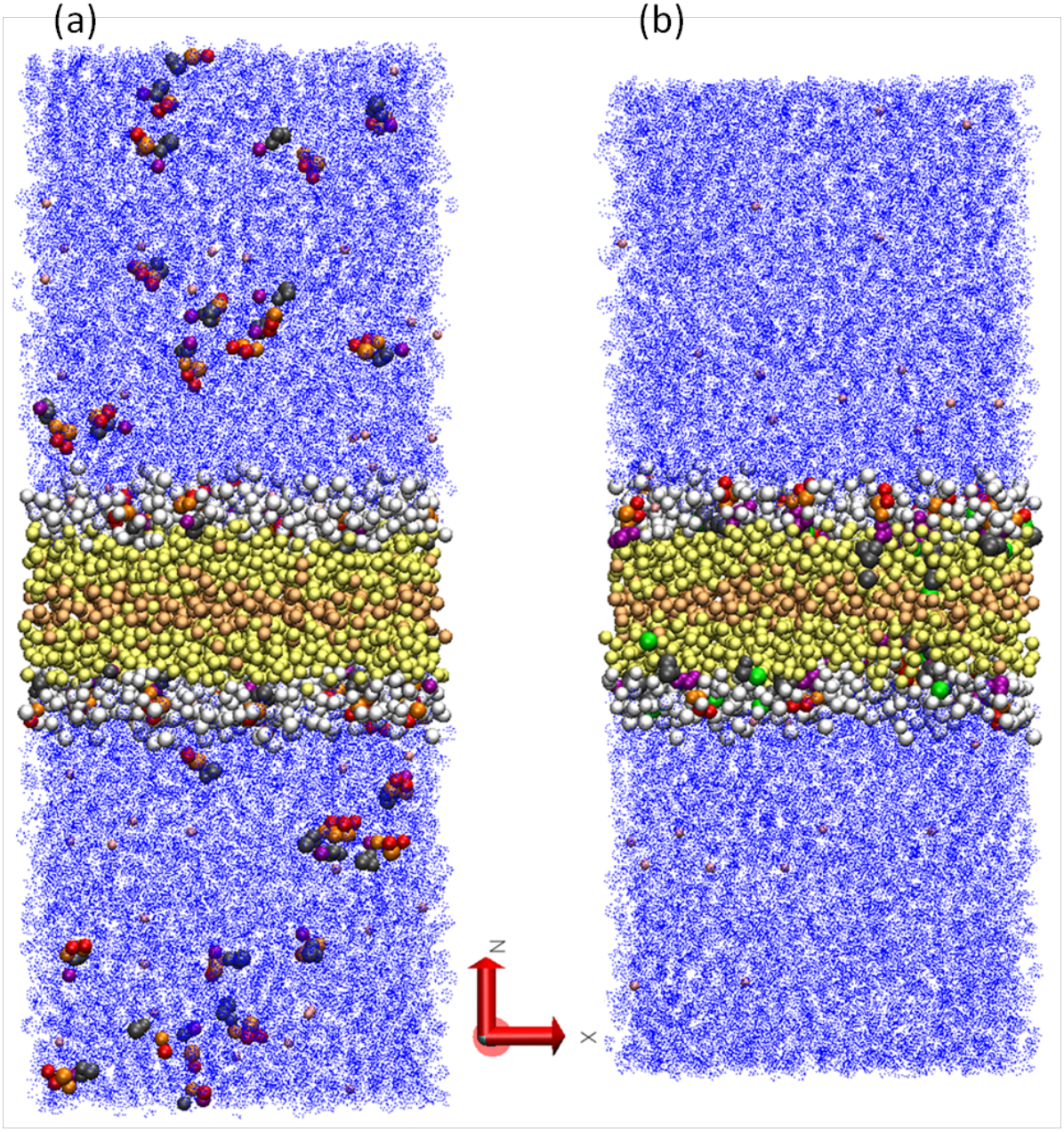

Figure 3-2: Snapshots of simulation cells containing fully equilibrated DPPC bilayers in water with warfarin (a) and brodifacoum (b) molecules taken after 320 ns of simulation time. DPPC polar head groups and glycerol backbones are represented by white spheres and the hydrophobic tails are yellow spheres with the terminal tail particle in orange. Water is depicted as blue dots and Na^+ counterions are shown as small pink spheres dispersed in the water. Warfarin and brodifacoum are colored as described in Figure 3-1.

3.4.2 **Transfer Free Energy for Bilayer Permeation**

Entry into the bilayer is an activated process for both warfarin and brodifacoum, with transport of each species exhibiting a free energy minimum in the region of the DPPC glycerol backbone (Figure 3-3). While the activation energy barrier for entry into a bare bilayer is similar for the two species (1.8 ± 0.6 k_BT and 1.4 ± 0.6 k_BT respectively for warfarin and brodifacoum), the intramembrane energy minimum is more pronounced for the more lipophilic molecule (-2.7 ± 0.9 k_BT vs. -5.9 ± 1.9 k_BT for warfarin and brodifacoum at 20 Å and 19 Å from the bilayer center respectively). Prepopulating the interface with additional hydroxycoumarin molecules only augments this difference in the thermodynamic landscapes, causing the free energy for warfarin to become essentially barrier-free with respect to escape from the interface (shallow minimum of -0.6 ± 1.1 k_BT, Figure 3-3 (a)). Indeed the spontaneous simulations demonstrated retention of brodifacoum without aqueous phase re-entry, whereas warfarin molecules were observed to undergo rapid entry into and escape from the bilayer interfacial region. Prepopulation of the bilayer with brodifacoum reduces the depth of the energy well (to 3.0 ± 1.0 k_BT), but does not eliminate the minimum. For both species, the activation barrier for bilayer association is essentially unchanged by prepopulation of the interface. This may reflect the association of each molecule with the interface being driven by interactions between the hydroxycoumarin ring and phospholipid head groups; retention within the bilayer is then mediated by the potential for favorable apolar interactions with the membrane hydrophobic core, which exists for brodifacoum more so than for warfarin.

Bilayer permeation subsequent to association with the interface is also an activated process. A thermodynamic barrier of ~21 ± 7 k_BT makes the bilayer crossing event kinetically

inaccessible in the spontaneous permeation simulations. No crossing events are observed for either species. However, fluctuations in system energy occur with a magnitude of ~ 213 k_BT, indicating that the crossing event should be possible even given the ionized state of the hydroxycoumarin.

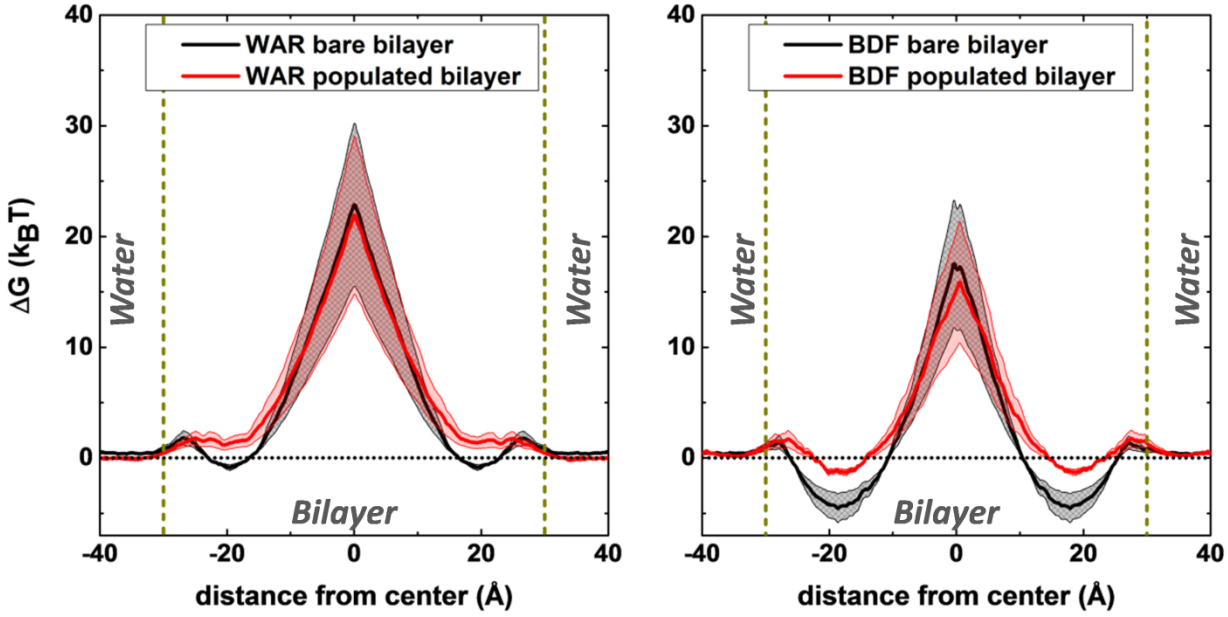

Figure 3-3: Free energy profiles of warfarin (left) and brodifacoum (right) as a function of distance through the bilayer. Statistical error bars are represented as shaded bands around the profiles.
Prepopulated systems are shown as red curves. Initially bare systems are black curves with crosshatched error bands. Approximate positions of DPPC polar head groups are indicated by vertical dashed lines. Brodifacoum and warfarin are abbreviated as BDF and WAR respectively.

3.4.3 **Lateral Expansion, Thinning and Curvature of the Bilayer**

Incorporation of either hydroxycoumarin at constant surface pressure caused the bilayer to expand laterally. At an interfacial warfarin mole fraction x_w = 0.11, an 11% expansion of the cross-sectional area was observed (i.e., from 59.5 ± 0.05 Å^2/lipid to 65.9 ± 0.03 Å^2/lipid), yielding an apparent area of 55 Å^2 per warfarin molecule. Brodifacoum, at a mole fraction x_b = 0.13, caused an expansion of 19%, with a corresponding apparent area per brodifacoum molecule of 75 Å^2. The lateral expansion of the DPPC bilayer was accompanied by overall thinning in the direction normal to the water/lipid interface. The thickness of the bilayer, measured as the distance between the phosphate groups of DPPC in each leaflet, was reduced by ~2 Å (4%) in the case of warfarin at the above-mentioned concentration. A similar concentration of brodifacoum reduced the bilayer thickness by ~5 Å (11%).

3.4.4 **Changes in the Transmembrane Pressure Distribution**

The aforementioned changes in bilayer structure are also reflected in the lateral forces acting between molecules of the interface. Changes in the configuration of the lateral pressure profile are known to serve as indicators of structural changes within a bilayer [151, 152]. The lateral pressure profiles in Figure 3-4 demonstrate the inhomogeneous distribution of forces within the bilayer and are represented as a function of position along the normal to the interface.

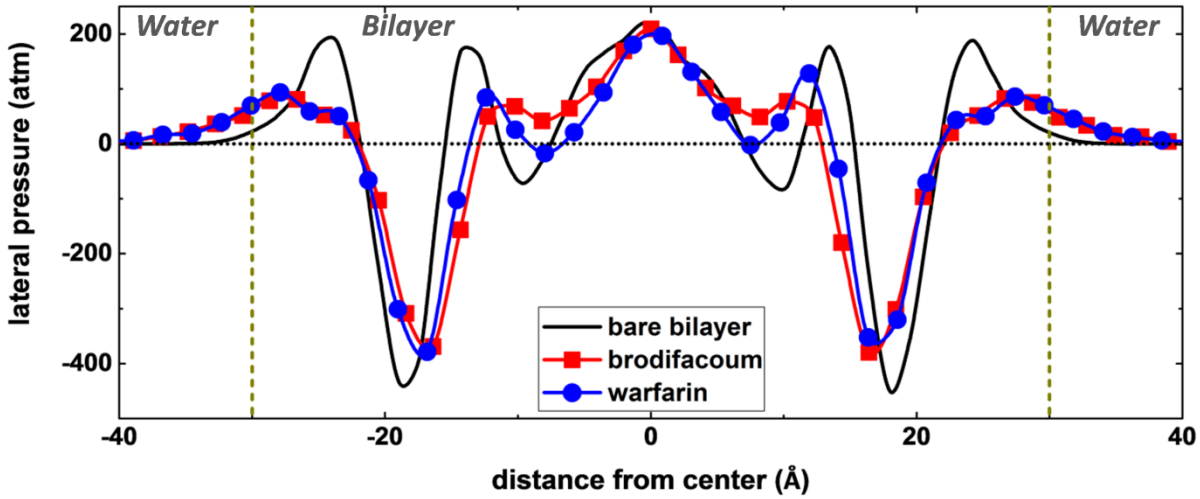

Figure 3-4: Lateral pressure profiles from simulations containing brodifacoum and warfarin (curves with square and circle symbols respectively) compared to a bare DPPC bilayer (solid black curve).
Vertical dashed lines indicate approximate positions of DPPC polar head groups.

Interactions between the amphiphilic phospholipid molecules give rise to positive peaks in the hydrophobic region (center of the bilayer) and head group regions, where interactions are repulsive. Negative pressures are observed at the polar/apolar interface, where cohesive forces produce a local tension. The presence of hydroxycoumarin molecules in the DPPC bilayer yields a broadening, outward shift, and reduction in magnitude of the peak in the head group region. An inward shift, reduction of magnitude, and broadening of the negative peak are observed in the interfacial region. As these data result from a zero surface-tension simulation, the repulsive and cohesive pressure components must sum to zero. Thus, decreases in repulsive interactions at one location must be accompanied by reduced cohesive forces in other parts of the bilayer. The resulting 'smoothing' of the pressure profile is indicative of the weakened intermolecular interactions that accompany a lateral expansion of the bilayer. Note, however,

that there is little change in the peak pressure at the center of the bilayer, suggesting that neither hydroxycoumarin molecule significantly perturbs this region and the expansion is primarily mediated by changes at the apolar/polar interface. Furthermore, the pressure distribution in the head group region is essentially identical for brodifacoum and warfarin, where the change with respect to the bare bilayer is a consequence primarily of hydroxycoumarin ring insertion between phosphate groups.

3.4.5 **Acyl Chain Packing Order**

Hydroxycoumarin incorporation at the interface does have an impact on the dynamics of the acyl chains forming the hydrophobic core of the bilayer. Here the presence of extraneous molecules manifests as an increase in the disorder of the DPPC tail groups. Orientational order, P_2, of the bonds in the acyl chains is evaluated as per Equation (3-1), where θ is the time-varying angle between the bond and the bilayer normal.

$$P_2 = \langle \frac{3\cos^2 \theta(t) - 1}{2} \rangle$$

(3-1)

The order parameter is evaluated as an ensemble average over the 200 phospholipid molecules constituting the bilayer and a time average over the duration of the simulation production run. Ranging between -0.5 and 1 (for anti-alignment and perfect alignment with the normal respectively), P_2 gives an indication of both the orientation of the bond in question and

the variability of that alignment across time and space within the bilayer. A P_2 value of zero indicates disorder, with no preferred orientation in the system.

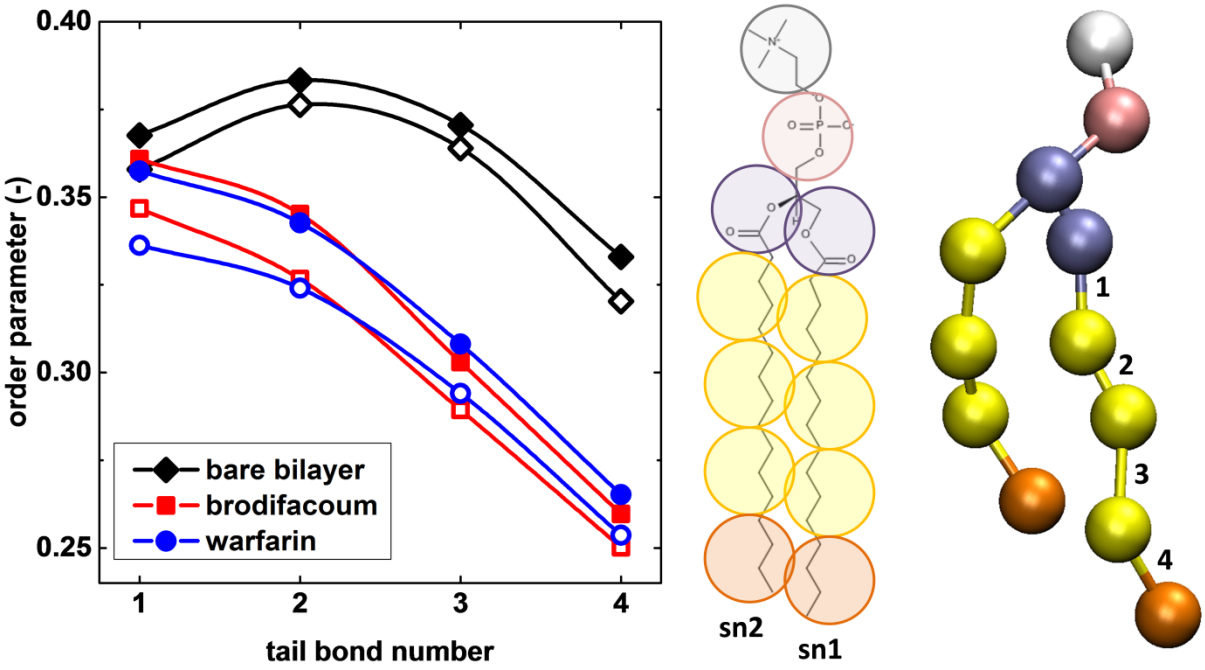

Figure 3-5: Left: order parameter profiles calculated along the bonds connecting coarse-grained sites in DPPC tails (bond numbering shown on the right). Open symbols represent the sn1 and closed symbols the sn2 tails of DPPC (illustrated on the right).
The bare bilayer is represented by black curves and diamond symbols; brodifacoum and warfarin containing bilayers are red and blue curves with square and circle symbols respectively. Right: two-dimensional structure of DPPC overlaid with the coarse-grained representation. Choline moiety is colored white, phosphate in pink, and glycerol backbone in purple. The sn1 and sn2 tails are both yellow, with the terminal particles in orange.

We find that both warfarin and brodifacoum reduce the orientational order of bonds in the phospholipid acyl chains, and they do so in a manner that increases with distance from the

glycerol backbone (Figure 3-5). The effect is of similar magnitude for the two hydroxycoumarin species, with the exception of the first bond in the sn-1 chain for the case of brodifacoum (i.e. the chain furthest from the phosphate group). Here, the bond displays a greater degree of alignment with the bilayer normal than in the case of warfarin uptake. The reduction of P_2 is indicative of an increase in fluidity of the bilayer, a logical consequence of the increased head group spacing induced by insertion of the hydroxycoumarin species in this region.

3.4.6 **Amphiphilic Structure and Dynamic Orientation of Interfacial Warfarin and Brodifacoum**

Although both molecules possess an amphiphilic character, brodifacoum has a longer lipophilic region as compared to the phenyl ring of warfarin (Figure 3-1). The tetralin and biphenyl ring moieties of brodifacoum provide favorable interactions with phospholipid acyl chains. In Figure 3-2 (b), several brodifacoum molecules are observed to be incorporated within the DPPC bilayer such that their lipophilic segments penetrate the hydrophobic core of the bilayer. The oxygen atoms in the hydroxycoumarin moiety lend a polar character to the head group common to both anticoagulants. In the case of brodifacoum, a second polar moiety arises. Electronic effects are transmitted to the brominated group of brodifacoum through conjugation by delocalized electrons in the phenyl rings, elevating the polarity of that group through the principle of vinylogy. Thus, rather than simply functioning as an amphiphile, brodifacoum has a bolaamphiphilic character. This allows for more than one preferred orientation in the bilayer. Indeed, simulations indicate a number of dynamic orientation effects.

Due to the larger hydrophobic region possessed by brodifacoum compared to warfarin, before incorporation into the bilayer, brodifacoum tends to self-aggregate rapidly in the aqueous phase. It forms micelle-like structures in an analogous fashion to surfactants, in order to shield its hydrophobic portion from the polar solvent. When the micelle enters the lipid bilayer, it breaks apart into its constituent molecules in order to interact with the amphiphilic phospholipids. This type of behavior is well studied for surface-active amphiphilic drugs which behave similarly to classical detergents [21, 180, 189-191].

It is clear from both the spontaneous simulations and the transfer free energy that both hydroxycoumarin species will preferentially partition into the lipid bilayer. Closer examination indicates initial association and subsequent retention of brodifacoum are mediated by directed interactions between the amphiphilic superwarfarin and the amphiphilic interface. For both warfarin and brodifacoum, association with the bilayer is facilitated by interactions between the hydroxycoumarin ring and the charge-bearing DPPC head group. Both species then reorient as they enter the interface to maintain this favorable interaction. Given that the length and apolar tetralin-biphenyl region of brodifacoum mimic to some extent the amphiphilic structure of the lipid layer, the molecule might be expected to intercalate with DPPC. However, the brominated moiety allows for other possibilities. Normalized density profiles in Figure 3-6 demonstrate the location of the brominated interaction site relative to the hydroxycoumarin moiety. The brominated site is predominately located in close proximity to the hydroxycoumarin rings, suggesting that the brodifacoum molecule orients parallel to the bilayer interface rather than the perpendicular orientation that would indicate intercalation. Both the

hydroxycoumarin rings and the brominated group are primarily localized in the polar regions of the bilayer.

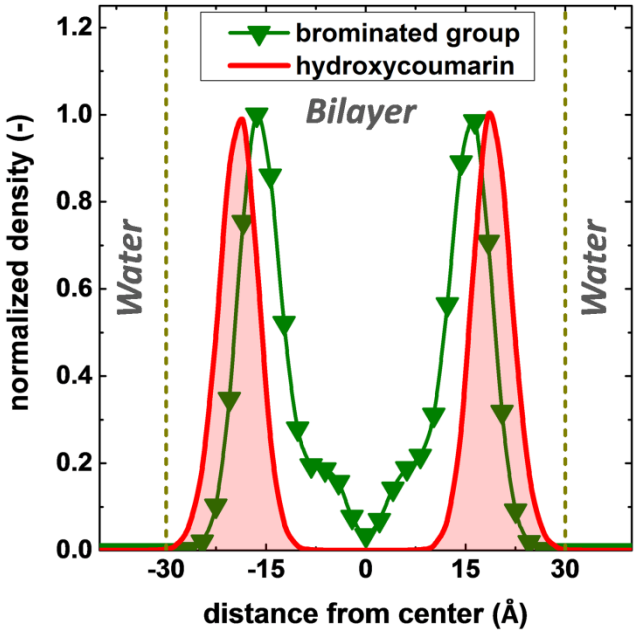

Figure 3-6: Normalized density profiles of the brodifacoum brominated (purple curve with triangle symbols) and hydroxycoumarin (shaded green curve) groups.
Vertical dashed lines indicate the approximate positions of the DPPC polar head groups.

Both warfarin and brodifacoum undergo dynamic conformational changes while interacting with lipids. In the case of warfarin, rotations are observed about the bond connecting the hydroxycoumarin and phenyl groups (colored red/orange and grey in Figure 3-7 (a) and (b)).

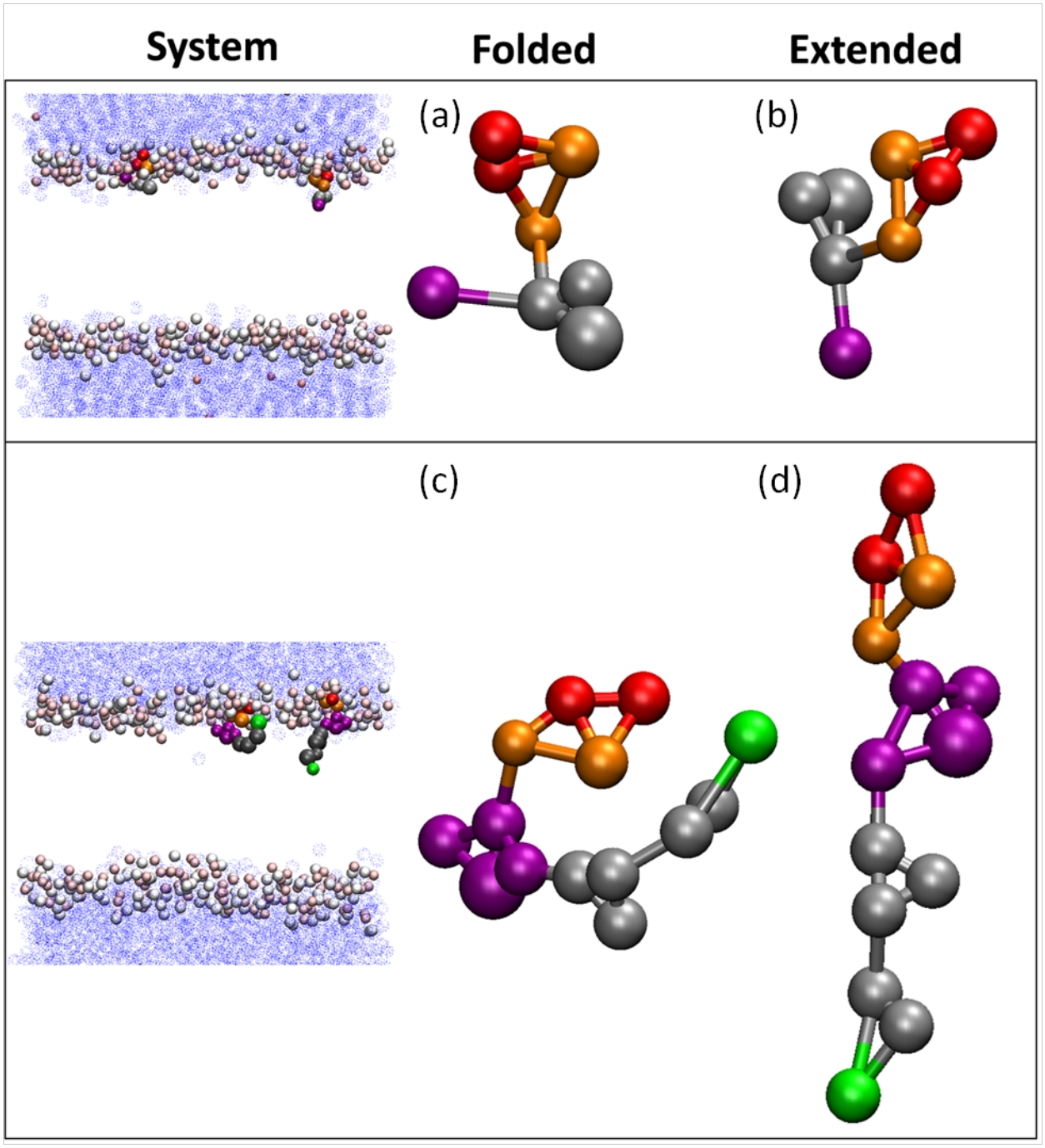

Figure 3-7: Snapshots of two possible configurations for warfarin (top) and brodifacoum (bottom) located within a DPPC bilayer near the polar choline (white spheres) and phosphate (pink spheres).
Glycerol backbones and DPPC tails are hidden for clarity. Water is represented as blue solvent spheres. Warfarin and brodifacoum have the same coloring as described in Figure 3-1.

When situated in the bilayer, brodifacoum has the potential to sweep out a large volume as it folds and extends about the tetralin structure (colored purple in Figure 3-7 (c) and (d)). These conformational changes alter the shape and effective size of brodifacoum such that the molecule's radius of gyration ranges from 3.7 Å (folded) to 6.7 Å (elongated). In contrast, warfarin is characterized by a radius of gyration measuring 3.4 ± 0.1 Å. The folded configuration of brodifacoum predominates, occurring 14 times as frequently as the elongated form. The larger size and dynamically changing conformation of brodifacoum likely contribute to the pronounced structural changes observed within the bilayer following brodifacoum incorporation.

3.4.7 **Transient Pore Formation, Water Permeation and Lipid Flip-Flop**

The presence of either warfarin or brodifacoum increases hydration of the simulated bilayer. This is particularly evident in steered simulations, where water solvates the hydroxycoumarin ring and is carried into the hydrophobic region along with the anticoagulant molecule (Figure 3-8). Much like a detergent molecule[21, 153], upon association with the bilayer, both warfarin and brodifacoum cause transient defects in the membrane structure. Phosphate and choline moieties in close proximity to the hydroxycoumarin are drawn inward, thinning the membrane and allowing water contact with the hydrophobic core. The effect is relatively brief for warfarin, with rebounding of the phospholipid head group to restore the structure of the membrane leaflet. The effect is prolonged for brodifacoum, for which hydroxycoumarin ring solvation continues even as the molecule crosses the center of the membrane.

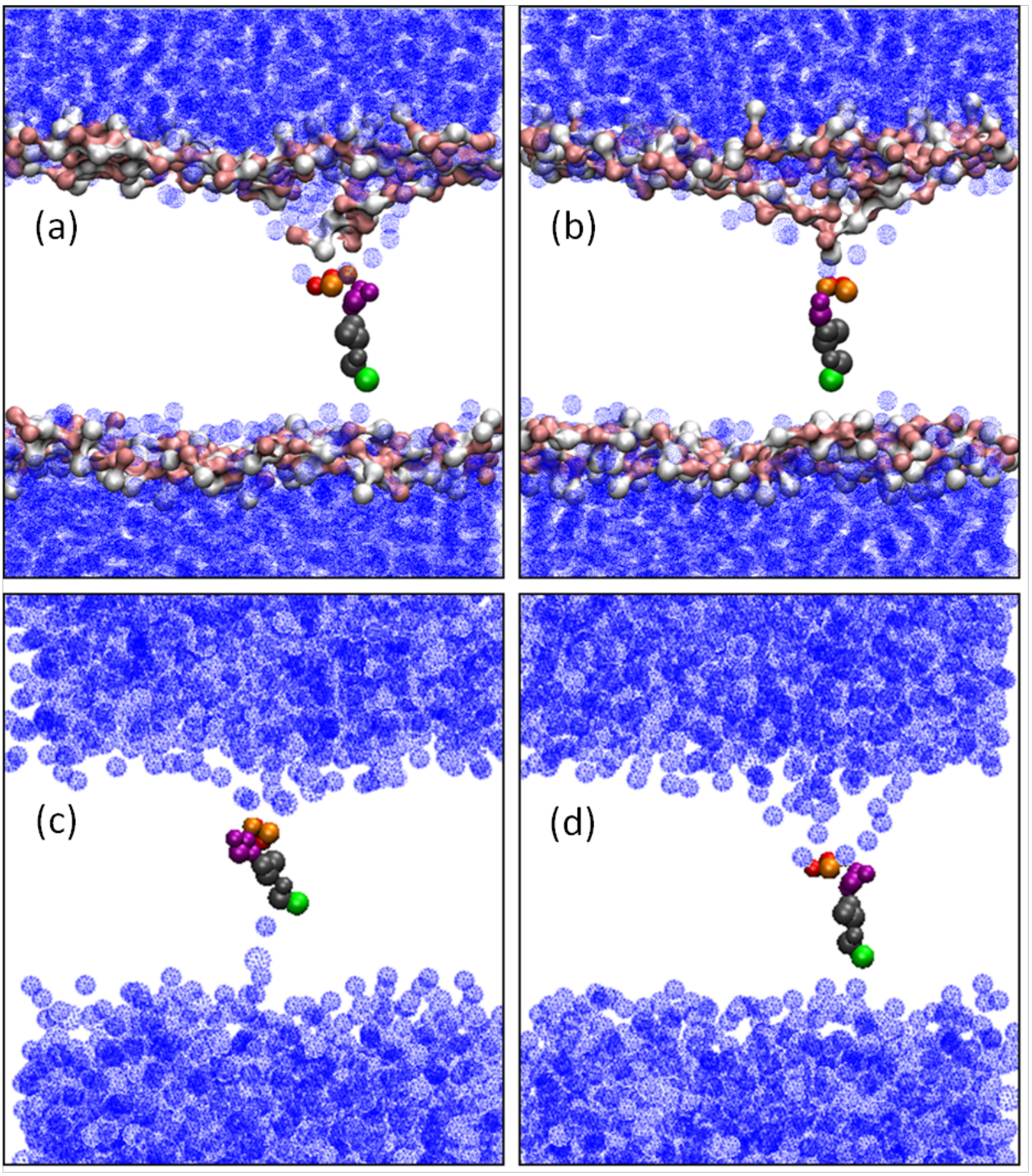

Figure 3-8: Snapshots of brodifacoum travelling through the DPPC bilayer.
In the top panel, only the polar choline (white) and phosphate (pink) groups of DPPC are shown in a solid surface representation. Glycerol backbones and DPPC tails are hidden for clarity. In the bottom panel, all DPPC molecules are hidden for clarity. Water is represented as blue solvent spheres. Brodifacoum has the same coloring as described in Figure 3-1.

Quantifying the extent of water permeation via the radial distribution function for water around the DPPC tail ends, we find that brodifacoum admits to the bilayer more than twice the amount of water that associates with warfarin (Figure 3-9).

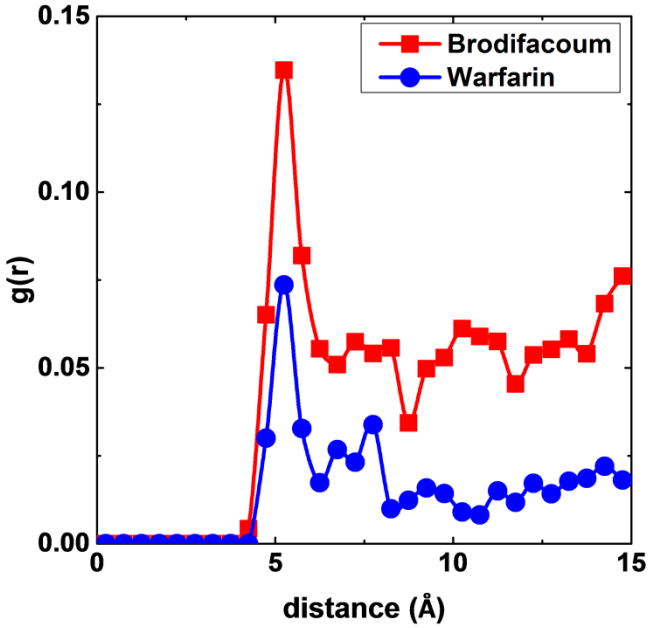

Figure 3-9: Radial distribution functions g(r) between the hydroxycoumarins and water in the center of the bilayer.
Brodifacoum and warfarin are red and blue curves with square and circle symbols respectively.

Furthermore, the larger size of brodifacoum accompanied by the slight polarity of the brominated group at the opposite extreme of the brodifacoum structure allows for water ingress from the opposing leaflet in order to solvate that moiety (Figure 3-8 (c)). Thus, a transient water pore is created. This occurs even before the molecule's center-of-mass reaches

the second leaflet due to the fact that the perturbation caused in the tails of the top leaflet by the large brodifacoum molecule gets translated into disruption of the structure of the second leaflet. Similar structural defects and water pores have been shown to aid in translocation of lipids from one leaflet of a bilayer to the other (known as flip-flop) as well as ion transport [39, 192, 193]. The water channel creates a favorable hydrophilic pathway for transit of these species through the hydrophobic bilayer. This phenomenon does not occur in simulations containing warfarin.

Snapshots in Figure 3-10 show DPPC molecules displaced from the plane of their leaflet and drawn into the hydrophobic core as they interact with brodifacoum. This is a consequence of the polar head groups of DPPC experiencing strong van der Waals interactions with the polar hydroxycoumarin ring and brominated particle. Electrostatic interactions also exist between the charge-bearing particles of the hydroxycoumarin ring and the oppositely charged DPPC choline particle. Having been displaced from the leaflet of origin, the DPPC molecule can undergo end-over-end flipping to facilitate insertion into the opposing leaflet. Although lipid flip-flop does not alter the bilayer composition in our model system – where the leaflets are identical – real cell membranes have asymmetric compositions and undergo regulated transverse lipid motion.[21, 194-197] In this case, increased lipid flip-flop rates may result in function-altering changes in leaflet composition. Consequences for membrane curvature and cell signaling mechanisms can lead to cell death.[39-41]

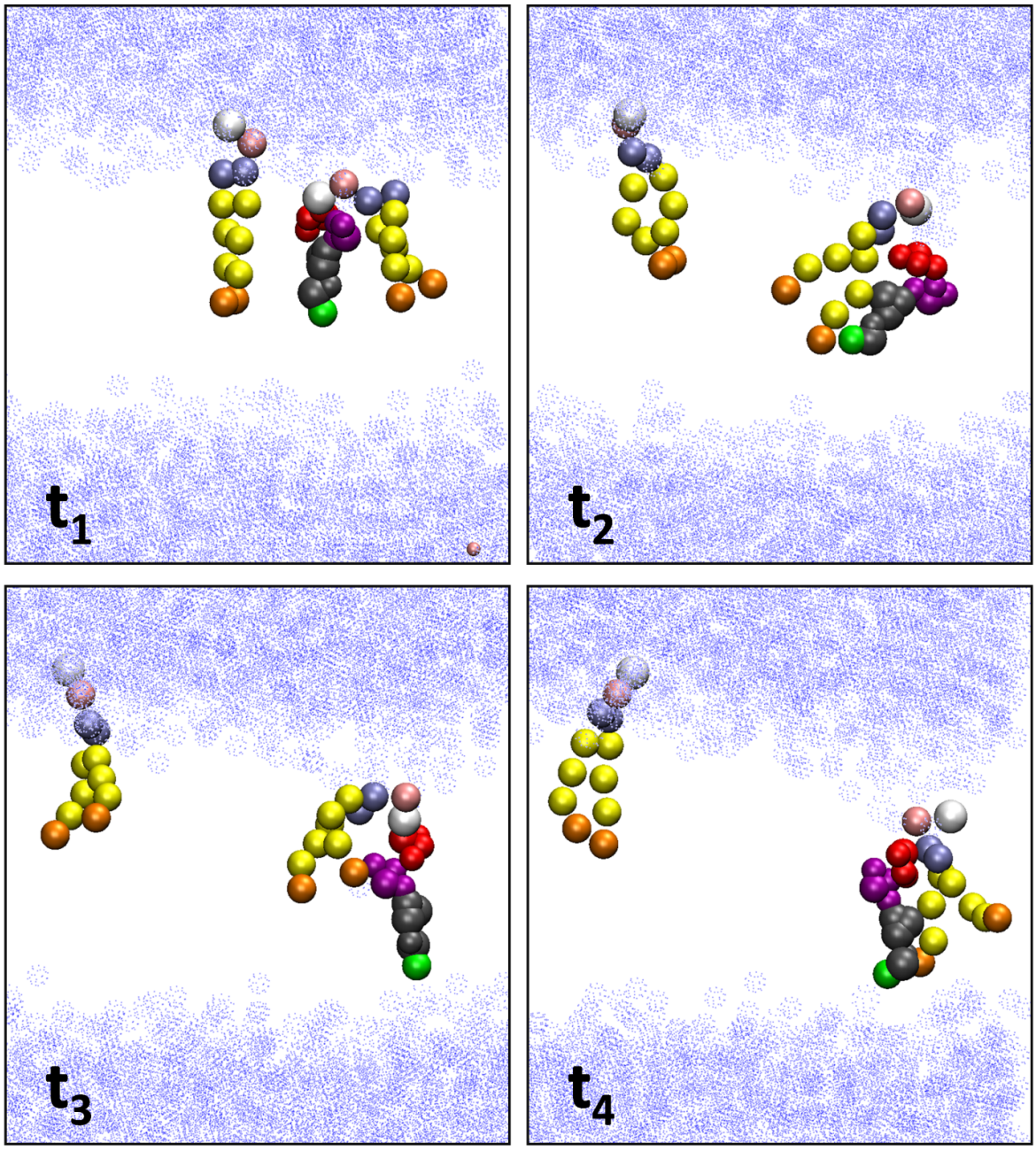

Figure 3-10: Simulation snapshots at four time points as brodifacoum travels through the DPPC bilayer.
Each snapshot illustrates an individual DPPC molecule pulled into the bilayer core by van der Waals and electrostatic interactions with brodifacoum. An additional DPPC molecule is shown in each snapshot to indicate the position of the other molecules in the leaflet. The rest of the DPPC molecules are hidden for clarity. The coloring of brodifacoum and the DPPC molecules is the same as in Figure 3-1 and Figure 3-5 respectively, with the exception of the orange charged particles in brodifacoum with are colored red here. Water is depicted as blue solvent spheres.

3.5 **Summary and Conclusion**

Our molecular dynamics simulations of hydroxycoumarin incorporation in a dipalmitoylphosphatidylcholine (DPPC) bilayer demonstrate that the physical structures and chemical properties unique to brodifacoum and warfarin molecules are responsible for their differential effects on the structure of DPPC bilayers. It is well established that the first stage of destabilization of lipid layers via a detergent-like mechanism involves adsorption of the extraneous molecules into the layer even at low concentrations [153, 192, 198]. This leads to perturbation of structure and formation of transient defects in the bilayer. Retention of such molecules promotes permeability and lowers the barrier function of the bilayer [191]. From our simulations, we observed that brodifacoum was retained within and associated more strongly with DPPC bilayers as compared to warfarin at all concentrations. This retention is of concern because this molecule is known to remain in human bodies much longer than warfarin, with a half-life of 10 to 70 days as opposed to 17 to 37 hours for warfarin [164, 165]. Thus, all the structural perturbation effects we observed would become longer lasting as a result of this increased brodifacoum retention, creating the potential for long-lasting impacts on cell viability.

Although both warfarin and brodifacoum induce changes in the configuration of the lateral pressure profile by decreasing the repulsive and cohesive stresses at various points in the bilayer, the effect of brodifacoum is more pronounced in the DPPC tail region as compared to warfarin. This would consequently lead to diminished barrier function of the bilayer. The reductions in tail orientational order in the presence of the hydroxycoumarins correspond with the reduced cohesion observed in the tail regions in the lateral pressure profiles. This decrease in order indicates that the DPPC tails have more space in which to move and can therefore

assume varied configurations, changing the internal structure and fluidizing the bilayer. Our results fall in line with microcalorimetric and fluorescence experimental observations that hydroxycoumarin molecules decrease the enthalpy required for phase transition by fluidizing DPPC bilayers [199].

In addition to fluidization and causing changes in the distribution of stresses in the membrane, our MD simulations demonstrate that anticoagulant permeation can permit water penetration and promote lipid flip-flop – both events capable of triggering cell death [21, 39-41]. The consequences of hydroxycoumarin penetration of the bilayer are more pronounced in the case of brodifacoum due both to its increased hydrophobicity and its elongated bolaamphiphilic structure. Indeed, its predominately deprotonated state at physiological pH and its similarity in length to the phospholipid constituents of the lipid bilayer cause brodifacoum to function in a manner analogous to an ionic surfactant.

Both hydroxycoumarin molecules undergo dynamic conformational changes while interacting with DPPC. In the case of warfarin, only minor rotations are observed about the bond connecting the hydroxycoumarin and phenyl groups. The larger size and dynamically changing conformation of brodifacoum is a major contribution to the pronounced structural changes observed in the bilayer. Brodifacoum sweeps out a large volume as it folds and extends about the tetralin structure in the bilayer. These conformational changes alter the shape and effective size of brodifacoum which results in more lateral expansion and thinning of the bilayer, greater structural disorder as evidenced by lateral pressure changes and lowering of the lipid tail order parameter, and permeation of water deeper into the bilayer. Overall, there is considerably more bilayer disruption by brodifacoum than by warfarin.

As brodifacoum moves through the bilayer in our steered simulations, the polar head groups of DPPC are redistributed and pulled inward to interact with the polar hydroxycoumarin ring, setting the stage for end-over-end flipping of phospholipid molecules. Indeed, the rate of lipid flip-flop has been shown to be increased by amphiphilic drug molecules [21, 192, 195-197]. We observed that this inward pulling of DPPC head groups creates a large hole and allows more water to enter the hydrophobic core of the bilayer. In fact, water does not only enter from the hole in the leaflet through which brodifacoum entered, we also observe water moving up through the opposite leaflet to meet brodifacoum in the hydrophobic core, creating a transient water pore. This phenomenon does not occur in simulations containing warfarin.

Finally, we observe that the DPPC choline particles (white spheres in Figure 3-8) in the vicinity of the penetrating brodifacoum molecule flip toward the interior of the membrane whereas the choline groups farther away flip out towards the water. That is, brodifacoum induces not only local perturbation and creates a hole in the leaflet, clearly seen in Figure 3-8 (a) and (b), but a concomitant change in the choline groups farther out in the bilayer. This leads to a ripple of effects in the rest of the bilayer.

Using equilibrium and steered molecular dynamics simulations, we have been able to show that hydroxycoumarins disrupt membrane barrier function by accumulation within and transit through the lipid bilayer. The detailed mechanisms by which warfarin and brodifacoum disrupt a lipid membrane have been revealed by elucidating the molecular phenomena that may underlie their differential cytotoxicity. The increased disruption in the structure and dynamics of cell membranes induced by brodifacoum, if accompanied by uncontrolled flux of

ions and other small molecules, would dysregulate the delicate homeostatic balance necessary to maintain cell health.

4. CONSCIOUSNESS IMPAIRMENT BY AN ENDOGENOUS METABOLITE

4.1 Introduction

Diabetes is one of the most prevalent diseases in the industrialized world, affecting nearly 30 million people in the United States, with a further nearly 90 million individuals qualifying as prediabetic [200]. As insulin is implicated in the proper functioning of most organs and tissues, the complications of diabetes can be fatal. Complications range from heart disease to blindness and kidney failure [201]. Neurological consequences also arise [45, 202]. Diabetes, along with other metabolic diseases, can lead to symptoms of impaired consciousness including dizziness, confusion and even coma [44, 45, 203].

While diabetes is a disease of the pancreas, its symptoms of consciousness impairment are shared by other disorders, such as acute liver failure and renal disease. The link between abdominal disease and neurological dysfunction is not altogether clear since these disorders impact different organs and thus alter different metabolic pathways; however, they affect the brain similarly. What they have in common is a deranged balance of physiological concentrations of endogenous metabolites [46, 48, 204-206]. When organs such as the kidneys, liver, and pancreas function incorrectly, the result is an elevation of particular species in the blood. Changes in these blood levels correlate with physiological consequences observed in organs such as the brain, which is far removed from the abdomen. It has been postulated that elevated concentrations of certain metabolites in the bloodstream may contribute to neurological dysfunction via a non-specific interaction of these species with neuronal cell membranes [51, 203].

Metabolites that correlate with impaired consciousness subsequent to metabolic disease are characterized by a broad range of physicochemical characteristics. Some are acids, some bases; some bear a charge at physiological pH, while others do not. They have varying degrees of lipophilicity, different sizes and chemical functional groups. Hence a non-specific mechanism of action is more plausible than a receptor-mediated phenomenon. Indeed, the impairment of consciousness via membrane absorption of small molecules has regained favor as a mechanism of action for general anesthetics, which are compounds specifically employed to alter consciousness [17, 207]. Furthermore, a recent report [51] demonstrates that lipid interfaces respond to the presence of a diabetes-associated metabolite in a similar fashion. Hsu et al. reported melting point depression and changes in morphology of a Langmuir monolayer upon absorption of *beta*-hydroxybutyric acid (BHB), a ketone whose concentration in blood is elevated in diabetic ketoacidosis. Bulk properties of the monolayer were demonstrably and concentration-dependently altered by incorporation of the metabolite – with clinically relevant concentrations producing a doubling of surface pressure.

We report here a molecular dynamics study of the interaction of BHB with a phospholipid bilayer and expand upon the molecular scale consequences of non-specific absorption of this metabolite into cell membranes. We confirm the observed concentration-dependent nature of changes in the properties of a dipalmitoylphosphatidylcholine (DPPC) membrane exposed to BHB. In our simulations, changes in the bilayer structure are observed to be initiated at low interfacial concentrations of this small metabolite. We find that as metabolite concentration increases, further changes are observed in morphological and mechanical properties including lipid tail order parameters, area per lipid, lateral pressure and apparent modulus of

compressibility. We find that a step change in these properties is observed at a threshold metabolite concentration. We propose that this may correspond to the clinically assessed transition between asymptomatic and symptomatic ketoacidosis [48, 206, 208, 209]. Furthermore, we relate our observed membrane response to BHB absorption to the similar behavior observed by others to result from membrane uptake of anesthetics [20, 26, 140, 159, 210].

4.2 **Coarse-Graining a Tiny Metabolite**

Coarse-grained molecular dynamics simulations of DPPC bilayers in water were employed to examine the molecular level causes of the bulk properties observed in the experimental Langmuir monolayer study by Hsu et al. [51]. The MARTINI coarse-graining approach and force field [79, 80] was employed to create the molecular topologies and to study the interactions of BHB with the DPPC bilayer. The DPPC and water geometries were downloaded from the MARTINI website (http://md.chem.rug.nl/cgmartini/). No topology for BHB currently exists; therefore we created a coarse-grained representation of the metabolite using the methods described in Section 2.4. This configuration is based on the centers-of-mass of the heavy atoms (Figure 4-1). We found it essential to use a three-site model; although BHB contains only 7 heavy atoms, no two-site model allowed for the correct reproduction of the octanol/water partition coefficient.

The BHB model was built from the available MARTINI interaction types. The carboxylic acid group was represented by a polar SP_3 interaction site, whereas the hydroxyl and associated carbon atoms were represented by two SN_{da} MARTINI groups to characterize the hydrogen bonding capability of the molecule. The equilibrium bond lengths and angles for the BHB molecule were selected to preserve the underlying geometry and molecule size.

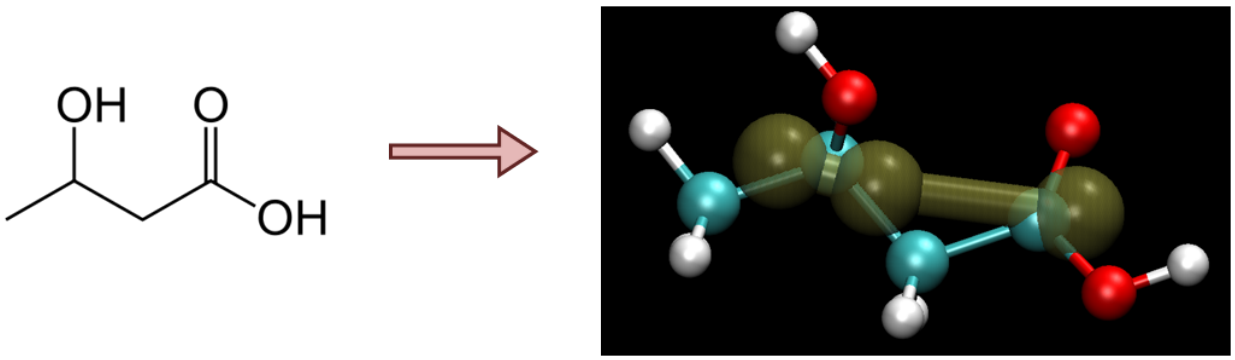

Figure 4-1: BHB structure (carbon-cyan, oxygen-red, hydrogen-white) overlaid with brown coarse-grained representation

This model was validated by reproducing the octanol/water partition coefficient using the BAR free energy difference method implemented in the Gromacs software package (details in Section 2.4.5). We estimated a partition coefficient ($\log P_{oct/wat}$) of -1.43 ± 0.17 from the free energy difference between BHB in water and in water-saturated octanol. This value is comparable to the $\log P_{oct/wat}$ value of -1.14 ± 0.21 predicted by the Advanced Chemistry Development, Inc. (ACD/Labs) ACD/PhysChem Suite log*P* prediction module used by the ChemSpider chemical structure database [211]. As this prediction module is based on empirical parameters obtained by fitting to a large octanol/water partition coefficient database, our simulated log*P* value is consistent with known structural correlations of a whole body of experimental partition coefficients.

4.3 Simulation System

Equilibrium MD simulations were performed using software described in Section 2.5. Each simulation system consisted of a DPPC bilayer containing 400 lipids in each leaflet. The

simulation box was structured such that a water slab was central and the two DPPC monolayer leaflets constituting the bilayer interacted with each other across the periodic boundaries at the top and bottom of the box. The polar head groups of this bilayer were solvated by 11,000 coarse-grained water particles (Figure 4-2). Eight systems containing various initial concentrations of BHB were constructed, resulting in BHB interfacial mol% ranging from of 1 to 20. These results are compared to a reference bare DPPC bilayer in water. BHB molecules become spontaneously incorporated into the bilayers over the course of the simulation.

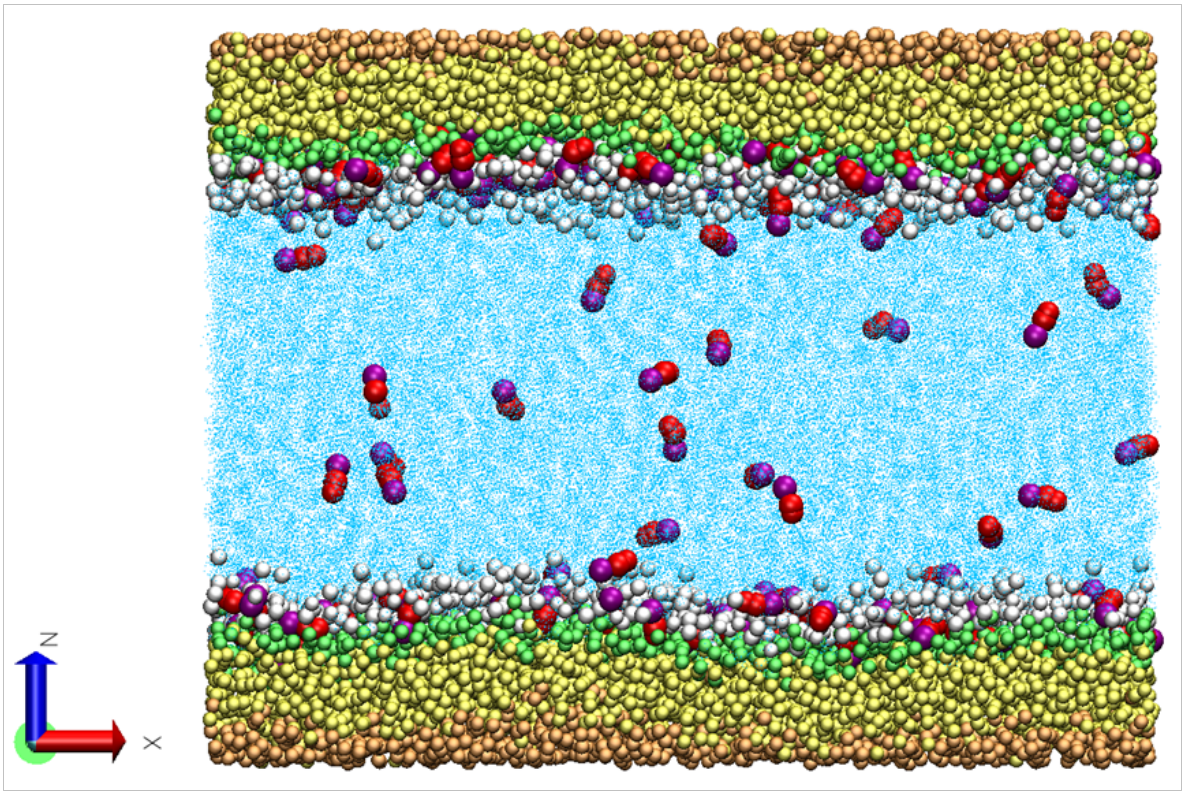

Figure 4-2: Snapshot of equilibrated DPPC bilayer in water containing 7 mol% BHB. Water is shown in blue, DPPC head groups in white, glycerol backbone in green, DPPC tails in yellow with terminal orange sites, BHB carboxylic acid in purple, and hydroxyl groups in red.

The general methods used in the simulations are described in Section 2.5. For this specific study in particular, we used an integration time step of 10 fs to improve the stability of the simulations because of short bond lengths in the BHB model. An isothermal-isobaric (NPT) ensemble was used which allowed the volume (and hence the cross sectional area) of the system to fluctuate freely. Each component of the system was coupled separately to a temperature bath using a Berendsen thermostat [127] with a coupling constant of 1.5 ps. A separate semi-isotropic Berendsen barostat was applied to each component to maintain the system pressure at 1 atm with a coupling constant of 5 ps. Semi-isotropic coupling was used to maintain a tensionless membrane. The simulations were each run for 1 μs with the last 500 ns used as the production run for data analysis. [It is important to note here that the Berendsen barostat used in this example did not reproduce the correct surface area for a bare DPPC bilayer at 323 K, although it allowed the system to approach equilibrium smoothly and quickly. We are currently performing subsequent simulations using a Parrinello-Rahman barostat and Nosé-Hoover thermostat to maintain a canonical ensemble and provide better estimates of the bilayer properties at equilibrium. The results presented here are from systems using Berendsen coupling protocols only. However, we expect to observe similar trends in the effects of BHB on the bilayer properties by using Parrinello-Rahman pressure and Nosé-Hoover temperature coupling.]

4.4 Simulation Results

In order to understand the molecular level mechanisms underlying the Langmuir-Blodgett minitrough observations of Hsu et al. [51], we interrogate our coarse-grained representation of the system to gain insights that can be provided by molecular dynamics simulations. Our simulations were initialized with the same number of phospholipids and water but different initial amounts of BHB. At equilibrium varying, concentrations of BHB were found to associate with the interface (averages shown in Table 4-1). Results are presented on the basis of these average interfacial concentrations of BHB over the course of the 500 ns production run.

TABLE 4-1: AVERAGE INTERFACIAL CONCENTRATIONS OF BHB

Initial Aqueous Amount of BHB (# of Molecules)	Equilibrium Interfacial Concentration (mol %)
16	1
48	2
80	3
120	5
160	7
320	12
480	15
800	20

4.4.1 Structural Changes in the Phospholipid Bilayer in the Presence of *Beta*-hydroxybutyric Acid

The concomitant effects of introducing BHB into our simulations and increasing its concentration in the aqueous phase include a change in the phospholipid density and lateral

expansion of the phospholipid membrane. A measure of this expansion is the average area per lipid (shown in Figure 4-3 (top)).

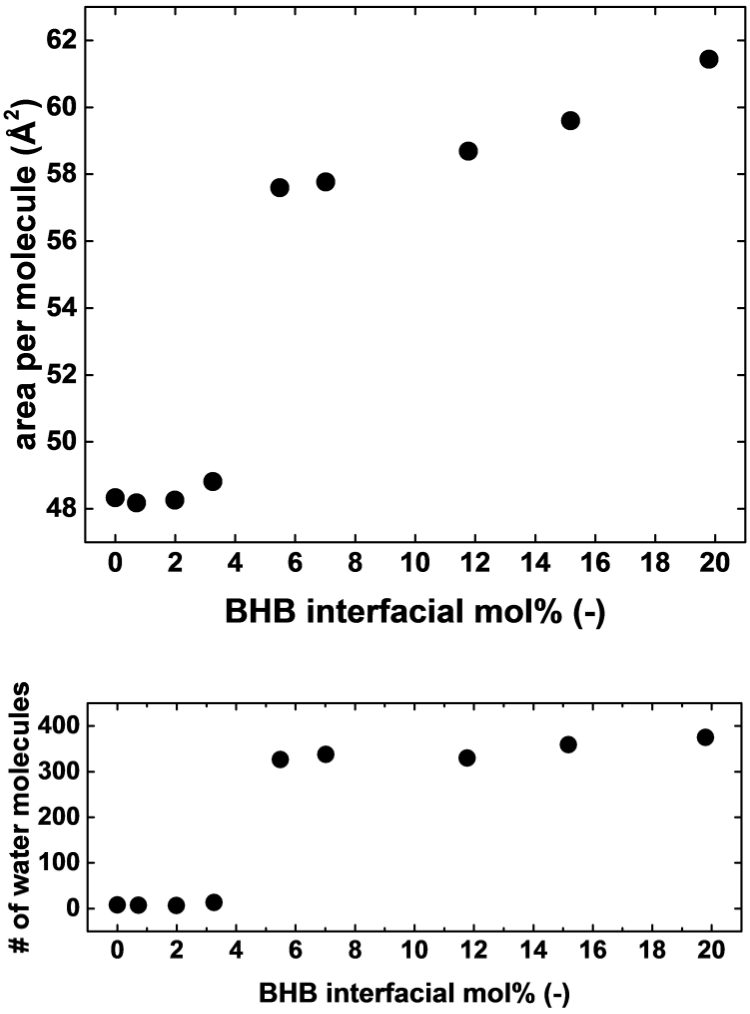

Figure 4-3: Average cross-sectional area per molecule (top) and water concentration (bottom) in DPPC bilayer as a function of BHB concentration. Error bars are located within each data point.

A non-monotonic change in area per lipid with increasing BHB concentration is observed, that is, negligible change in area per lipid at low BHB concentrations, until 5 mol%, at which point the area per lipid rises sharply. An increase in molecular area with increasing BHB concentration is consistent with the results of Langmuir-Blodgett trough experiments by Hsu et al. The lateral expansion of the phospholipid bilayer is accompanied by water penetration farther into the membrane. This is seen in Figure 4-3 (bottom). With increasing BHB concentration, the number of water molecules found within the DPPC bilayer (in the interior of the membrane, past the DPPC head groups) is seen to follow a similar trend to that observed in area per lipid changes.

A further structural change we observe is a change in the stress distribution of the membrane. A measure of this is the mean lateral pressure across the membrane. The effect of BHB on the mean lateral pressure is shown in Figure 4-4. We observed that at 5 mol%, the mean lateral pressure of the phospholipid layer is more than doubled and continues to increase with higher concentrations of BHB. In additionally, a change is observed in the orientation of the phospholipid head groups. A measure of this average orientation is given by the average tilt angle for the phosphate-to-choline vector (P-N bond) away from the bilayer normal. (This is shown in Figure 4-5).

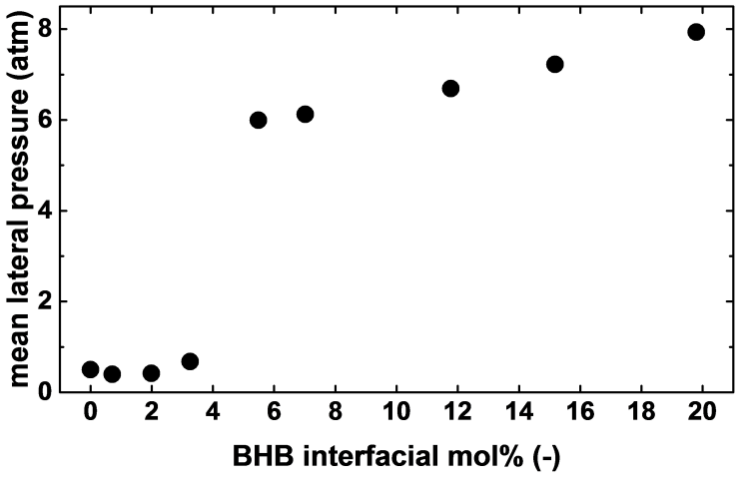

Figure 4-4: Effect of BHB on mean lateral pressure across DPPC bilayer. Error bars are located within each data point.

The tilt angle initially non-monotonically decreases with increasing BHB concentration, indicating that the phospholipid head groups, which in the absence of BHB are nearly parallel to the interface, tend to tilt upwards toward the normal with increasing BHB concentration. This decrease in the head group tilt angle may be caused by BHB molecules inserting themselves between the phospholipid head groups causing the choline to tilt outwards into water to make room for BHB. At 5 mol% once again, the trend changes as the tilt angle shoots up to 81.2° (a value higher than the tilt angle observed in the reference bare bilayer), before slowly decreasing again with increasing BHB concentration. The tilt angle does not appear to return to the initial value at these higher BHB concentrations, but remains elevated, possibly indicating a persistent change in the packing and interactions between phospholipid molecules.

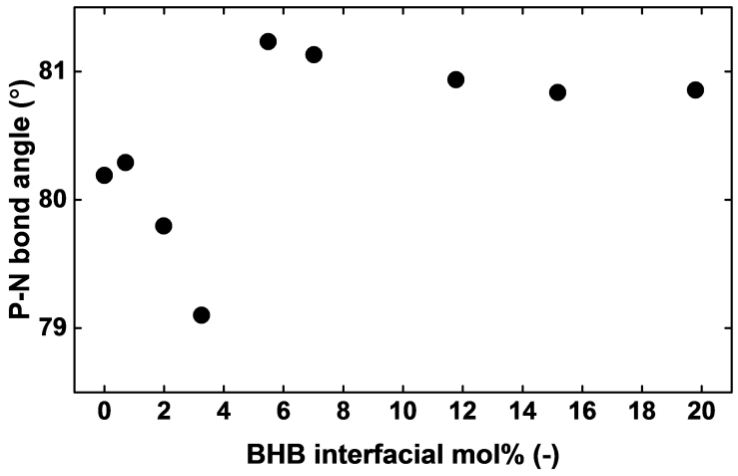

Figure 4-5: Average angle formed between the P-N (phosphate to choline) vector and the interface normal at different BHB concentrations.

The effects of BHB are not limited to the phospholipid head group region only; we observe a change in the orientation and alignment of the DPPC tails as well. This is measured by the order parameter, depicted in Figure 4-6.

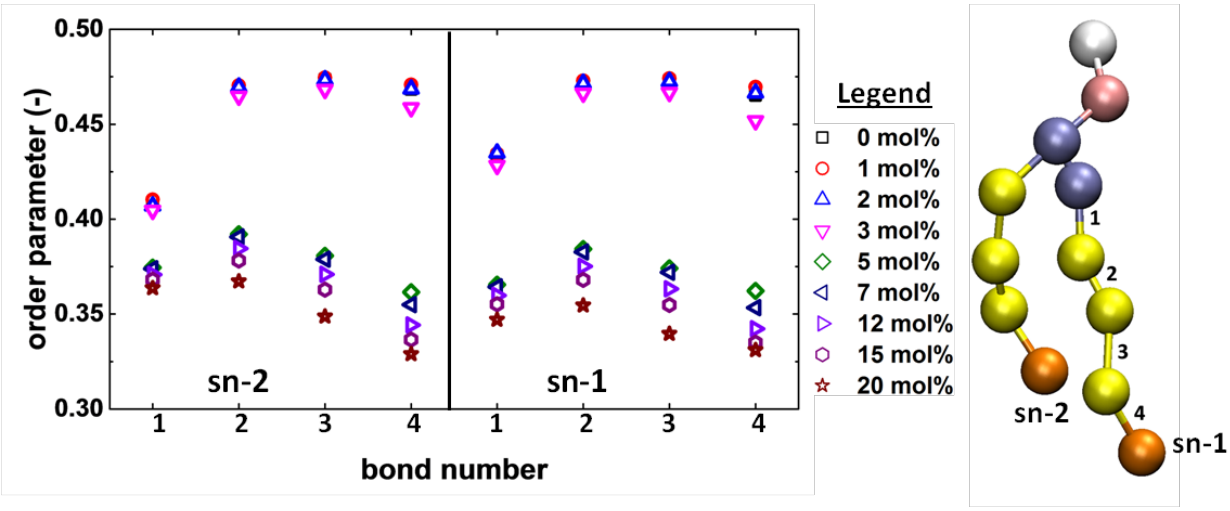

Figure 4-6: Coarse-grained order parameter profiles calculated along the bonds (vectors) connecting CG sites constituting DPPC tails for different BHB concentrations.

Here, the presence of BHB at concentrations below 5 mol% has little effect on the order parameter. However, at higher concentrations, the order parameter decreases considerably, indicating that the phospholipid tails become more disordered. The orientational order of phospholipid tails relates to the packing and fluidity of the membrane, with lower order implying looser packing and greater fluidity.

4.4.2 Distribution and Orientation of *Beta*-hydroxybutyric Acid

Our simulations indicate that the majority of BHB molecules reside near the phospholipid head groups and do not penetrate into the tail region of the membrane. This can be observed both in the simulation snapshot in Figure 4-2 as well as in the density plots in Figure 4-7. These normalized mass density plots show the relative positions of all the species in

a system containing 1 mol% BHB; they indicate that the majority of BHB molecules reside near the phospholipid head groups in the bilayer and close to the water phase.

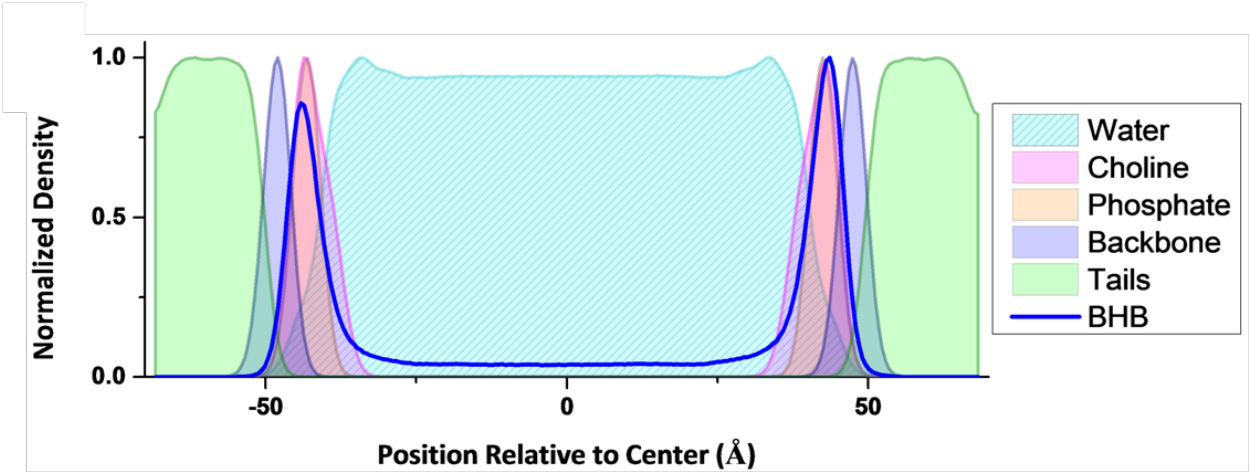

Figure 4-7: Normalized mass density distribution of DPPC bilayer containing 1 mol% BHB.

Simulation snapshots reveal that when interacting with phospholipids, BHB assumes specific orientations with respect to the normal to the interface depending on concentration. A measure of this orientation is the angle between the interface normal and the vector connecting the carboxyl group to the terminal hydroxyl group in the CG representation of BHB (Figure 4-1).

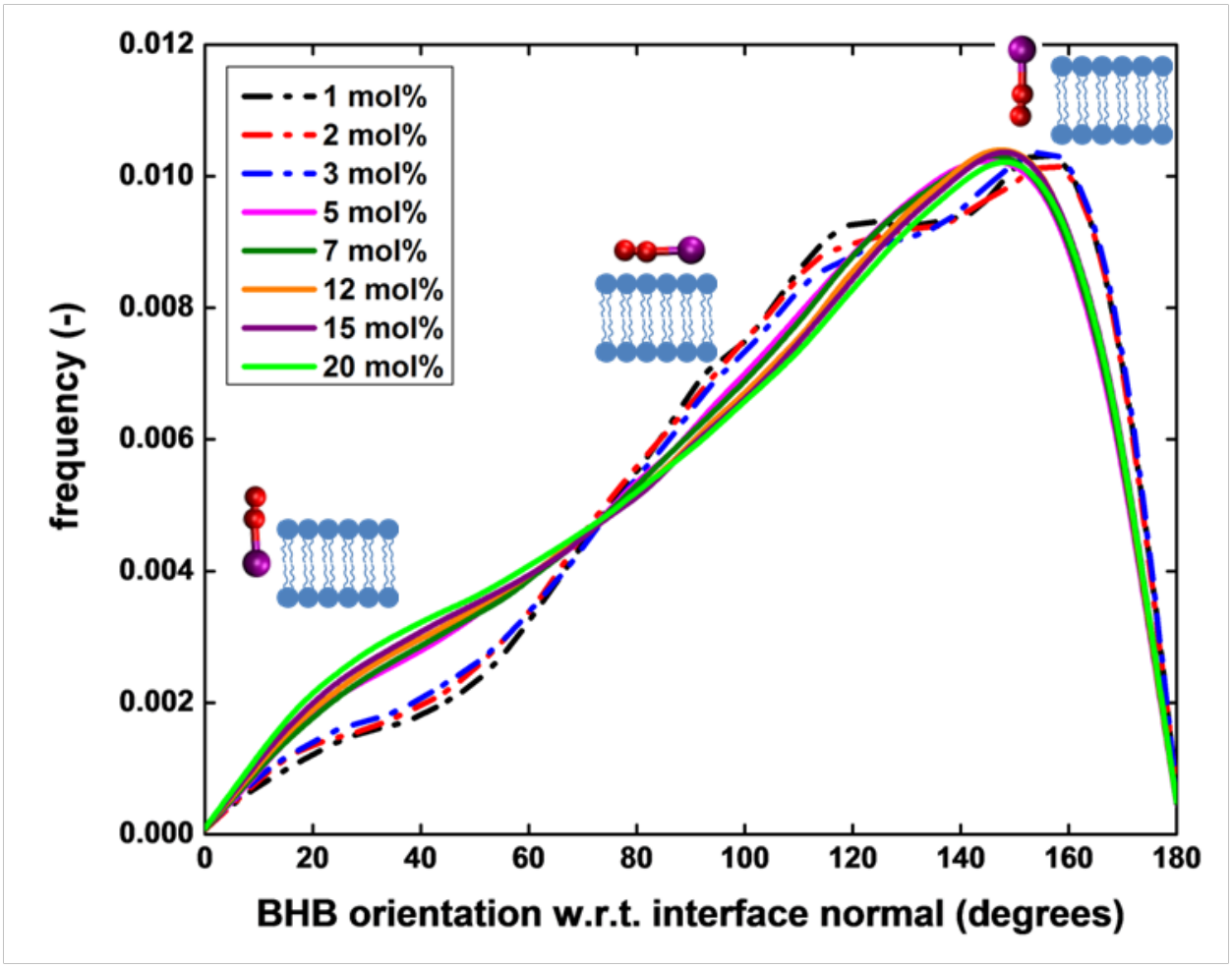

Figure 4-8: Comparison of the distributions of tilt angle between the interface normal and a vector connecting the carboxyl group to the terminal hydroxyl group of BHB embedded in DPPC membrane.
Overlaid: approximate orientations of BHB in relation to bilayer at various angles (not drawn to scale).

Distributions of tilt angle between the interface normal and the BHB carboxyl-hydroxyl vector of molecules embedded in DPPC membranes are shown in Figure 4-8. These distributions show a preference for larger tilt angles (peak at approximately 160 degrees), indicating the vector connecting the carboxyl group to the terminal hydroxyl group of BHB molecules lies virtually

anti-parallel to the interface normal. The preference for larger tilt angles for BHB suggests a preferential specific interaction with the phospholipid molecule. Concentrations below 5 mol% appear to have a narrower distribution of BHB tilt angles possibly indicating that these smaller concentrations experience more confined or restricted environments.

Since BHB appears to have a preferred location and orientation within the bilayer, we investigated if interactions between BHB molecules play a role in the observed step function phenomena. We show the BHB-BHB pair radial distribution functions – g(r) (the probability of finding a second BHB molecule at a distance r from a BHB molecule) in Figure 4-9 at various concentrations. From these bimolecular distributions of BHB we observed no appreciable differences with increasing concentration of BHB. Ignore the plot for 1 mol%, which appears to indicate that fewer BHB molecules would be found within 4.7 Å of other molecules; this perceived lower radial distribution is due to poor sampling at this low concentration. Since, BHB-BHB radial distribution functions do not show any steep changes with concentration, we can rule out specific BHB-BHB interactions as the driving mechanism for the phenomenon of a step change in properties observed at 5 mol% BHB.

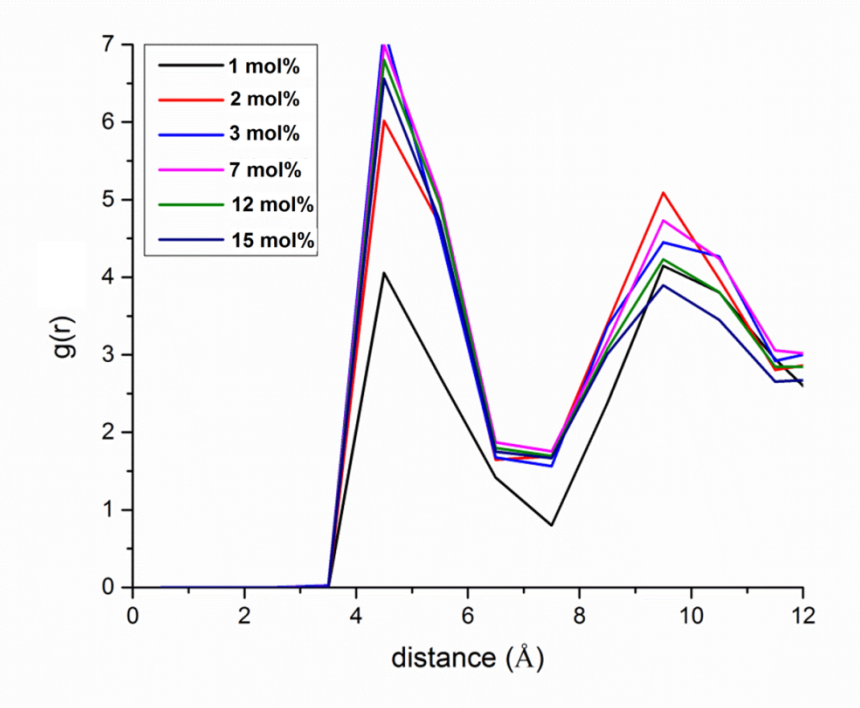

Figure 4-9: BHB pair radial distribution functions for various BHB concentrations.

4.4.3 **Local Effects of *Beta*-hydroxybutyric Acid in Phospholipid Bilayers**

Up to this point, we have considered only the average membrane properties in the presence of BHB. The results indicate that increasing concentrations of BHB results in structural and dynamical changes over the whole interface. We also observe that most properties change dramatically at and above a BHB interfacial concentration of 5 mol%. We now ask the question: Are there any phospholipid characteristics that are changed by the local presence of one or more BHB molecules? To answer this, we look at properties of specific molecules or groups of molecules.

First, we observe the diffusion dynamics of BHB at the interface. Do the BHB molecules interact with the same set of phospholipid molecules over time while in the bilayer or do they "travel" around? In Figure 4-10 we plot the random walks of single BHB molecules for a particular MD run for a system with a lower interfacial concentration of BHB (3 mol%) and compare this with that of single BHB molecules for a system with a higher concentration of BHB (7 mol%). We note that at lower concentrations, the BHB molecules explore rather limited areas, whereas they explore a much larger surface area at the higher concentration.

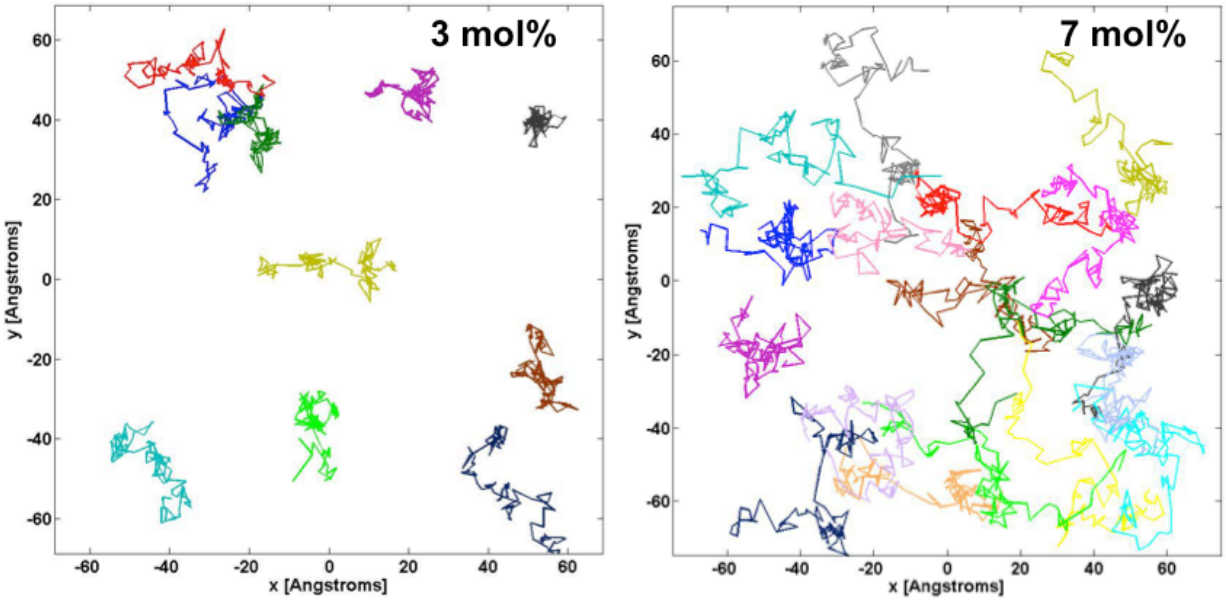

Figure 4-10: Random walk trajectories of several BHB molecules in DPPC bilayers at interfacial concentrations of 3 mol% (left) and 7 mol% (right). Each molecule trajectory is shown in a different color.

Finally, we interrogate our bilayer cross section to understand the effects of differential BHB diffusion on the phospholipids. Measures of this are spatially resolved two-dimensional (2D) maps of phospholipid properties. In Figure 4-11, we show the spatial mapping of the order parameters of DPPC tail bonds.

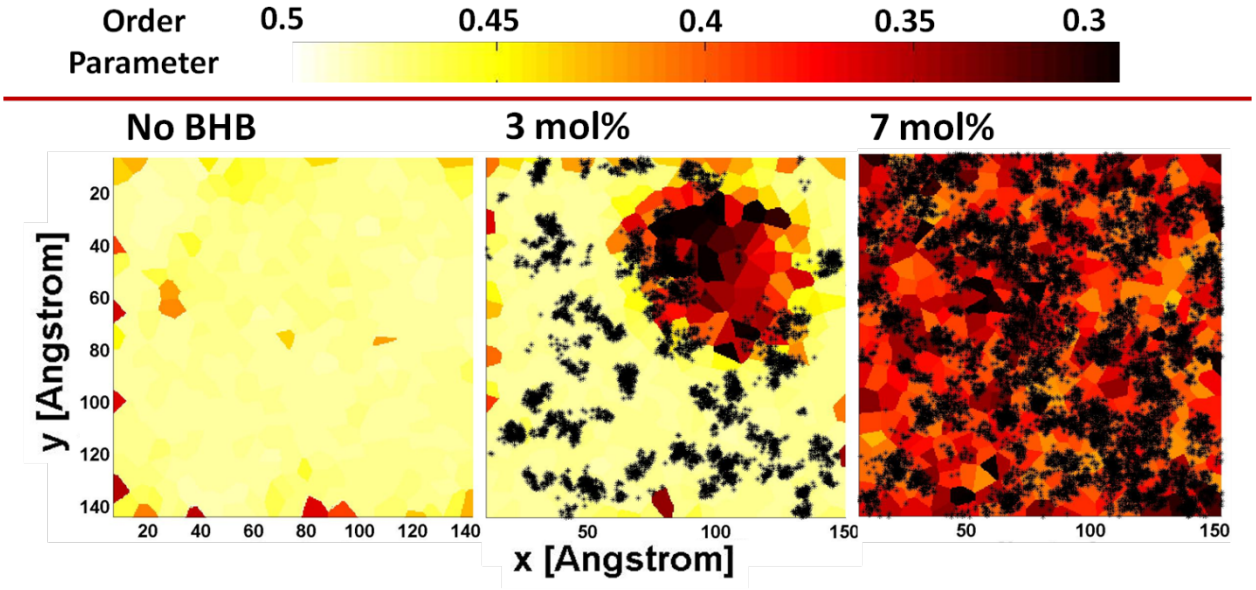

Figure 4-11: Spatially resolved and time averaged 2D order parameter maps for DPPC membranes at BHB concentrations of zero (left), 3 mol% (middle) and 7 mol% (right). Each polygon represents one DPPC molecule with color scale indicating degree of order. Instantaneous positions of BHB molecules at each time point are overlaid as black dots.

These color-coded 2D plots show the order parameter (tilt angle) of bond number 3 in the sn-1 acyl tail (see bond numbering on DPPC molecule in Figure 4-6) of all the phospholipids in one leaflet of the membrane, averaged over time. (Similar results are produced irrespective of

which bond is chosen.) Darker colors indicate greater disorder and lighter colors show bonds that are more aligned with the membrane normal. Each polygon represents the time-averaged order parameter of the sn-1 bond #3 of one DPPC molecule. The instantaneous positions of BHB molecules at every time point are overlaid as black dots. These BHB positions are not averaged over time.

By disaggregating the average properties of the system, we find localized structural changes in the bilayer. In the 2D grid display in Figure 4-11, we illustrate that changes in the local order parameter are not homogeneous. In fact, we observe that lower concentrations of BHB stimulate small, localized regions of disorder; these grow in area with increasing BHB concentration. At higher concentrations, the regions of disorder coalesce into larger areas and expand to include the entire membrane. At the threshold concentration of 3 mol% above which many properties of the membrane change dramatically, the disordering effect corresponds to an area that covers about 15% of the interface. We have seen in Figures Figure 4-3 to Figure 4-6 that several average characteristics of the phospholipid bilayer exhibit this threshold phenomenon (step function) with respect to BHB concentration; i.e., the changes are small at lower concentrations and then a sudden jump to more pronounced values at a particular concentration, then only slight changes with further concentration increases. We find in Figure 4-11 that looking at the localized structural changes engendered by individual BHB molecules leads to a better understanding of the step function behavior, the eventual coalescence of ever-widening areas of influence of BHB molecules with increasing concentration at the interface.

4.5 **Discussion and Conclusion**

When BHB interacts with the phospholipid membrane, it alters the characteristics of the bilayer. The phospholipid head groups begin to tilt toward the water initially but suddenly snap back to an almost parallel configuration at 5 mol% BHB. This sudden change may indicate a loss of membrane integrity as it coincides with a dramatic disordering of the DPPC tails. These molecular changes cause the membrane as a whole to expand laterally, which increases the average area per lipid, permitting water to penetrate farther into the bilayer. At the same time, the mean lateral pressure of the membrane increases. What is interesting about these changes is that they are non-monotonic with increasing BHB concentration. At low concentrations, the effects on the membrane characteristics are relatively small but a steep change occurs at interfacial BHB concentrations of 5 mol%. This is observed for area per lipid in Figure 4-3, for mean lateral pressure in Figure 4-4, and for average order parameters in Figure 4-6. Higher concentrations more than double the surface pressure of the phospholipid membrane, which is in line with experimental observations by Hsu et al. [51] [Caveat: The MARTINI force field is known to underestimate surface pressure, however the trend qualitatively compares well with experimental observations.]

To investigate the nature of this phenomenon further, we considered the possibility that the steep change may be due to BHB-BHB interactions becoming crucial to some alteration of the lipid membrane. However, BHB-BHB radial distribution functions do not show any steep changes with concentration. Therefore, we can rule out specific BHB-BHB interactions as the driving mechanism for the phenomenon.

While viewing the trajectories of individual BHB molecules projected onto the interfacial surface, we discovered the random walks of the BHB to be fairly tight at lower concentrations, whereas they covered a very wide area at higher concentrations (Figure 4-10). This suggested that in the latter case, the membrane had expanded sufficiently, such as to begin to lose its integrity, thereby permitting the BHB molecules to explore a very wide area. Viewing individual BHB trajectories in this manner led us to quantify the increasing phospholipid disorder by constructing spatially resolved 2D maps, as shown in Figure 4-11 – the spatial distribution of the local order parameter in a grid display. It can be observed here that low concentrations of BHB stimulate small, localized regions of disorder. These individual regions of disorder grow in size with increasing concentration of BHB molecules at the interface. At high concentrations, the regions of disorder have expanded to include the whole interface. At some critical BHB interfacial concentration (5 mol% in our simulations) the lipid disorder has propagated to the entire membrane and possibly compromised its integrity. The effective range of the BHB molecule (its radius of influence) can be considered in terms of the number of neighboring lipids that become disordered by virtue of BHB interaction with the membrane. We speculate that as the concentration of BHB is increased, these areas of influence could eventually touch each other. At a high enough concentration, the localized disorder becomes propagated throughout the entire membrane and the average properties undergo a steep change.

We believe this may be a non-specific effect, that is, another metabolite molecule with its own chemical functional groups interacting with a lipid membrane would have its own specific radius of influence, but the propagation of the disorder throughout the entire membrane occurring when these areas of influence eventually touch each other could be a more general

phenomenon. That is, the threshold effect at a specific concentration is likely not unique to BHB. For example, the observed response by the phospholipid bilayer to BHB absorption is similar to that observed from membrane uptake of anesthetics [20, 26, 140, 159].

We may have demonstrated in this example, a general mechanism by which small molecules (drugs, metabolites) change membrane properties. In turn, the altered membranes can modulate protein receptor or protein channel function. It is important to note here that diabetic patients and animals exhibiting consciousness-impairment symptoms have been shown to have BHB blood concentrations above about 5 mM [48, 206, 208, 209]. Patients with blood concentrations below this value tend to be asymptomatic. This distinguishes subclinical concentrations from clinical ones. In fact, blood concentrations of BHB below 5 mM are used in clinical settings to induce ketoacidosis in epileptic patients [212, 213]. At these lower concentrations, consciousness impairment symptoms are not observed, however, the slightly elevated metabolite concentrations appear to have a therapeutic effect on the epileptic patients. Our simulations may have inadvertently stumbled upon an important physical phenomenon that relates interfacial concentrations of BHB to the occurrence of consciousness impairment symptoms in patients.

The BHB molecule possesses a hydroxyl group and a carboxylic acid group at the two ends. To discover if there are any essential chemical functional groups required for a metabolite to cause similar effects as those observed for BHB, it will be necessary to investigate other metabolites and anesthetic molecules using the same approach we have used here. A systematic investigation of metabolites and drugs that impair consciousness by this approach would help define the role of membranes as drug targets.

5. LIPID EMULSIONS FOR THE RAPID REVERSAL OF DRUG TOXICITY

5.1 Introduction

In the United States, unintentional poisoning is the leading cause of death from injuries, surpassing even motor vehicle accidents and suicide [214]. Of these mortalities, over 90% are due to drug intoxications. Drug overdoses from legal medication or illegal drugs occur frequently and unpredictably. Whether an overdose is accidental or intentional, the reversal of drug toxicity remains a serious clinical challenge [215]. This is because most pharmaceutical agents have no known antidote. In many cases, the compound causing intoxication is unknown or is only one agent in a polysubstance overdose [216, 217]. Currently, the treatment of patients suffering systemic toxicity and cardiac failure following an overdose relies primarily on a set of advanced cardiovascular life support (ACLS) methods, with varied outcomes [218, 219]. These urgent treatment methods include cardiopulmonary resuscitation (CPR) and defibrillation. Unfortunately, in some cases, patients remain unresponsive to the ACLS interventions.

5.1.1 Reversal of Drug Toxicity by Lipid Emulsions

Clinical reports, case studies, and *in vivo* experiments suggest that intravenous infusion of a simple oil-in-water formulation (a lipid emulsion) rapidly resuscitates patients from cardiac arrest and reverses the toxic effects of a range of pharmaceutical agents [52-56]. These parenteral nutrition emulsions have been traditionally used in clinical settings to intravenously supply patients with vital nutrients in situations where the gastrointestinal tract is compromised [91, 220].

Patient resuscitation using lipid emulsions, dubbed 'lipid rescue', has been used successfully in patients before the onset of cardiac arrest to facilitate rapid reversal of systemic toxicity [115, 116, 221, 222]. It has also been shown to be effective for resuscitation after intoxication in situations involving local anesthetic drug overdose in both animal studies and human patient cases. Specific pharmaceutical agents for which lipid therapy has been successful in remediating toxicity include antidepressants [216, 223], calcium-channel blockers [224], beta blockers [225], anticonvulsants [216], atypical antipsychotics [217], selective serotonin reuptake inhibitors (SSRIs) [217], and nitrovasodilators [56]. Patients that were unresponsive to traditional ACLS approaches were able to rapidly regain a spontaneous cardiac output (in as few as 60 seconds in one case [226]).

Intravenous lipid emulsions may prove to be a 'silver bullet' for the treatment of drug overdoses as well as toxicity due to chemical warfare agents, pesticide poisonings, and even snake venom [215]. Although treatment of overdoses with lipid emulsions has been shown to be effective with few side effects [226, 227], many clinical practitioners will not consider using lipid therapy because questions still remain. Questions such as how this treatment should be combined with other drugs, concerns about the safety of the high doses of lipid emulsion used [227], as well as the actual mechanism of action of detoxification, still need to be addressed.

5.1.2 **Hypothesized Mechanisms of Action**

Recent reports incorporating small animal experiments and pharmacokinetic modeling [228-231] indicate that the action of lipid emulsions as detoxification agents is multifaceted. One mechanism, which is specific to the cardiotoxic local anesthetic drug bupivacaine, posits

that this drug inhibits fatty acid metabolism and suppresses ATP production. The intravenous delivery of lipid droplets provides excess fatty acids to overcome this inhibition. Another mechanism of action is the direct increase in the strength of heart muscle contractions by the cardiotonic effect of the lipid emulsion.

The most prevalent theory of the action mechanism of lipid emulsions is a physicochemical scavenging known as the 'lipid sink' [56, 57]. A key feature of the lipid emulsion is the ability of its constituent particles to act as toxin scavengers. This scavenging action is commonly believed to be limited to acting only on highly lipophilic toxins, with hydrophobic partitioning as the primary driving force. In the lipid sink mechanism, oil droplets are thought to bind or sequester the lipophilic drug molecules in the blood plasma through a non-specific mechanism. In the body, the concentration of the drug in tissues is related to the unbound concentration of drug in the blood plasma. Thus, a scavenging mechanism by the lipid emulsion droplets would sequester drugs within droplets (Figure 5-1); this would shift the equilibrium and cause drugs to be released from tissues back into the blood stream, resulting in reduced overall tissue drug concentrations. Hence, the toxin concentration in critical organs such as the heart is lowered, and these organs are able to recover. It is thought that lipid droplets provide a discrete oil phase with which lipophilic molecules may preferentially associate. A 2011 report [232] claimed that knowledge of the drug lipid partition coefficient and volume of distribution are sufficient to predict the efficacy of lipid therapy based on the lipid sink effect.

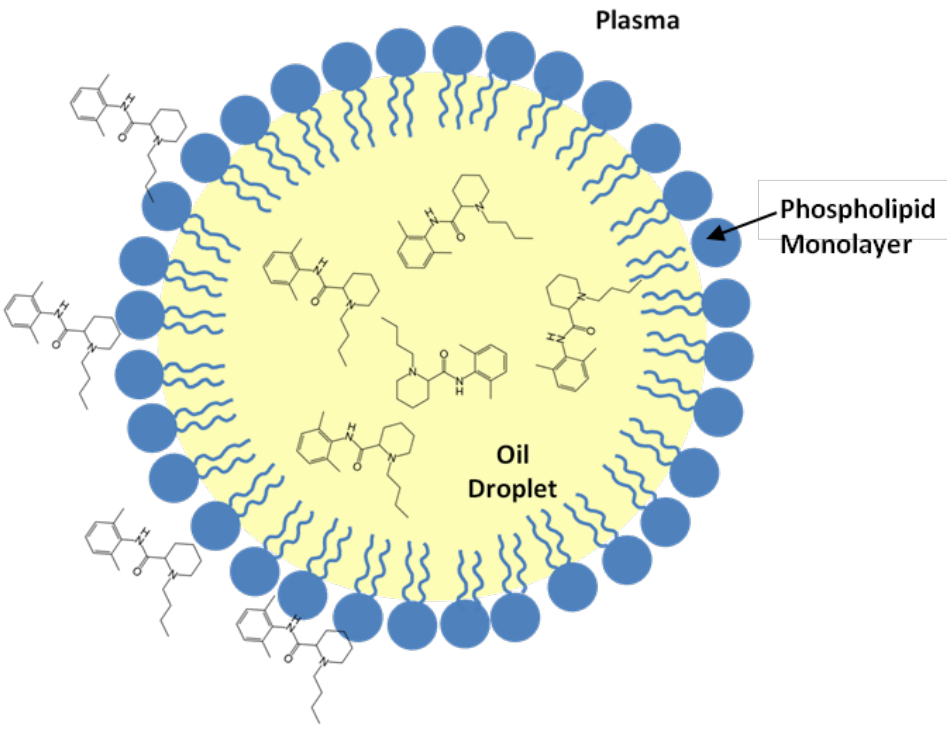

Figure 5-1: Schematic of theoretical lipid sink mechanism of toxin sequestration by an oil droplet.

The overarching question remains however: to what extent is a lipid droplet capable of non-specific binding of drug molecules? Underlying that is the fundamental question: what properties of this colloidal formulation dictate its interaction with small molecules in an aqueous environment? As noted earlier, the prevailing hypothesis is that lipophilic drug molecules are sequestered by lipid droplets by virtue of their ability to easily partition into the oil phase. However, many of the compounds for which toxicity has been reversed by this therapy exist in a predominantly ionized state at physiological pH (based on pKa values). These ions are more capable of hydrogen or dative covalent bonding (depending on charge) and therefore remain more soluble in aqueous environments. Nevertheless, lipid therapy has been

shown to be very effective for intoxication with these types of drugs. In addition, during cardiac arrest, the possibility of acidosis occurring is high [233-237], further reducing blood pH levels and increasing the degree of molecular protonation for positively charged species.

The surfaces of lipid droplets are composed of zwitterionic and anionic phospholipid molecules [238, 239], therefore electrostatic interactions are likely to play an important role in driving the sequestration of toxins. Furthermore, clinical reports exist that credit lipid droplets with reversing toxicities even for drugs of moderate lipophilicity [240]. It has also been observed that structurally dissimilar molecules appear to associate with lipid dispersions. While it is apparent that only one hypothesized mechanism is insufficient to fully describe the action of lipid emulsion therapy, for a rational application of lipid biodetoxification, it is first necessary to clarify the key physicochemical characteristics that govern the association of toxin molecules with lipid droplets.

It is clear that direct lipophilic partitioning cannot be the only molecular mechanism by which drugs are sequestered by lipid emulsions. Because many of the toxins shown to be susceptible to lipid therapy exist in a predominantly ionized state at physiological pH, electrostatic interactions would exist between the ionized toxins and the zwitterionic or charged phospholipid interface. The unprotonated fraction of drug molecules may, on the other hand, cross over and reside within the core of the lipid droplet, although the phospholipids present a barrier to entry due to their amphiphilic structure and close-packed configuration. Thus, the association of the toxin molecules with the emulsion particulates may be influenced by one or more of the following factors: (i) the charge of the constituent phospholipids (since membranes containing anionic phospholipids have been shown to sequester more toxin

molecules [241-243]), (ii) the pKa of the toxin molecules (because higher pKa values correspond to higher fractions of protonated species at physiological pH), (iii) the acyl tail ordering caused by interactions between phospholipid and triglyceride tails (since this may alter phospholipid to packing), and (iv) the size, shape and distribution of polar groups of the toxin molecules.

In this chapter, we use molecular dynamics simulations to understand the molecular mechanisms that constitute the lipid emulsion – toxin molecule encounter. This molecular dynamics approach is one part of a larger study of lipid therapy in our research group, which includes pharmacokinetic/pharmacodynamic modeling and collaborative small animal studies [228-231]. None of these other studies can reveal the molecular details, however. By coupling the molecular dynamics results with experimental measures of binding performance and pharmacokinetic/ pharmacodynamic models, the validity of the lipid sink hypothesis can be assessed from a multi-scale viewpoint.

To probe the association of toxin molecules with emulsion particulates, we employ a coarse-grained molecular dynamics scheme to clarify the relative roles of lipophilicity, charge, size and other factors in mediating toxin sequestration. This particular approach has not previously been applied to a monolayer system of this type and will allow the study of a sufficiently large system over adequately long timescales to obtain structural, dynamic and thermodynamic information about transport through the phospholipid monolayer. In this work, both neutral and ionized coarse-grained topologies are developed for six small toxin molecules with varying levels of lipophilicity and differing degrees of protonation at physiological pH. These topologies are then incorporated into a multiphase droplet system consisting of a dipalmitoylphosphatidylcholine (DPPC) monolayer at an aqueous/lipid interface.

We find some similarities among the toxins in their association with the oil droplet, even for molecules of low lipophilicity where association with oil droplets would not conventionally be expected. We investigate the role in the toxin – droplet interaction of molecular attributes such as protonation state, size, and the presence of polar moieties. Furthermore, we explore the partitioning of toxins between the aqueous phase, the droplet interface, and the lipid core.

5.2 **Creating an Oil Droplet Model**

The emulsion generally used in lipid therapy is a dispersion of soybean oil in an aqueous medium stabilized by soybean or egg yolk phospholipids [244, 245], which are mostly zwitterionic with a small percentage of anionic lipids [238, 239]. These emulsions are FDA approved for use in humans and are readily available in clinical settings as a source of intravenous nutrition. The emulsions are generally recognized as safe – even for this off-label application, and consist of particulates including lipid droplets, liposomes, and other more complex structures [246]. Commercial lipid emulsion formulations vary substantially in their composition. Some are formulated from natural oils such as soybean [220, 247, 248], safflower [247], olive [249], and fish oil [248]. While others are formulated with structured triglycerides, which are fatty acid chains of different lengths esterified to the same glycerol backbone [250].

In order to investigate the molecular level association of toxin molecules with an oil droplet, we created a model system using a dipalmitoylphosphatidylcholine (DPPC) monolayer at the interface between water and glycerine trioleate (triolein). A simple model of this type can provide insight into the molecular consequences of interactions between small molecules and oil droplets without confounding the results with variable composition. The knowledge

gleaned from this method can be used as a tool to predict which molecules will interact favorably with droplets and the mechanism by which they will be sequestered.

5.2.1 **Molecular Dynamics Simulations**

Coarse-grained molecular dynamics (MD) simulations of DPPC monolayers at water/triolein interfaces were employed in this thesis to study the nature of the interactions between small toxin molecules and lipid droplets. Steered MD simulations were performed using LAMMPS software described in Section 2.5. Partition coefficient estimation simulations were performed using the BAR implemented in Gromacs (details in Section 2.4.5).

5.2.2 **Molecule Topologies**

The MARTINI coarse-graining approach and force field [79, 80] was employed to create molecule topologies and to study the interactions of toxin molecules with fully solvated DPPC monolayers at the interface between water and the symmetrical triglyceride – triolein. The coarse-grained geometries for DPPC, glycerine trioleate (triolein), and water were downloaded from the MARTINI website (http://md.chem.rug.nl/cgmartini/).

Due to its close association with the history of lipid emulsion therapy and extensive studies in the literature [53, 55, 115-117], the cardiotoxic local anesthetic drug bupivacaine is an excellent initial candidate for molecular investigation. Five other potentially toxic drugs with higher and lower lipophilicity values were compared to bupivacaine (Table 5-1). Bupivacaine is lipophilic and highly protonated at physiological pH. In contrast, though also protonated at physiological pH (with a larger pKa value than bupivacaine), a drug such as the hepatotoxic pain

and fever reducing drug, acetaminophen [118-120] is much more polar and therefore more soluble in aqueous environments. The hydrophilic nature of this molecule makes the acetaminophen/oil droplet interaction study a useful comparison to that of bupivacaine, since its behavior can provide important insight into whether electrostatics plays a significant role in drug molecule sequestration by emulsion droplets.

Mepivacaine, another local anesthetic, is almost identical in structure to bupivacaine, with the exception of the terminal butyl group possessed by bupivacaine. Although the two molecules are similar, and successful resuscitations of patients with mepivacaine toxicity, among other drugs, have occurred [53, 54, 251], mepivacaine is less lipophilic than bupivacaine and has been predicted by experimental techniques to be sequestered to a lesser extent than bupivacaine by lipid emulsions [252]. Bupropion is another drug for which successful resuscitation has occurred after onset of toxicity [216]. Unlike bupivacaine and mepivacaine, however, it is an antidepressant and smoking cessation aid [253, 254], but has a log*P* value similar to that of bupivacaine.

The drugs introduced above are all highly protonated at physiological pH. In contrast, the anticoagulants warfarin and brodifacoum are negatively charged at physiological pH. Brodifacoum has a log*P* value much larger than that of bupivacaine, while the partition coefficient of warfarin is only slightly smaller than that of bupivacaine. By understanding the interactions of these six drugs with a lipid droplet model, insight may be gained into the mechanism of toxin sequestration by lipid emulsions in general.

TABLE 5-1: TOXIN PROPERTIES

Toxin	Literature log*P* [255]	pKa	Physiological charge	% ionized	Simulation log*P*
Acetaminophen	0.46	9.38	+1	99	0.39 ± 0.14
Mepivacaine	1.95	7.6	+1	61	2.03 ± 0.21
Warfarin	2.7	5.08	-1	99.5	3.10 ± 0.16
Bupropion	3.2	8	+1	80	3.21 ± 0.18
Bupivacaine	3.41	8.21	+1	87	3.38 ± 0.19
Brodifacoum	8.5	4-5	-1	99+	8.65 ± 0.59

We based our coarse-grained representations of the toxin molecules on the centers-of-mass of grouped heavy atoms corresponding to interaction sites. The properties of the toxin molecules we studied are listed in Table 5-1 and chemical structures along with coarse-grained representations for each of the toxins are illustrated in Figure 5-2. The interaction sites were characterized using the standard MARTINI interaction types; the coarse-graining scheme was developed in each case using methods described in Section 2.4. The equilibrium bond lengths and angles for all toxin molecules were selected to preserve the underlying geometry and molecule size. Since they all exist as acid-base pairs and are predominantly found in their ionized states at physiological pH, we considered both neutral and charged forms in our simulations.

These coarse-grained models were initially validated by reproducing the drug octanol/water partition coefficients. The log*P* values we estimated by the free energy difference between the molecules in water and water-saturated octanol from simulations are listed in the last column of Table 5-1. These values are comparable to the experimental and predicted octanol/water partition coefficients found in the literature for each neutral species;

therefore we are confident that our coarse-graining scheme for these species can be used for the molecular dynamics simulations.

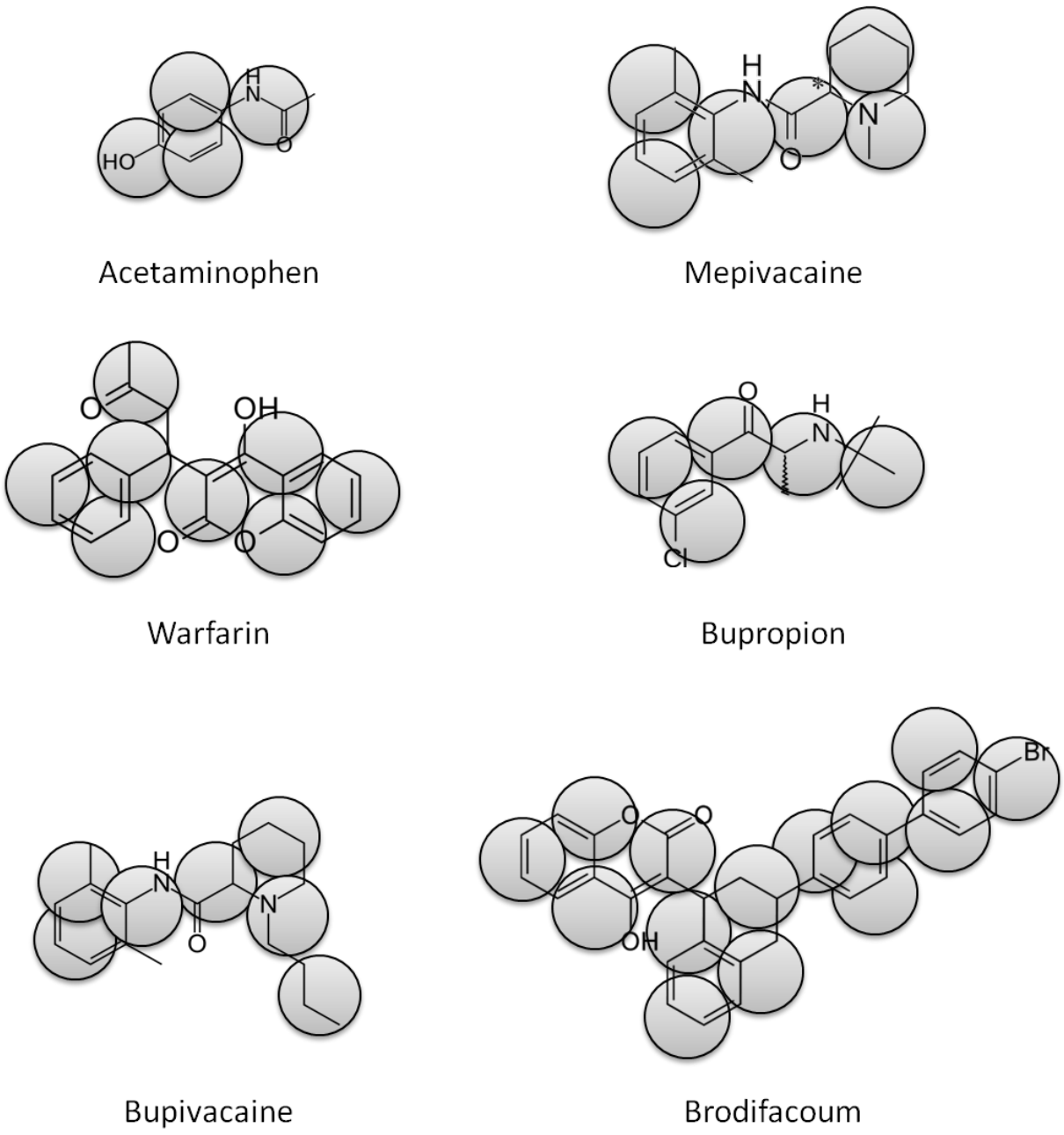

Figure 5-2: Two-dimensional structures of toxins overlaid with the coarse-grained representation of each molecule.

5.2.3 **Simulation System**

Each simulation system consists of a central oil core containing 1000 triolein molecules, surrounded on both sides by water slabs containing 4000 coarse-grained water particles each (Figure 5-3). At each interface between oil and water is a phospholipid monolayer containing 100 DPPC molecules in each leaflet. The polar head groups of DPPC are fully solvated in the water phase and the hydrophobic tails associated with the triolein molecules. We start with either a neutral or charged toxin molecule in the aqueous phase. For the simulations containing an ionized molecule, depending on the physiological charge of the toxin, a Cl^- or Na^+ counter ion was added to maintain charge neutrality.

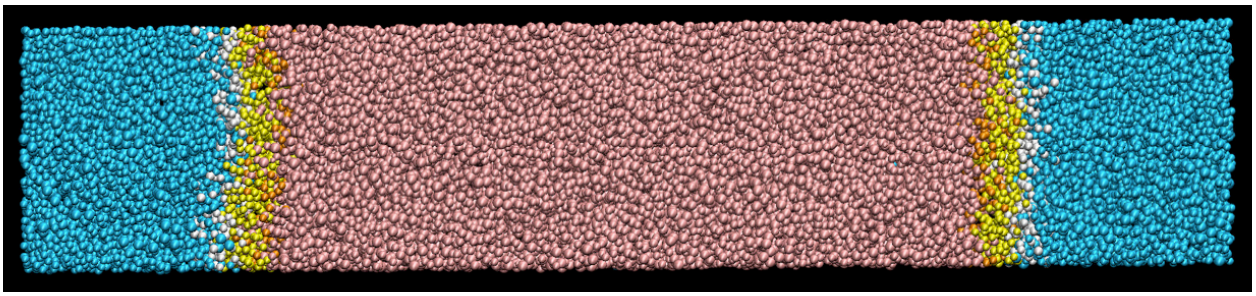

Figure 5-3: Snapshot of simulation cell containing fully equilibrated DPPC monolayers at the water/triglyceride interface.
DPPC head groups and glycerol backbones are shown in white, while tails are in yellow with orange terminals. Triglycerides are pink and water is blue.

5.2.4 **Constant Velocity Steered Molecular Dynamics Simulations**

To estimate the thermodynamic free energy profiles for moving toxins from an aqueous phase into the oil droplet, we performed steered molecular dynamics simulations in which a toxin molecule was pulled from water through the DPPC monolayer into triolein, as described in Section 2.5.4. Each simulation run consisted of a 450 ns equilibration phase during which the target toxin molecule was constrained in the bulk water phase by tethering the center-of-mass to a fixed z-position using a harmonic spring potential. A further 10 ns short post-equilibration simulation was performed to obtain a distribution of initial toxin configurations for constant velocity simulations.

Each steered simulation production run was for 200 ns using a spring constant of 40 Kcal/mol/ $Å^2$ and a pulling velocity of 1 Å/ns. This pulling velocity is over 1000 orders of magnitude smaller than the root mean square thermal velocity (Equation (5-1)) of 1048 Å/ns for DPPC, thereby ensuring that the layer is not needlessly perturbed as the toxin molecule is pulled through.

$$v_{pull} \ll v_{th} = \sqrt{\frac{3k_B T}{m}}$$

(5-1)

To estimate the free energy change of moving toxins into the oil droplet from the work performed as they transited through the system, we used the isobaric-isothermal Jarzynski equality (see Section 2.5.4 and Equation (2-16)). Because the transition of toxins from water to oil was very slow, we assumed that the process was reversible (due to our small pulling velocity

of 1 Å/ns) and used the first order cumulant expansion average (Equation (2-17)) to obtain estimates of the free energy as well. Free energy profiles for moving toxins from water, through a DPPC monolayer and into an oil phase were obtained in the manner described in Section 2.5.4. Each steered molecular dynamics simulation was replicated 10 times in order to reduce systematic errors in estimating the free energy differences. Each iteration corresponded to a different initial configuration as derived from the z-constrained post-equilibration simulations.

The general methods used in the simulations are described in Section 2.5. A time step of 20 fs was used to integrate the equations of motion [130-132]. An isothermal-isobaric (NPT) ensemble was maintained which allowed the volume (and hence the cross sectional area) of the systems to fluctuate freely. During equilibration, Berendsen [127] protocols were used for both temperature and pressure coupling. After equilibration, each component of the simulation systems were coupled separately to a temperature bath using Nose-Hoover protocols [184-186] with a coupling constant of 1.5 ps as well as to a semi-isotropic barostat at 1 atm with a coupling constant of 5 ps using a Parrinello-Rahman scheme [132]. Semi-isotropic pressure coupling was used to maintain a tensionless monolayer.

5.3 Results and Discussion

A snapshot of one fully equilibrated droplet system is shown in Figure 5-3. Occasionally during our simulations, water particles crossed the phospholipid monolayer on one side, through the triglyceride slab and across the monolayer on the other side. This ability of water to cross the triolein layer was not mentioned in an atomistic oil droplet simulation of similar structure to ours [91], although that may be due to their much shorter simulation (50 ns). We note that triolein has been shown to contain up to 5.1 mol% of water at 25 °C [256]. We observed a high degree of intercalation between the DPPC tails and the triolein tails. DPPC and triolein molecules in our system, however, never exited their respective domains.

5.3.1 Averaging Method Choice for Work Profiles

Each steered molecular dynamics simulation produced a work profile representing the force needed to keep the toxin molecule tethered as the tether point was moved from water into oil. The ensemble of 10 work profiles for every toxin molecule was averaged using Equations (2-16) and (2-17). These averages represent the Gibbs free energy change associated with movement of each toxin molecule from water, through the DPPC monolayer, into the oil phase. The exponential average from the Jarzynski equality (Equation (2-16)) is difficult to estimate because this average is dominated by cases for which the work value is small [155, 156]. Such cases are rare and, therefore, not often sampled in simulations. We show in Figure 5-4, the difference in averaging techniques for two representative toxins (acetaminophen and bupivacaine).

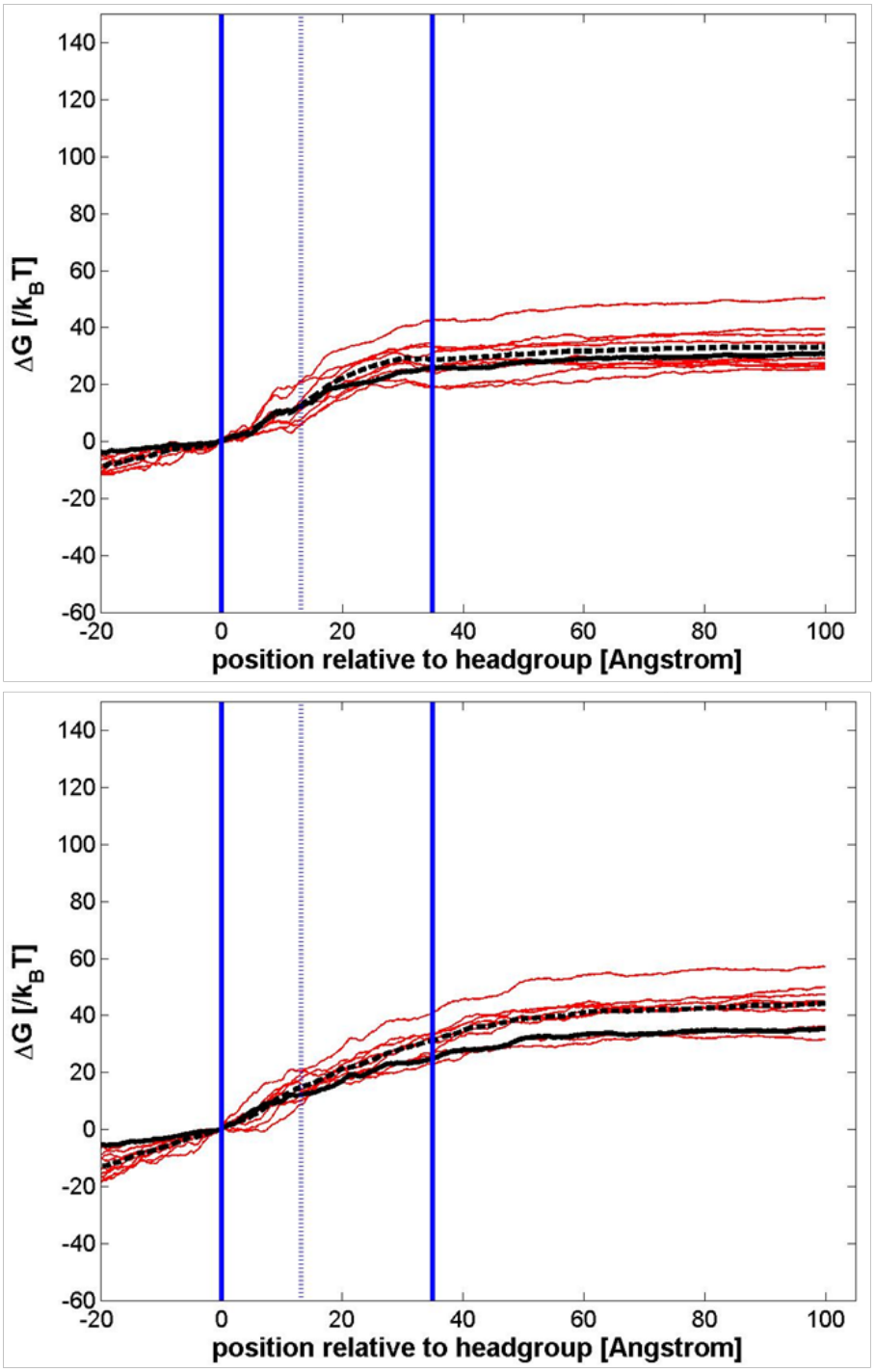

Figure 5-4: Comparison of work profile (red lines) averaging methods for acetaminophen (top) and bupivacaine (bottom).
The exponential average is a solid black line and the first order cumulant expansion average is a dotted black line.

The work profiles for each of the 10 steered simulation runs are shown as red curves with the associated Jarzynski average overlaid as a solid black curve. The first order cumulant expansion average is shown as a dotted black curve in Figure 5-4. The mean position of the DPPC monolayer in the z-direction is indicated by solid blue vertical lines and the glycerol backbone position is a dashed blue vertical line. The average DPPC head group position was made the reference state for all work profiles before averaging; hence both the z-position and the Gibbs free energy at that position were set to zero, i.e., $\Delta G(z=0\ \text{Å}) = 0\ k_B T$.

It is clear from the bupivacaine work profiles in Figure 5-4 (bottom) that the Jarzynski exponential average (solid black curve) is heavily weighted by the smaller work profiles. This causes a large discrepancy between the exponential average and the first order cumulant average (dashed black curve), except in the case of acetaminophen Figure 5-4 (top), for which the difference is not large. For all six of the toxins we considered here, we used the first order cumulant expansion average to estimate free energy differences for transfer of the toxins to various points in the simulation systems.

5.3.2 **Effects of lipophilicity and charge**

5.3.2.1 **Activation Energy: Water to Oil**

For all toxins, the maximum free energy value occurs in the oil phase, indicating a lower affinity of these molecules for this phase compared to other locations in the system. We find that passage through the DPPC monolayer and entry into the droplet is an activated process. The difference in free energy between water and oil corresponds to the activation energy required to enter the oil phase from water. The magnitude of this activation energy differs for

each toxin and between neutral and charged species (Table 5-2). In most cases (except for acetaminophen), the neutral species have lower activation energies for crossing the DPPC monolayer into oil than charged species. For acetaminophen, however, the magnitudes of the activation energy for neutral and charged species are nearly identical. Activation energies for neutral species increase with the following trend: bupropion < acetaminophen < bupivacaine < mepivacaine < warfarin < brodifacoum.

TABLE 5-2: ACTIVATION ENERGIES FOR ENTRY INTO OIL FROM WATER

Toxin	log*P*	Water to Oil Activation Energy [k_BT]	
		Neutral	Charged
Acetaminophen	0.46	29.3 ± 1.9	27.5 ± 1.5
Mepivacaine	1.95	34.8 ± 2.3	59.3 ± 2.7
Warfarin	2.7	48.2 ± 2.6	71.6 ± 5.1
Bupropion	3.2	23.5 ± 2.1	44.8 ± 3.0
Bupivacaine	3.41	31.2 ± 1.7	60.6 ± 4.8
Brodifacoum	8.5	52.9 ± 2.1	78.5 ± 4.0

Charged species follow a similar trend in activation energy increase to that of the neutral species with the exception of acetaminophen and bupropion, which are interchanged. The higher activation energies we observed for charged forms indicate that it may be less likely that these molecules will cross the DPPC monolayer to reside within the oil phase.

Contrary to prevailing thought [232], lipophilicity alone (as characterized by the partition coefficient - listed in Table 5-2 for comparison) does not predict the association of the toxins with oil droplets in either their neutral or charged forms. The differences in affinity of the

toxins for the droplet may depend on several other factors including protonation state, size, and the distribution of polarity within each small molecule.

5.3.2.2 **Activation Energy: Piecewise**

Although we observe that all six toxin species required an activation energy to enter the oil phase from water and that the neutral species generally required less energy, an interesting picture emerges when we break down the process of association with the droplet into two distinct parts. First, how much energy is required for a toxin to enter the phospholipid monolayer from water? Second, how much energy does this toxin need once it is in the monolayer to travel into the oil? The answers to these questions may shed some light on the mechanism by which different toxins are sequestered by oil droplets.

To obtain the activation energies for entry into the DPPC monolayer from water, we took the difference between the ΔG value in water and the maximum ΔG value in the head group or backbone regions of the monolayer. Those values are listed in Table 5-3.

TABLE 5-3: ACTIVATION ENERGIES FOR ENTRY INTO DPPC FROM WATER AND INTO OIL FROM DPPC

Toxin	log*P*	Water to DPPC Activation Energy [k_BT]		DPPC to Oil Activation Energy [k_BT]	
		Neutral	Charged	Neutral	Charged
Acetaminophen	0.46	13.1 ± 1.7	11.9 ± 1.9	16.2 ± 2.5	15.6 ± 2.4
Mepivacaine	1.95	12.2 ± 1.8	14.0 ± 1.9	22.6 ± 2.9	45.2 ± 3.3
Warfarin	2.7	19.5 ± 2.4	34.8 ± 3.5	28.7 ± 3.5	36.8 ± 6.2
Bupropion	3.2	7.8 ± 1.1	13.1 ± 1.5	15.7 ± 2.4	31.7 ± 3.3
Bupivacaine	3.41	15.0 ± 1.4	28.9 ± 3.8	16.2 ± 2.2	31.7 ± 6.1
Brodifacoum	8.5	22.4 ± 1.7	25.2 ± 3.5	30.5 ± 2.7	53.3 ± 5.3

For three of the toxins (acetaminophen, mepivacaine, brodifacoum), there is no real difference in affinity of neutral and charged species with the monolayer. In fact, for many of the toxins, the ΔG values for entry into the monolayer are low enough that fluctuations in system energy (which occur with a magnitude on the order of ~ 200 k_BT) could be sufficient to overcome the energy barrier, even for the charged species.

The situation is different, however, for entry into oil once toxins are in the monolayer. From the ΔG values shown in Table 5-3, the neutral forms of bupivacaine, bupropion and acetaminophen may be expected to enter the oil phase from the monolayer quite readily. For charged species here, once again, there is a steeper energy penalty for migration into the oil phase, with all species (except acetaminophen) showing higher ΔG values than for neutral species. Since all these toxins are highly ionized at physiological pH, this higher activation energy could prevent the majority of molecules from crossing from the DPPC monolayer into the oil. The charged molecules would also experience strong electrostatic interactions with the zwitterionic DPPC molecule head groups, making this location more preferable than the oil core. The effect of lipophilicity on the association of the six toxins with an oil droplet is summarized in Figure 5-5. There does not appear to be much correlation between log*P* and activation energy for any of the processes.

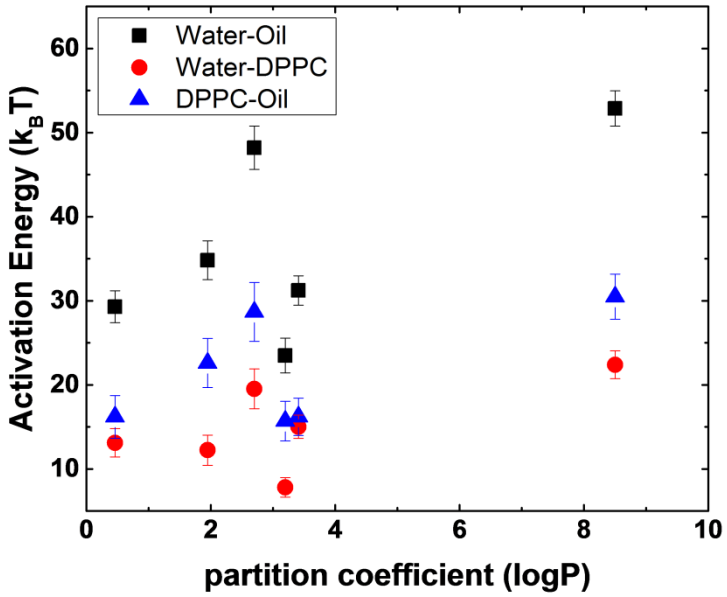

Figure 5-5: Effect of log*P* on activation energies for neutral toxin molecules

5.3.3 **Effects of structure and size**

The structure of each toxin molecule and the distribution of polar groups may determine its ease of partitioning. A parameter, known as the polar surface area (PSA), can be calculated for each toxin, which provides a quantitative measure of the amount of surface area of the molecule, occupied by polar groups. PSA is often used in medicinal and computational chemistry and has been shown to predict rates of passive transport of molecules through membranes [257-262]. For structurally diverse model drugs, a strong correlation has been found between PSA (providing standard error of regression R^2 values from 0.56 to 0.91 in a sigmoidal relationship) with various measures of bioavailability such as absorbed fraction after oral administration of a drug, intestinal permeability (measured by *in vitro* rabbit or rat colonic permeability), permeability across a monolayer of Caco-2 cells (the *in vitro* model of the human

intestinal mucosa), and drug transport across various *in vitro* models of the blood-brain barrier. Drugs with PSA < ~ 63 Å^2 are completely absorbed whereas drugs with PSA > ~ 140 Å^2 are poorly absorbed [258, 263]. To our knowledge, our study is the first to correlate PSA with activation energies from MD simulations of the transport of drug molecules across a phospholipid layer. It is important to point out that this parameter does not correlate with log*P* (see Table 5-4), as indeed was found also by others calculating PSA [264].

TABLE 5-4: COMPARISON OF POLAR SURFACE AREA AND RELATIVE SIZE OF EACH TOXIN

Toxin	**log*P***	**Polar Surface Area**[255] (Å^2)	**Radius of Gyration (Å)**	
			Neutral	**Charged**
Acetaminophen	0.46	49.3	2.6 ± 0.1	2.6 ± 0.1
Mepivacaine	1.95	32.3	2.9 ± 0.1	2.9 ± 0.1
Warfarin	2.7	63.6	3.4 ± 0.1	3.4 ± 0.1
Bupropion	3.2	29.1	3.0 ± 0.2	3.0 ± 0.2
Bupivacaine	3.41	32.3	3.5 ± 0.2	3.3 ± 0.2
Brodifacoum	8.5	46.5	5.4 ± 0.5	5.5 ± 0.6

We tested if the distribution of polar groups in each toxin molecule had an effect on uptake by the oil droplet. This correlation can be observed in plots of activation energy versus polar surface area for both neutral and charged species (Figure 5-6). In both cases, there appears to be a strong correlation between these two properties for toxins crossing into oil from water (black square markers). There also appears to be a correlation between these properties for toxins entering the monolayer from water and entering oil from the monolayer.

The trend is more distinct for smaller PSA values and appears to plateau in most cases at PSA values above approximately 45 $Å^2$.

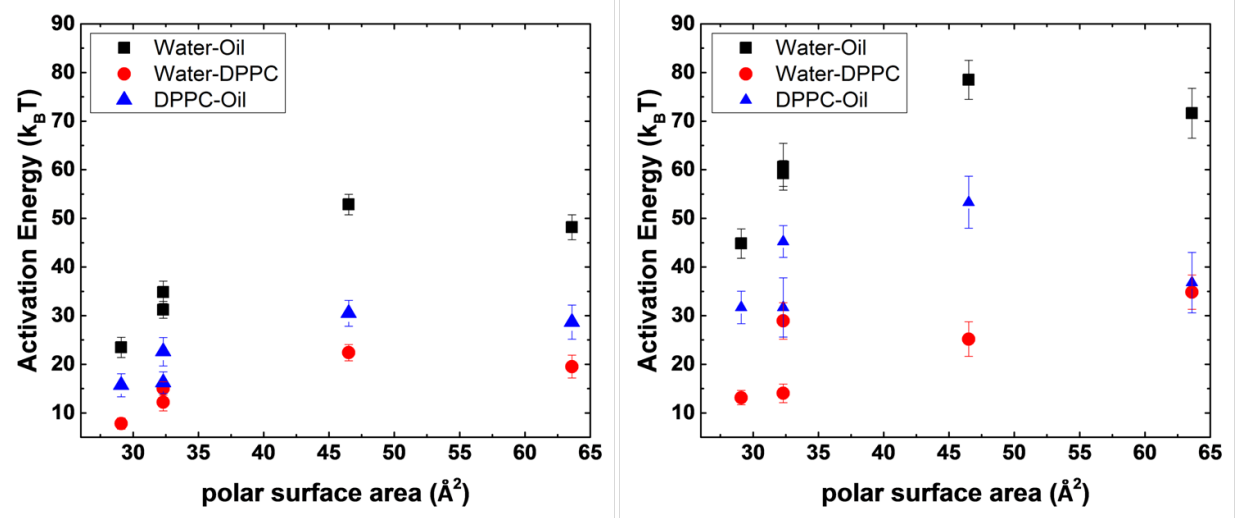

Figure 5-6: Effect of polar surface area on activation energies for neutral (left) and charged (right) toxin species. Values for acetaminophen are not included.

Since activation energies, and hence ease of uptake of toxins by the oil droplet, appear to be correlated with polar surface area, we investigated if the size of each toxin had an effect on the activation energies. We estimated the relative size of each toxin from our simulations using the radius of gyration (R_g), which is calculated as the root mean square distance between the center of mass of the molecule and its ends. This parameter gives an indication of how compact (folded) or stretched out the molecule is on average during the simulation. Average radius of gyration values for neutral and charged forms of the six toxins are listed in Table 5-4.

We did not observe much difference between the charged and neutral average radii. We note here that in general, the R_g values increased as the toxin partition coefficients increased. Since these two parameters were correlated, we tested whether or not the R_g values were correlated with activation energies.

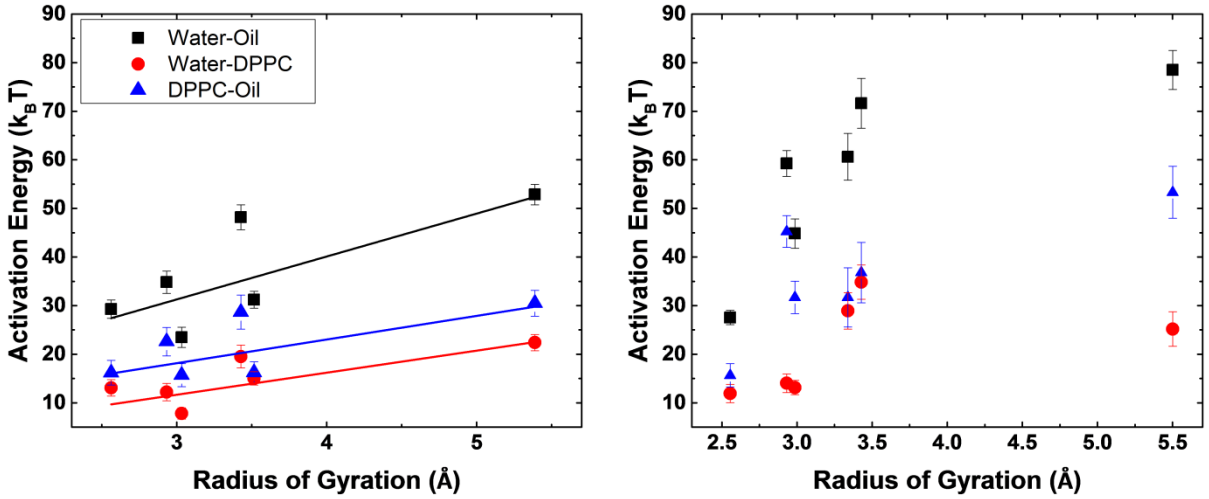

Figure 5-7: Effect of radius of gyration on activation energies for neutral (left) and charged (right) toxin species. Solid lines placed to guide the eye.

From the plots in Figure 5-7, it is clear that there is a correlation between molecular size and ease of entry into the oil droplet. For neutral species (Figure 5-7 (left)), this appears to be a linear relationship, while for charged toxin species (Figure 5-7 (right)), we observe a plateau behavior similar to that shown in Figure 5-6 for polar surface area. For charged toxin molecules travelling from the DPPC monolayer to oil, however, there does not appear to be a strong

correlation with size (shown as blue triangles in Figure 5-7 (right)). Clearly, although size follows a similar trend to log*P*, it appears to have a correlation with entry into the oil droplet, which log*P* does not.

5.3.4 **Effects of Prepopulation**

Up to this point, we have shown free energies of activation for moving toxin molecules from water into and through a pristine DPPC monolayer. These free energy values are likely to be affected by the presence of other similar toxin molecules already in the interface. To test this, we performed steered molecular dynamics simulations in which a single toxin molecule was pulled through a simulation system containing 49 other toxin molecules of the same type. The activation energies obtained for these prepopulated systems for two of the toxins are listed in Table 5-5 and compared to the results from bare monolayer systems reported above.

TABLE 5-5: COMPARISON OF ACTIVATION ENERGIES BETWEEN BARE AND PREPOPULATED INTERFACES

Toxin	Water to Oil Activation Energy [k_BT]		Water to DPPC Activation Energy [k_BT]		DPPC to Oil Activation Energy [k_BT]	
Monolayer State	**Bare**	**Prepopulated**	**Bare**	**Prepopulated**	**Bare**	**Prepopulated**
Mepivacaine	34.8 ± 2.3	34.9 ± 2.1	12.2 ± 1.8	14.7 ± 1.9	22.6 ± 2.9	20.3 ± 2.8
Bupivacaine	31.2 ± 1.7	40.4 ± 4.2	15.0 ± 1.4	24.5 ± 4.6	16.2 ± 2.2	15.9 ± 6.2

There appears to be a small increase in activation energies for going from water to DPPC and from water to oil for monolayers prepopulated with bupivacaine. Prepopulation has no

effect on mepivacaine transfer. From this table, it is not entirely clear what effect prepopulation would have on the activation energies in general. It may be necessary test various concentrations and several different toxin species to obtain a clearer picture on the effects of prepopulation on the ease of sequestration of toxins by oil droplets.

5.4 **Summary and Conclusion**

Lipophilicity (measured by the octanol/water partition coefficient - log*P*) has generally been assumed to be the driving force for the association of toxin molecules with lipid emulsions [56, 232, 240]. We found from our simulations that lipophilicity alone does not appear to correlate well with ease of partitioning of six representative toxin molecules into an oil droplet model. In fact, the least lipophilic toxin we studied (acetaminophen) has one of the smallest energy barriers to association with the droplet, in both its neutral and its protonated state. According to predictions made from *in vitro* studies [232], a molecule such as acetaminophen should not be predicted to be susceptible to sequestration by lipid droplets due to its low lipophilicity. We observe the opposite from our simulations. We expect the protonated form of acetaminophen to be even more susceptible to oil droplet sequestration from the lower activation energies for crossing from water to oil that we observe for this species. Indeed, as most of these toxins are highly ionized at physiological pH, the log*P* value is not an appropriate measure of their actual partitioning capability. A significant result of our molecular dynamics simulations is that lipophilicity alone does not predict the association of toxin molecules with oil droplets.

Although the octanol/water partition coefficient does not correlate well with sequestration of toxins, we do find correlations between activation energies and the size (measured as the radius of gyration) and the polar surface area of each toxin. In general, activation barriers increase with increasing molecule size and polar area, up to a plateau. The partitioning of toxins between the aqueous phase, the droplet interface, and the lipid core may be predicted by our steered simulations. High activation energies indicate that the toxin

molecules may not easily enter particular regions of the system. Most of the charged toxin species have higher activation energies for entry into oil than neutral species, so we would not expect them to reside in the oil phase. Most of the charged species have comparable activation energies for entry into the DPPC monolayer from water. Coupled with electrostatic interactions with the phospholipid head groups, we would predict that the monolayer would be a favorable location for these charged toxins.

Our simulations have therefore demonstrated that lower lipophilicity does not prevent molecules from being sequestered by the oil droplet, in contrast to the prevailing thought. We would like to note here that our model system composed of DPPC and triolein is much simpler than the actual composition of egg phospholipid and soybean triglyceride emulsions. We have not considered the effects of charged phospholipids and varying compositions, which may change many of the correlations be have observed. However, DPPC is a particularly stable phospholipid which is often used for model systems [265-267]; therefore changes in properties measured here during interaction of molecules with the DPPC monolayer may be even more enhanced when layers composed of less stable phospholipids are employed.

6. **CONCLUSIONS**

The studies presented in this thesis demonstrate the essential role that computational molecular dynamics methods play in elucidating molecular level mechanisms by which small toxins associate with and alter the physicochemical properties of phospholipid layers. We have illustrated the creation of coarse-grained representations of small molecules using the MARTINI force field, which was previously used predominantly for biomacromolecules. Our CG topologies have been computationally verified by correctly replicating experimentally predicted octanol/water partition coefficients. We have been able to show through our simulations that different toxic molecules associate with phospholipid layers to varying extents and modify the properties of these layers.

To demonstrate the phospholipid layer property-modulating capacity of endogenous and exogenous toxins, we consider three biomedically relevant examples. In each example, toxin molecules associate with and perturb a phospholipid layer, thereby compromising its ability to carry out its function, which is to enclose specific structures and mediate transport of material. The length and time scales we consider and the detail that our simulations provide give insight into molecular mechanisms that would be difficult to assess using experimental techniques alone.

In Chapter 3, we demonstrate that the physical structures and chemical properties unique to two anticoagulant molecules are responsible for their differential effects on the structure of phospholipid bilayers. From our simulations, we observe that the larger and more lipophilic anticoagulant, brodifacoum, is retained within DPPC bilayers, in contrast to the smaller warfarin molecule. This retention could cause the bilayer structural perturbation that we also observe,

to become longer lasting; the potential consequences of this perturbation on cell viability may be devastating. Through equilibrium and steered molecular dynamics simulations, we have shown that hydroxycoumarins disrupt membrane barrier function by accumulation within and transit through phospholipid bilayers. The detailed mechanisms by which these molecules disrupt the membrane have been revealed by elucidating the molecular phenomena that underlie their differential cytotoxicity. In physiological conditions, the increased disruption in cell membrane integrity induced by brodifacoum, if accompanied by uncontrolled flux of ions and other small molecules, would dysregulate the delicate homeostatic balance necessary to prevent cell death.

In the second example, we explored the mechanisms behind consciousness impairment associated with increases in concentration of endogenous metabolites as a consequence of metabolic disease. By comparison with experimental observations in the literature [51], we demonstrate that the loss of atomistic detail in the coarse-grained representation of the small molecule does not prevent semi-quantitative reproduction of the effect of the metabolite on the structure and dynamics of a phospholipid bilayer. The presence of the metabolite alters membrane structure and dynamics by expanding the phospholipid bilayer, increasing its fluidity, and doubling its lateral pressure in a concentration-dependent manner. We also identify a potential key membrane disruption mechanism that relates a threshold interfacial metabolite concentration to the occurrence of consciousness impairment symptoms in patients. This important physical phenomenon may distinguish subclinical concentrations from clinical ones. We demonstrate what may yet be a general mechanism by which a small molecule can alter membrane properties that is non-linear in concentration at the interface.

In our third example, we investigate the relative roles played by electrostatics, lipophilicity, charge and other factors in mediating toxin sequestration by lipid emulsion droplets. The model we develop helps to elucidate the mechanisms underlying the effectiveness of lipid emulsion therapy for the treatment of drug overdose. Using steered molecular dynamics simulations, we examine the changes induced by a range of pharmaceutical agents on the thermodynamic landscape of a phospholipid monolayer at the oil/water interface. We conclude that, contrary to prevailing thought, the octanol/water partition coefficient is not a good predictor of toxin sequestration by emulsion droplets. We find correlations instead between both the size and the polar surface area of the toxin molecules and the activation energies. We also predict from our steered molecular dynamics simulation results that, at physiological conditions, most of the toxins studied would likely not partition into the lipid droplet core, but would associate instead with the interfacial phospholipid monolayer.

Based on these three examples, we understand that different molecular properties (size, polar surface area, charge, conformational dynamics) lead to different associations of toxins with phospholipid layers; so that different orientations, different preferred locations of the toxin molecules along the interfacial region, and different degrees of disruption of physical properties of the lipid layer accompany the toxin molecule's interaction with the phospholipid interface. Likewise, different molecular properties lead to different free energy profiles for penetration of the molecule through the layer. What all three examples show in common is the ability of this approach (coarse-grained molecular dynamics simulations to reveal molecular details of the consequences of interactions of a small molecule with the phospholipid layer) to provide molecular-level information on the absorption, transport, and partitioning of the toxin

molecule in the model membrane. We have shown various ways in which the results of an MD simulation run may be interrogated to find unprecedented levels of detailed information for a given toxin molecule interacting with and possibly penetrating the interface. We have seen three relevant problems for which the approach provides new information toward resolution of the problem. The nature of model membrane disruption caused by some molecules suggests the membrane barrier function can be seriously compromised.

6.1 **Recommendations for Future Work**

As noted in Section 5.4, our phospholipid model systems are homogeneous in the sense that they are all composed of a single type of phospholipid molecule (DPPC) and in the case of the lipid droplet, only one type of triglyceride molecule (triolein). The choice to use simpler models was made to ensure that the results were not confounded by variable compositions, in order to obtain general mechanisms that could then be extrapolated to many other situations.

Now that some mechanisms have been identified, we could examine ways in which composition may alter them. For example, considering the membrane-altering effects of the metabolite *beta*-hydroxybutyric acid, it would be necessary to investigate other metabolites and molecules with potential anesthetic-like effects using the same approach we have used here. A systematic investigation of consciousness-impairing drugs by this approach would help elucidate the role of cell membranes as drug targets for these types of drugs. Also, it could be useful to create a membrane model that contains a variety of phospholipids and other structures found in physiological membranes (such as cholesterol).

Along the same lines, for further studies on drug sequestration by lipid emulsions, it would be informative to model the actual composition of egg phospholipid and soybean triglyceride emulsions. The compositions of commercial lipid emulsion formulations vary significantly. They are made with natural oils (e.g. soybean, safflower, olive, fish oil) or synthetic structured triglycerides with different acyl tail lengths. Phospholipid emulsifiers are also derived from varied sources such as soybean lecithin or egg yolk that contain both zwitterionic and anionic molecules. These differences in composition may cause differential uptake of pharmaceutical agents, therefore our approach could be easily extended to take the various compositions into account. Furthermore, lipid emulsions contain structures such as liposomes in addition to oil droplets [238]. Therefore, a similar approach to that described in Chapter 5 could be used to predict the association of a range of pharmaceutical agents with liposomes.

Finally, the coarse-grained phospholipid layer models we developed for the lipid emulsion droplet can be extended to other potential applications including studying the viability of lipid therapy for other poisonous and toxic substances. Our oil droplet simulation method could also be extended to study microemulsions used as drug delivery vehicles. These emulsions have been found to be very stable, form readily, and have many potential applications [268-270]. Microemulsions are useful for various types of drug delivery, including oral, dermal and transdermal. However, their physicochemical properties are not well understood. Molecular dynamics simulations of these oil/water/surfactant systems could help elucidate some of these properties.

CITED LITERATURE

1. Pritchard, J.B. and D.S. Miller, *Mechanisms mediating renal secretion of organic anions and cations.* Physiological Reviews, 1993. **73**(4).

2. Ullrich, K.J., *Specificity of transporters for 'organic anions' and 'organic cations' in the kidney.* Biochimica et Biophysica Acta (BBA)-Reviews on Biomembranes, 1994. **1197**(1): p. 45-62.

3. Koepsell, H., *Organic cation transporters in intestine, kidney, liver, and brain.* Annual review of physiology, 1998. **60**(1): p. 243-266.

4. Inui, K.-I., S. Masuda, and H. Saito, *Cellular and molecular aspects of drug transport in the kidney.* Kidney international, 2000. **58**(3): p. 944-958.

5. Wright, S.H. and W.H. Dantzler, *Molecular and cellular physiology of renal organic cation and anion transport.* Physiological Reviews, 2004. **84**(3): p. 987-1049.

6. Singer, S. and G.L. Nicolson, *The fluid mosaic model of the structure of cell membranes.* Day and Good Membranes and viruses in immunopathology, 1972: p. 7-47.

7. Clandinin, M., S. Cheema, C. Field, M. Garg, J. Venkatraman, and T. Clandinin, *Dietary fat: exogenous determination of membrane structure and cell function.* The FASEB journal, 1991. **5**(13): p. 2761-2769.

8. Vuignier, K., J. Schappler, J.-L. Veuthey, P.-A. Carrupt, and S. Martel, *Drug-protein binding: a critical review of analytical tools.* Analytical and Bioanalytical Chemistry, 2010. **398**(1): p. 53-66.

9. Scholz, A., *Mechanisms of (local) anaesthetics on voltage-gated sodium and other ion channels.* British Journal of Anaesthesia, 2002. **89**(1): p. 52-61.

10. Teague, S.J., *Implications of protein flexibility for drug discovery.* Nature Reviews Drug Discovery, 2003. **2**(7): p. 527-541.

11. Oravcova, J., B. Bo, and W. Lindner, *Drug-protein binding studies new trends in analytical and experimental methodology.* Journal of Chromatography B: Biomedical Sciences and Applications, 1996. **677**(1): p. 1-28.

12. Vanholder, R., R. De Smet, G. Glorieux, A. Argilés, U. Baurmeister, P. Brunet, W. Clark, G. Cohen, P.P. De Deyn, and R. Deppisch, *Review on uremic toxins: classification,*

concentration, and interindividual variability. Kidney international, 2003. **63**(5): p. 1934-1943.

13. Arkin, M.R. and J.A. Wells, *Small-molecule inhibitors of protein-protein interactions: progressing towards the dream.* Nature Reviews Drug Discovery, 2004. **3**(4): p. 301-317.

14. Young, J.A. and R.J. Collier, *Anthrax toxin: receptor binding, internalization, pore formation, and translocation.* Annu. Rev. Biochem., 2007. **76**: p. 243-265.

15. Pasenkiewicz-Gierula, M., T. Róg, J. Grochowski, P. Serda, R. Czarnecki, T. Librowski, and S. Lochyński, *Effects of a carane derivative local anesthetic on a phospholipid bilayer studied by molecular dynamics simulation.* Biophysical journal, 2003. **85**(2): p. 1248-1258.

16. Cantor, R.S., *The lateral pressure profile in membranes: a physical mechanism of general anesthesia.* Biochemistry, 1997. **36**(9): p. 2339-2344.

17. Cantor, R.S., *Breaking the Meyer-Overton rule: predicted effects of varying stiffness and interfacial activity on the intrinsic potency of anesthetics.* Biophysical journal, 2001. **80**(5): p. 2284-2297.

18. Wood, A.J., J.A. Campagna, K.W. Miller, and S.A. Forman, *Mechanisms of actions of inhaled anesthetics.* New England Journal of Medicine, 2003. **348**(21): p. 2110-2124.

19. Harris, R.A. and F. Schroeder, *Effects of barbiturates and ethanol on the physical properties of brain membranes.* Journal of Pharmacology and Experimental Therapeutics, 1982. **223**(2): p. 424-431.

20. Frangopol, P.T. and D. Mihailescu, *Interactions of some local anesthetics and alcohols with membranes.* Colloids and Surfaces B: Biointerfaces, 2001. **22**(1): p. 3-22.

21. Schreier, S., S.n.V. Malheiros, and E. de Paula, *Surface active drugs: self-association and interaction with membranes and surfactants. Physicochemical and biological aspects.* Biochimica et Biophysica Acta (BBA)-Biomembranes, 2000. **1508**(1): p. 210-234.

22. Finkelstein, A., L.L. Rubin, and M.-C. Tzeng, *Black widow spider venom: effect of purified toxin on lipid bilayer membranes.* Science, 1976. **193**(4257): p. 1009-1011.

23. Kiss, T., A. Vehovszky, L. Hiripi, A. Kovács, and L. Vörös, *Membrane effects of toxins isolated from a cyanobacterium, Cylindrospermopsis raciborskii, on identified molluscan*

neurones. Comparative Biochemistry and Physiology Part C: Toxicology & Pharmacology, 2002. **131**(2): p. 167-176.

24. Paiva, J.G., P. Paradiso, A.P. Serro, A. Fernandes, and B. Saramago, *Interaction of local and general anaesthetics with liposomal membrane models: a QCM-D and DSC study.* Colloids and Surfaces B: Biointerfaces, 2012. **95**: p. 65-74.

25. Högberg, C.-J. and A.P. Lyubartsev, *Effect of local anesthetic lidocaine on electrostatic properties of a lipid bilayer.* Biophysical journal, 2008. **94**(2): p. 525-531.

26. Tsuchiya, H. and M. Mizogami, *Interaction of Local Anesthetics with Biomembranes Consisting of Phospholipids and Cholesterol: Mechanistic and Clinical Implications for Anesthetic and Cardiotoxic Effects.* Anesthesiology Research and Practice, 2013. **2013**: p. 18.

27. Tsuchiya, H. and M. Mizogami, *The membrane interaction of drugs as one of mechanisms for their enantioselective effects.* Medical Hypotheses, 2012. **79**(1): p. 65-67.

28. Egberts, E., S.-J. Marrink, and H.J. Berendsen, *Molecular dynamics simulation of a phospholipid membrane.* European Biophysics Journal, 1994. **22**(6): p. 423-436.

29. Hofsäß, C., E. Lindahl, and O. Edholm, *Molecular dynamics simulations of phospholipid bilayers with cholesterol.* Biophysical journal, 2003. **84**(4): p. 2192-2206.

30. Berger, O., O. Edholm, and F. Jähnig, *Molecular dynamics simulations of a fluid bilayer of dipalmitoylphosphatidylcholine at full hydration, constant pressure, and constant temperature.* Biophysical journal, 1997. **72**(5): p. 2002.

31. Feller, S.E., D. Yin, R.W. Pastor, and A.D. MacKerell Jr, *Molecular dynamics simulation of unsaturated lipid bilayers at low hydration: parameterization and comparison with diffraction studies.* Biophysical journal, 1997. **73**(5): p. 2269.

32. Patocka, J., G. Petroianu, and K. Kuca, *Toxic potential of Superwarfarin: Brodifacoum.* Mil. Med. Sci. Lett., 2013. **82**(1): p. 32-38.

33. Zolcinski, M., A. Padjas, and J. Musial, *Intoxication with three different superwarfarin compounds in an adult woman.* Thrombosis and haemostasis, 2008. **100**(1): p. 156.

34. Palmer, R.B., P. Alakija, J. de Baca, and K.B. Nolte, *Fatal brodifacoum rodenticide poisoning: autopsy and toxicologic findings.* Journal of forensic sciences, 1999(44): p. 851-5.

35. Kruse, J.A. and R.W. Carlson, *Fatal rodenticide poisoning with brodifacoum.* Annals of emergency medicine, 1992. **21**(3): p. 331-336.

36. Chua, J.D. and W.R. Friedenberg, *Superwarfarin poisoning.* Archives of internal medicine, 1998. **158**(17): p. 1929-1932.

37. Park, J., *Can we more efficiently save patients with vitamin K-dependent coagulopathy caused by superwarfarin intoxication?* The Korean journal of internal medicine, 2014. **29**(4): p. 430-433.

38. Caravati, E.M., A.R. Erdman, E.J. Scharman, A.D. Woolf, P.A. Chyka, D.J. Cobaugh, P.M. Wax, A.S. Manoguerra, G. Christianson, and L.S. Nelson, *Long-acting anticoagulant rodenticide poisoning: an evidence-based consensus guideline for out-of-hospital management.* Clinical Toxicology, 2007. **45**(1): p. 1-22.

39. Gurtovenko, A.A. and I. Vattulainen, *Molecular mechanism for lipid flip-flops.* The Journal of Physical Chemistry B, 2007. **111**(48): p. 13554-13559.

40. Balasubramanian, K. and A.J. Schroit, *Aminophospholipid asymmetry: a matter of life and death.* Annual review of physiology, 2003. **65**(1): p. 701-734.

41. Boon, J.M. and B.D. Smith, *Chemical control of phospholipid distribution across bilayer membranes.* Medicinal research reviews, 2002. **22**(3): p. 251-281.

42. *Injury Prevention & Control: Data & Statistics.* Office of Statistics and Programming, Centers for Disease Control and Prevention, (accessed May 9, 2014).

43. Hoyert DL, X.J., *Deaths: Preliminary Data for 2011.* National Vital Statistics Reports, 2012. **61**(6).

44. Sass, D.A. and A.O. Shakil, *Fulminant hepatic failure.* Liver Transplantation, 2005. **11**(6): p. 594-605.

45. Brouns, R. and P.P. De Deyn, *Neurological complications in renal failure: a review.* Clinical Neurology and Neurosurgery, 2004. **107**(1): p. 1-16.

46. Brosnan, R.J., L. Yang, P.S. Milutinovic, J. Zhao, M.J. Laster, E.I.I. Eger, and J.M. Sonner, *Ammonia Has Anesthetic Properties.* Anesthesia & Analgesia, 2007. **104**(6): p. 1430-1433.

47. Boado, R., O. Colombo, and A.A. Zaninovich, *Effects of diabetes, Beta-hydroxybutyric acid and metabolic acidosis on the pituitary-thyroid axis in the rat.* Journal of Endocrinological Investigation, 1985. **8**(2): p. 107-111.

48. Yang, L., J. Zhao, P.S. Milutinovic, R.J. Brosnan, E.I.I. Eger, and J.M. Sonner, *Anesthetic Properties of the Ketone Bodies Beta-Hydroxybutyric Acid and Acetone.* Anesthesia & Analgesia, 2007. **105**(3): p. 673-679.

49. Yang, L. and J.M. Sonner, *The Anesthetic-Like Effects of Diverse Compounds on Wild-Type and Mutant Gamma-Aminobutyric Acid Type A and Glycine Receptors.* Anesthesia & Analgesia, 2008. **106**(3): p. 838-845.

50. Tsuchiya, H. and M. Mizogami, *The membrane interaction of drugs as one of mechanisms for their enantioselective effects.* Medical Hypotheses. **79**(1): p. 65-67.

51. Hsu, T.T., D.L. Leiske, L. Rosenfeld, J.M. Sonner, and G.G. Fuller, *3-Hydroxybutyric Acid Interacts with Lipid Monolayers at Concentrations That Impair Consciousness.* Langmuir, 2013. **29**(6): p. 1948-1955.

52. Litz, R.J., M. Popp, S.N. Stehr, and T. Koch, *Successful resuscitation of a patient with ropivacaine-induced asystole after axillary plexus block using lipid infusion.* Anaesthesia, 2006. **61**(8): p. 800-801.

53. Rosenblatt, M.A., M. Abel, G.W. Fischer, C.J. Itzkovich, and J.B. Eisenkraft, *Successful use of a 20% lipid emulsion to resuscitate a patient after a presumed bupivacaine-related cardiac arrest.* Anesthesiology, 2006. **105**(1): p. 217-218.

54. Warren, J.A., R.B. Thoma, A. Georgescu, and S.J. Shah, *Intravenous lipid infusion in the successful resuscitation of local anesthetic-induced cardiovascular collapse after supraclavicular brachial plexus block.* Anesthesia and Analgesia, 2008. **106**(5): p. 1578-1580.

55. Zimmer, C., K. Piepenbrink, G. Riest, and J. Peters, *Cardiotoxic and neurotoxic effects after accidental intravascular bupivacaine administration - Therapy with lidocaine propofol and lipid emulison.* Anaesthesist, 2007. **56**(5): p. 449-453.

56. Samuels, T.L., J.W. Willers, D.R. Uncles, R. Monteiro, C. Halloran, and H. Dai, *In vitro suppression of drug-induced methaemoglobin formation by Intralipid® in whole human blood: observations relevant to the 'lipid sink theory'.* Anaesthesia. **67**(1): p. 23-32.

57. Weinberg, G.L., *Lipid infusion therapy: Translation to clinical practice.* Anesthesia and Analgesia, 2008. **106**(5): p. 1340-1342.

58. Lyubartsev, A.P. and A.L. Rabinovich, *Recent development in computer simulations of lipid bilayers.* Soft Matter. **7**(1): p. 25-39.

59. Noguchi, H., *Membrane Simulation Models from Nanometer to Micrometer Scale.* Journal of the Physical Society of Japan, 2009. **78**(4): p. 041007-1-041007-9.

60. Kjaer, K., J. Als-Nielsen, C. Helm, L. Laxhuber, and H. Möhwald, *Ordering in lipid monolayers studied by synchrotron X-ray diffraction and fluorescence microscopy.* Physical Review Letters, 1987. **58**(21): p. 2224.

61. Helm, C., H. Möhwald, K. Kjaer, and J. Als-Nielsen, *Phospholipid monolayers between fluid and solid states.* Biophysical journal, 1987. **52**(3): p. 381.

62. Yang, X.M., D. Xiao, S.J. Xiao, and Y. Wei, *Domain structures of phospholipid monolayer Langmuir-Blodgett films determined by atomic force microscopy.* Applied Physics A, 1994. **59**(2): p. 139-143.

63. Seelig, A. and J. Seelig, *Dynamic structure of fatty acyl chains in a phospholipid bilayer measured by deuterium magnetic resonance.* Biochemistry, 1974. **13**(23): p. 4839-4845.

64. Honig, B. and A. Nicholls, *Classical electrostatics in biology and chemistry.* Science, 1995. **268**(5214): p. 1144-1149.

65. Brannigan, G., L.L. Lin, and F.H. Brown, *Implicit solvent simulation models for biomembranes.* European Biophysics Journal, 2006. **35**(2): p. 104-124.

66. Nelson, D.R., T. Piran, and S. Weinberg, *Statistical mechanics of membranes and surfaces*. 2004, River Edge, N.J.: World Scientific Pub.

67. Venturoli, M., M.M. Sperotto, M. Kranenburg, and B. Smit, *Mesoscopic models of biological membranes.* Physics Reports, 2006. **437**(1): p. 1-54.

68. Venturoli, M., M. Maddalena Sperotto, M. Kranenburg, and B. Smit, *Mesoscopic models of biological membranes.* Physics Reports, 2006. **437**(1â€“2): p. 1-54.

69. Parkar, N.S., B.S. Akpa, L.C. Nitsche, L.E. Wedgewood, A.T. Place, M.S. Sverdlov, O. Chaga, and R.D. Minshall, *Vesicle formation and endocytosis: function, machinery, mechanisms, and modeling.* Antioxidants & redox signaling, 2009. **11**(6): p. 1301-1312.

70. Gompper, G. and D.M. Kroll, *Fluctuations of polymerized, fluid and hexatic membranes: Continuum models and simulations.* Current Opinion in Colloid & Interface Science, 1997. **2**(4): p. 373-381.

71. Ayton, G. and G.A. Voth, *Bridging microscopic and mesoscopic simulations of lipid bilayers.* Biophys J, 2002. **83**(6): p. 3357-70.

72. Drouffe, J.M., A.C. Maggs, and S. Leibler, *Computer simulations of self-assembled membranes.* Science, 1991. **254**(5036): p. 1353-1356.

73. Ayton, G.S., J.L. McWhirter, and G.A. Voth, *A second generation mesoscopic lipid bilayer model: Connections to field-theory descriptions of membranes and nonlocal hydrodynamics.* The Journal of Chemical Physics, 2006. **124**(6): p. 064906.

74. Tieleman, D.P., S.J. Marrink, and H.J. Berendsen, *A computer perspective of membranes: molecular dynamics studies of lipid bilayer systems.* Biochim Biophys Acta, 1997. **1331**(3): p. 235-70.

75. Marrink, S.-J. and H.J.C. Berendsen, *Simulation of water transport through a lipid membrane.* The Journal of Physical Chemistry, 1994. **98**(15): p. 4155-4168.

76. Heller, H., M. Schaefer, and K. Schulten, *Molecular dynamics simulation of a bilayer of 200 lipids in the gel and in the liquid crystal phase.* The Journal of Physical Chemistry, 1993. **97**(31): p. 8343-8360.

77. Tieleman, D.P. and H.J.C. Berendsen, *Molecular dynamics simulations of a fully hydrated dipalmitoylphosphatidylcholine bilayer with different macroscopic boundary conditions and parameters.* The Journal of Chemical Physics, 1996. **105**(11): p. 4871-4880.

78. Marrink, S.J., A.H. de Vries, and D.P. Tieleman, *Lipids on the move: simulations of membrane pores, domains, stalks and curves.* Biochim Biophys Acta, 2009. **1788**(1): p. 149-68.

79. Marrink, S.J., H.J. Risselada, S. Yefimov, D.P. Tieleman, and A.H. De Vries, *The MARTINI force field: coarse grained model for biomolecular simulations.* The Journal of Physical Chemistry B, 2007. **111**(27): p. 7812-7824.

80. Marrink, S.J., A.H. De Vries, and A.E. Mark, *Coarse grained model for semiquantitative lipid simulations.* The Journal of Physical Chemistry B, 2004. **108**(2): p. 750-760.

81. Noguchi, H. and M. Takasu, *Self-assembly of amphiphiles into vesicles: a Brownian dynamics simulation.* Phys Rev E Stat Nonlin Soft Matter Phys, 2001. **64**(4 Pt 1): p. 041913.

82. Chandrasekhar, I., M. Kastenholz, R.D. Lins, C. Oostenbrink, L.D. Schuler, D.P. Tieleman, and W.F. van Gunsteren, *A consistent potential energy parameter set for lipids: dipalmitoylphosphatidylcholine as a benchmark of the GROMOS96 45A3 force field.* European Biophysics Journal, 2003. **32**(1): p. 67-77.

83. van Gunsteren, W.F., X. Daura, and A.E. Mark, *GROMOS Force Field*, in *Encyclopedia of Computational Chemistry*. 2002, John Wiley & Sons, Ltd.

84. Hermans, J., H.J.C. Berendsen, W.F. Van Gunsteren, and J.P.M. Postma, *A consistent empirical potential for water–protein interactions.* Biopolymers, 1984. **23**(8): p. 1513-1518.

85. Schuler, L.D., X. Daura, and W.F. van Gunsteren, *An improved GROMOS96 force field for aliphatic hydrocarbons in the condensed phase.* Journal of Computational Chemistry, 2001. **22**(11): p. 1205-1218.

86. MacKerell, A.D., D. Bashford, M. Bellott, R. Dunbrack, J. Evanseck, M.J. Field, S. Fischer, J. Gao, H. Guo, and S.a. Ha, *All-atom empirical potential for molecular modeling and dynamics studies of proteins.* The Journal of Physical Chemistry B, 1998. **102**(18): p. 3586-3616.

87. MacKerell, A.D., J. Wiorkiewicz-Kuczera, and M. Karplus, *An all-atom empirical energy function for the simulation of nucleic acids.* Journal of the American Chemical Society, 1995. **117**(48): p. 11946-11975.

88. Wang, J., R.M. Wolf, J.W. Caldwell, P.A. Kollman, and D.A. Case, *Development and testing of a general amber force field.* Journal of Computational Chemistry, 2004. **25**(9): p. 1157-1174.

89. Jójárt, B. and T.A. Martinek, *Performance of the general amber force field in modeling aqueous POPC membrane bilayers.* Journal of Computational Chemistry, 2007. **28**(12): p. 2051-2058.

90. Henneré, G., P. Prognon, F. Brion, V. Rosilio, and I. Nicolis, *Molecular dynamics simulation of a mixed lipid emulsion model: Influence of the triglycerides on interfacial phospholipid organization.* Journal of Molecular Structure: THEOCHEM, 2009. **901**(1-3): p. 174-185.

91. Henneré, G., P. Prognon, F. Brion, and I. Nicolis, *Molecular dynamics study of a phospholipid monolayer at a water/triglyceride interface: towards lipid emulsion modelling.* Chemistry and Physics of Lipids, 2009. **157**(2): p. 86-93.

92. Lenz, O. and F. Schmid, *A simple computer model for liquid lipid bilayers.* Journal of Molecular Liquids, 2005. **117**(1): p. 147-152.

93. Izvekov, S. and G.A. Voth, *A multiscale coarse-graining method for biomolecular systems.* The Journal of Physical Chemistry B, 2005. **109**(7): p. 2469-2473.

94. Shelley, J.C., M.Y. Shelley, R.C. Reeder, S. Bandyopadhyay, and M.L. Klein, *A coarse grain model for phospholipid simulations.* The Journal of Physical Chemistry B, 2001. **105**(19): p. 4464-4470.

95. Stevens, M.J., *Coarse-grained simulations of lipid bilayers.* The Journal of Chemical Physics, 2004. **121**(23): p. 11942-11948.

96. Brannigan, G. and F.L. Brown, *Solvent-free simulations of fluid membrane bilayers.* The Journal of Chemical Physics, 2004. **120**(2): p. 1059-1071.

97. Chanda, J. and S. Bandyopadhyay, *Molecular dynamics study of surfactant monolayers adsorbed at the oil/water and air/water interfaces.* J Phys Chem B, 2006. **110**(46): p. 23482-8.

98. Yong, N.A., A. Gupta, A. Chauhan, and D.I. Kopelevich, *Molecular Transport through Surfactant-Covered Oil-Water Interfaces: Role of Physical Properties of Solutes and Surfactants in Creating Energy Barriers for Transport.* Langmuir, 2011. **27**(6): p. 2420-2436.

99. Lopez, C.A., A.J. Rzepiela, A.H. de Vries, L. Dijkhuizen, P.H. Huì^nenberger, and S.J. Marrink, *Martini Coarse-Grained Force Field: Extension to Carbohydrates.* Journal of Chemical Theory and Computation, 2009. **5**(12): p. 3195-3210.

100. Monticelli, L., S.K. Kandasamy, X. Periole, R.G. Larson, D.P. Tieleman, and S.-J. Marrink, *The MARTINI Coarse-Grained Force Field: Extension to Proteins.* Journal of Chemical Theory and Computation, 2008. **4**(5): p. 819-834.

101. Rossi, G., L. Monticelli, S.R. Puisto, I. Vattulainen, and T. Ala-Nissila, *Coarse-graining polymers with the MARTINI force-field: polystyrene as a benchmark case.* Soft Matter, 2011. **7**(2): p. 698-708.

102. Marrink, S.J. and D.P. Tieleman, *Perspective on the Martini model.* Chemical Society Reviews, 2013. **42**(16): p. 6801-6822.

103. Yuan, H., C.J. Jameson, and S. Murad, *Diffusion of gases across lipid membranes with OmpA channel: a molecular dynamics study.* Molecular Physics. **108**(12): p. 1569-1581.

104. Yuan, H., C.J. Jameson, and S. Murad, *Exploring gas permeability of lipid membranes using coarse-grained molecular dynamics.* Molecular Simulation, 2009. **35**(10-11): p. 953-961.

105. Vorobyov, I., W.F.D. Bennett, D.P. Tieleman, T.W. Allen, and S. Noskov, *The Role of Atomic Polarization in the Thermodynamics of Chloroform Partitioning to Lipid Bilayers.* Journal of Chemical Theory and Computation. **8**(2): p. 618-628.

106. Baron, R., A.H. de Vries, P.H. Hunenberger, and W.F. van Gunsteren, *Configurational entropies of lipids in pure and mixed bilayers from atomic-level and coarse-grained molecular dynamics simulations.* J Phys Chem B, 2006. **110**(31): p. 15602-14.

107. Cabeca, L.F., M. Pickholz, E. de Paula, and A.J. Marsaioli, *Liposome-prilocaine interaction mapping evaluated through STD NMR and molecular dynamics simulations.* J Phys Chem B, 2009. **113**(8): p. 2365-70.

108. MacCallum, J.L., D.P. Tieleman, and E.F. Scott, *Chapter 8 Interactions between Small Molecules and Lipid Bilayers*, in *Current Topics in Membranes*. 2008, Academic Press. p. 227-256.

109. Bagatolli, L. and P.B. Sunil Kumar, *Phase behavior of multicomponent membranes: Experimental and computational techniques.* Soft Matter, 2009. **5**(17): p. 3234-3248.

110. Lopez, C.F., S.O. Nielsen, P.B. Moore, J.C. Shelley, and M.L. Klein, *Self-assembly of a phospholipid Langmuir monolayer using coarse-grained molecular dynamics simulations.* Journal of Physics: Condensed Matter, 2002. **14**(40): p. 9431.

111. Pickholz, M., O.N. Oliveira, Jr., and M.S. Skaf, *Molecular dynamics simulations of neutral chlorpromazine in zwitterionic phospholipid monolayers.* J Phys Chem B, 2006. **110**(17): p. 8804-14.

112. Giner Casares, J.J., L. Camacho, M.T. Martín-Romero, and J.J. López Cascales, *Effect of Na+ and Ca2+ Ions on a Lipid Langmuir Monolayer: An Atomistic Description by Molecular Dynamics Simulations.* Chemphyschem, 2008. **9**(17): p. 2538-2543.

113. Hac-Wydro, K. and P. Dynarowicz-Latka, *The impact of sterol structure on the interactions with sphingomyelin in mixed langmuir monolayers.* J Phys Chem B, 2008. **112**(36): p. 11324-32.

114. Notter, R.H., *Lung Surfactants: Basic Science and Clinical Applications*. 2000: Marcel Dekker.

115. Spence, A.G., *Lipid reversal of central nervous system symptoms of bupivacaine toxicity.* Anesthesiology, 2007. **107**(3): p. 516-517.

116. Foxall, G., R. McCahon, J. Lamb, J.G. Hardman, and N.M. Bedforth, *Levobupivacaine-induced seizures and cardiovascular collapse treated with Intralipid (R).* Anaesthesia, 2007. **62**(5): p. 516-518.

117. Di Gregorio, G., D. Schwartz, R. Ripper, K. Kelly, D.L. Feinstein, R.D. Minshall, M. Massad, C. Ori, and G.L. Weinberg, *Lipid emulsion is superior to vasopressin in a rodent model of resuscitation from toxin-induced cardiac arrest.* Critical Care Medicine, 2009. **37**(3): p. 993-999.

118. Smilkstein, M.J., G.L. Knapp, K.W. Kulig, and B.H. Rumack, *Efficacy of oral N-acetylcysteine in the treatment of acetaminophen overdose. Analysis of the national multicenter study (1976 to 1985).* The New England journal of medicine, 1988. **319**(24): p. 1557-1562.

119. Rumack, B.H., R.C. Peterson, G.G. Koch, and I.A. Amara, *Acetaminophen overdose: 662 cases with evaluation of oral acetylcysteine treatment.* Archives of internal medicine, 1981. **141**(3): p. 380.

120. Rivera-Penera, T., R. Gugig, J. Davis, S. McDiarmid, J. Vargas, P. Rosenthal, W. Berquist, M.B. Heyman, and M.E. Ament, *Outcome of acetaminophen overdose in pediatric patients and factors contributing to hepatotoxicity.* The Journal of pediatrics, 1997. **130**(2): p. 300.

121. *National Center for Biotechnology Information.* PubChem Compound Database, CID=2474. http://pubchem.ncbi.nlm.nih.gov/summary/summary.cgi?cid=2474 (accessed October 22, 2012).

122. *National Center for Biotechnology Information.* PubChem Compound Database, CID=1983. http://pubchem.ncbi.nlm.nih.gov/summary/summary.cgi?cid=1983 (accessed October 22, 2012).

123. Plimpton, S., *Fast parallel algorithms for short-range molecular dynamics.* Journal of computational physics, 1995. **117**(1): p. 1-19.

124. Yesylevskyy, S.O., L.V. Schäfer, D. Sengupta, and S.J. Marrink, *Polarizable water model for the coarse-grained MARTINI force field.* PLoS Comput Biol, 2010. **6**(6): p. e1000810.

125. Hess, B., Kutzner, C., van der Spoel, D., Lindahl, E., *GROMACS 4: Algorithms for Highly Efficient, Load-Balanced, and Scalable Molecular Simulation.* J. Chem. Theory Comp., 2008. **4**(3): p. 435–447.

126. Bennett, C.H., *Efficient Estimation of Free Energy Differences from Monte-Carlo Data.* Journal of Computational Physics, 1976. **22**(2): p. 245-268.

127. Berendsen, H.J.C., J.P.M. Postma, W.F. Vangunsteren, A. Dinola, and J.R. Haak, *Molecular-Dynamics with Coupling to an External Bath.* Journal of Chemical Physics, 1984. **81**(8): p. 3684-3690.

128. Martínez, L., R. Andrade, E.G. Birgin, and J.M. Martínez, *PACKMOL: A package for building initial configurations for molecular dynamics simulations.* Journal of computational chemistry, 2009. **30**(13): p. 2157-2164.

129. Tuckerman, M.E., J. Alejandre, R. López-Rendón, A.L. Jochim, and G.J. Martyna, *A Liouville-operator derived measure-preserving integrator for molecular dynamics simulations in the isothermal–isobaric ensemble.* Journal of Physics A: Mathematical and General, 2006. **39**(19): p. 5629.

130. Shinoda, W., M. Shiga, and M. Mikami, *Rapid estimation of elastic constants by molecular dynamics simulation under constant stress.* Physical Review B, 2004. **69**(13): p. 134103.

131. Martyna, G.J., D.J. Tobias, and M.L. Klein, *Constant pressure molecular dynamics algorithms.* The Journal of Chemical Physics, 1994. **101**(5): p. 4177-4189.

132. Parrinello, M. and A. Rahman, *Polymorphic transitions in single crystals: A new molecular dynamics method.* Journal of Applied physics, 1981. **52**(12): p. 7182-7190.

133. Harvey, S.C., R.K.-Z. Tan, and T.E. Cheatham III, *The flying ice cube: Velocity rescaling in molecular dynamics leads to violation of energy equipartition.* Journal of computational chemistry, 1998(19): p. 726-740.

134. Humphrey, W., A. Dalke, and K. Schulten, *VMD: visual molecular dynamics.* Journal of molecular graphics, 1996. **14**(1): p. 33-38.

135. Högberg, C.-J., A. Maliniak, and A.P. Lyubartsev, *Dynamical and structural properties of charged and uncharged lidocaine in a lipid bilayer.* Biophysical Chemistry, 2007. **125**(2): p. 416-424.

136. Feller, S.E., R.M. Venable, and R.W. Pastor, *Computer Simulation of a DPPC Phospholipid Bilayer: Structural Changes as a Function of Molecular Surface Area.* Langmuir, 1997. **13**(24): p. 6555-6561.

137. Feller, S.E., Y. Zhang, and R.W. Pastor, *Computer simulation of liquid/liquid interfaces. II. Surface tension-area dependence of a bilayer and monolayer.* The Journal of Chemical Physics, 1995. **103**(23): p. 10267-10276.

138. Poger, D. and A.E. Mark, *On the Validation of Molecular Dynamics Simulations of Saturated and cis-Monounsaturated Phosphatidylcholine Lipid Bilayers: A Comparison with Experiment.* Journal of Chemical Theory and Computation, 2010. **6**(1): p. 325-336.

139. Kučerka, N., M.-P. Nieh, and J. Katsaras, *Fluid phase lipid areas and bilayer thicknesses of commonly used phosphatidylcholines as a function of temperature.* Biochimica et Biophysica Acta (BBA) - Biomembranes, 2011. **1808**(11): p. 2761-2771.

140. Pickholz, M., L.F. Fraceto, and E. de Paula, *Preferential location of prilocaine and etidocaine in phospholipid bilayers: A molecular dynamics study.* Synthetic Metals, 2009. **159**(21-22): p. 2157-2158.

141. *CRC Handbook of Chemistry and Physics*. 77th edition ed, ed. D.R. Lide. 1996-1997: CRC Press.

142. Cascales, J.J.L., T. Otero, A.J.F. Romero, and L. Camacho, *Phase transition of a DPPC bilayer induced by an external surface pressure: from bilayer to monolayer behavior. a molecular dynamics simulation study.* Langmuir, 2006. **22**(13): p. 5818-5824.

143. Exarchos, N.C., M. Tasioula-Margari, and I.N. Demetropoulos, *Viscosities and Densities of Dilute Solutions of Glycerol Trioleate + Octane, + p-Xylene, + Toluene, and + Chloroform.* Journal of Chemical & Engineering Data, 1995. **40**(3): p. 567-571.

144. Pape, E.H., K. Klott, and W. Kreutz, *The determination of the electron density profile of the human erythrocyte ghost membrane by small-angle x-ray diffraction.* Biophysical journal, 1977. **19**(2): p. 141-161.

145. Herbette, L., P. DeFoor, S. Fleischer, D. Pascolini, A. Scarpa, and J.K. Blasie, *The separate profile structures of the functional calcium pump protein and the phospholipid bilayer within isolated sarcoplasmic reticulum membranes determined by X-ray and neutron diffraction.* Biochimica et Biophysica Acta (BBA) - Biomembranes, 1985. **817**(1): p. 103-122.

146. Adachi, T., H. Takahashi, K. Ohki, and I. Hatta, *Interdigitated structure of phospholipid-alcohol systems studied by x-ray diffraction.* Biophysical journal, 1995. **68**(5): p. 1850-1855.

147. Nagle, J.F. and M.C. Wiener, *Relations for lipid bilayers. Connection of electron density profiles to other structural quantities.* Biophysical journal, 1989. **55**(2): p. 309-313.

148. Jeffrey, G.A., *An introduction to hydrogen bonding*. Vol. 12. 1997: Oxford university press New York.

149. Pandey, P.R. and S. Roy, *Headgroup Mediated Water Insertion into the DPPC Bilayer: A Molecular Dynamics Study.* The Journal of Physical Chemistry B, 2011. **115**(12): p. 3155-3163.

150. Oldfield, E., D. Chapman, and W. Derbyshire, *Deuteron resonance: a novel approach to the study of hydrocarbon chain mobility in membrane systems.* FEBS letters, 1971. **16**(2): p. 102-104.

151. Baoukina, S., S.J. Marrink, and D.P. Tieleman, *Lateral pressure profiles in lipid monolayers.* Faraday discussions, 2009. **144**: p. 393-409.

152. Patra, M., *Lateral pressure profiles in cholesterol-DPPC bilayers.* European Biophysics Journal, 2005. **35**(1): p. 79-88.

153. Henriksen, J.R., T.L. Andresen, L.N. Feldborg, L. Duelund, and J.H. Ipsen, *Understanding detergent effects on lipid membranes: a model study of lysolipids.* Biophysical journal, 2010. **98**(10): p. 2199-2205.

154. Jarzynski, C., *Nonequilibrium equality for free energy differences.* Physical Review Letters, 1997. **78**(14): p. 2690.

155. Park, S., F. Khalili-Araghi, E. Tajkhorshid, and K. Schulten, *Free energy calculation from steered molecular dynamics simulations using Jarzynski's equality.* The Journal of Chemical Physics, 2003. **119**(6): p. 3559-3566.

156. Park, S. and K. Schulten, *Calculating potentials of mean force from steered molecular dynamics simulations.* The Journal of Chemical Physics, 2004. **120**(13): p. 5946-5961.

157. Liu, H., J. Chen, Q. Shen, W. Fu, and W. Wu, *Molecular insights on the cyclic peptide nanotube-mediated transportation of antitumor drug 5-fluorouracil.* Molecular pharmaceutics, 2010. **7**(6): p. 1985-1994.

158. Raczyński , P., K. Górny, M. Pabiszczak, and Z. Gburski, *Nanoindentation of biomembrane by carbon nanotubes – MD simulation.* Computational Materials Science, 2013. **70**: p. 13-18.

159. Vemparala, S., L. Saiz, R.G. Eckenhoff, and M.L. Klein, *Partitioning of anesthetics into a lipid bilayer and their interaction with membrane-bound peptide bundles.* Biophysical journal, 2006. **91**(8): p. 2815-2825.

160. Betten, D.P., R.B. Vohra, M.D. Cook, M.J. Matteucci, and R.F. Clark, *Antidote use in the critically ill poisoned patient.* Journal of intensive care medicine, 2006. **21**(5): p. 255-277.

161. Chua J, F.W.R., *Superwarfarin Poisoning.* Archives of Internal Medicine, 1998. **158**(17): p. 1929-1932.

162. Morgan, B.W., C. Tomaszewski, and I. Rotker, *Spontaneous hemoperitoneum from brodifacoum overdose.* The American journal of emergency medicine, 1996. **14**(7): p. 656-659.

163. Park, B.K. and J.B. Leck, *A comparison of vitamin K antagonism by warfarin, difenacoum and brodifacoum in the rabbit.* Biochemical pharmacology, 1982. **31**(22): p. 3635-3639.

164. Spahr, J.E., J.S. Maul, and G.M. Rodgers, *Superwarfarin poisoning: a report of two cases and review of the literature.* American journal of hematology, 2007. **82**(7): p. 656-660.

165. Kotsaftis, P., F. Girtovitis, A. Boutou, G. Ntaios, and P.E. Makris, *Haemarthrosis after superwarfarin poisoning.* European journal of haematology, 2007. **79**(3): p. 255-257.

166. De Paula, E.V., S.A.L. Montalvao, P.R. Madureira, R. Jose Vieira, J.M. Annichino-Bizzacchi, and M.C. Ozelo, *Simultaneous bleeding and thrombosis in superwarfarin poisoning.* Thrombosis research, 2009. **123**(4): p. 637-639.

167. Barnett, V., F. Bergmann, H. Humphrey, and J. Chediak, *Diffuse alveolar hemorrhage secondary to superwarfarin ingestion.* CHEST Journal, 1992. **102**(4): p. 1301-1302.

168. Kahn, R.A., S.A. Johnson, and A.F. DeGraff, *Effects of sodium warfarin on capillary ultrastructure.* The American journal of pathology, 1971. **65**(1): p. 149.

169. Leithäuser, B., C. Mrowietz, B. Hiebl, G. Pindur, and F. Jung, *Capillary bleeding under oral anticoagulation.* Clinical Hemorheology and Microcirculation, 2009. **43**: p. 167-171.

170. Kataranovski, M., V. Prokić, D. Kataranovski, L. Zolotarevski, and I. Majstorović, *Dermatotoxicity of epicutaneously applied anticoagulant warfarin.* Toxicology, 2005. **212**(2): p. 206-218.

171. André, C., C. Guyon, and Y.C. Guillaume, *Rodenticide–humic acid adsorption mechanisms and role of humic acid on their toxicity on human keratinocytes: chromatographic approach to support the biological data.* Journal of Chromatography B, 2004. **813**(1): p. 295-302.

172. Vermeer, C. and L.J. Schurgers, *A comprehensive review of vitamin K and vitamin K antagonists.* Hematology/oncology clinics of North America, 2000. **14**(2): p. 339-353.

173. Cain, D., S.M. Hutson, and R. Wallin, *Assembly of the warfarin-sensitive vitamin K 2, 3-epoxide reductase enzyme complex in the endoplasmic reticulum membrane.* Journal of Biological Chemistry, 1997. **272**(46): p. 29068-29075.

174. Wajih, N., S.M. Hutson, and R. Wallin, *Disulfide-dependent Protein Folding Is Linked to Operation of the Vitamin K Cycle in the Endoplasmic Reticulum A PROTEIN DISULFIDE ISOMERASE-VKORC1 REDOX ENZYME COMPLEX APPEARS TO BE RESPONSIBLE FOR VITAMIN K1 2, 3-EPOXIDE REDUCTION.* Journal of Biological Chemistry, 2007. **282**(4): p. 2626-2635.

175. Sugano, K., M. Kansy, P. Artursson, A. Avdeef, S. Bendels, L. Di, G.F. Ecker, B. Faller, H. Fischer, G. Gerebtzoff, H. Lennernaes, and F. Senner, *Coexistence of passive and carrier-mediated processes in drug transport.* Nature Reviews Drug Discovery, 2010. **9**(8): p. 597-614.

176. Camenisch, G., G. Folkers, and H. van de Waterbeemd, *Review of theoretical passive drug absorption models: Historical background, recent developments and limitations.* Pharmaceutica Acta Helvetiae, 1996. **71**(5): p. 309-327.

177. Ghosh, A., D.O. Scott, and T.S. Maurer, *Towards a unified model of passive drug permeation I: Origins of the unstirred water layer with applications to ionic permeation.* European Journal of Pharmaceutical Sciences, 2014. **52**(0): p. 109-124.

178. Grinberg, S., N. Kipnis, C. Linder, V. Kolot, and E. Heldman, *Asymmetric bolaamphiphiles from vernonia oil designed for drug delivery.* European Journal of Lipid Science and Technology, 2010. **112**(1): p. 137-151.

179. Meister, A., K. Köhler, S. Drescher, B. Dobner, G. Karlsson, K. Edwards, G. Hause, and A. Blume, *Mixing behaviour of a symmetrical single-chain bolaamphiphile with phospholipids.* Soft Matter, 2007. **3**(8): p. 1025-1031.

180. Attwood, D., *The mode of association of amphiphilic drugs in aqueous solution.* Advances in Colloid and Interface Science, 1995. **55**: p. 271-303.

181. Moss, R.A., T. Fujita, and Y. Okumura, *Dynamics of a bolaamphiphilic lipid in a bilayer liposome.* Langmuir, 1991. **7**(11): p. 2415-2418.

182. Longo, G.S., D.H. Thompson, and I. Szleifer, *Stability and phase separation in mixed monopolar lipid/bolalipid layers.* Biophysical journal, 2007. **93**(8): p. 2609-2621.

183. Moss, R.A. and J.M. Li, *Bilayer-bridging bolaamphiphilic lipids.* Journal of the American Chemical Society, 1992. **114**(23): p. 9227-9229.

184. Nosé, S., *A unified formulation of the constant temperature molecular dynamics methods.* The Journal of Chemical Physics, 1984. **81**(1): p. 511-519.

185. Nosé, S., *A molecular dynamics method for simulations in the canonical ensemble.* Molecular physics, 1984. **52**(2): p. 255-268.

186. Hoover, W.G., *Canonical dynamics: equilibrium phase-space distributions.* Physical Review A, 1985. **31**(3): p. 1695.

187. Mousavi, S.Z., S. Amjad-Iranagh, Y. Nademi, and H. Modarress, *Carbon nanotube-encapsulated drug penetration through the cell membrane: an investigation based on steered molecular dynamics simulation.* The Journal of membrane biology, 2013. **246**(9): p. 697-704.

188. Allen, W.J. and D.R. Bevan, *Steered molecular dynamics simulations reveal important mechanisms in reversible monoamine oxidase B inhibition.* Biochemistry, 2011. **50**(29): p. 6441-6454.

189. Atherton, A.D. and B.W. Barry, *Micellar properties of phenothiazine drugs: a laser light scattering study.* Journal of Colloid and Interface Science, 1985. **106**(2): p. 479-489.

190. Mouritsen, O.G. and K. Jørgensen, *Dynamical order and disorder in lipid bilayers.* Chemistry and Physics of Lipids, 1994. **73**(1): p. 3-25.

191. Mouritsen, O.G. and K. Jørgensen, *A new look at lipid-membrane structure in relation to drug research.* Pharmaceutical Research, 1998. **15**(10): p. 1507-1519.

192. Contreras, F.-X., L. Sánchez-Magraner, A. Alonso, and F.M. Goñi, *Transbilayer (flip-flop) lipid motion and lipid scrambling in membranes.* FEBS letters, 2010. **584**(9): p. 1779-1786.

193. Gurtovenko, A.A. and I. Vattulainen, *Pore formation coupled to ion transport through lipid membranes as induced by transmembrane ionic charge imbalance: atomistic molecular dynamics study.* Journal of the American Chemical Society, 2005. **127**(50): p. 17570-17571.

194. Seigneuret, M. and P.F. Devaux, *ATP-dependent asymmetric distribution of spin-labeled phospholipids in the erythrocyte membrane: relation to shape changes.* Proceedings of the National Academy of Sciences, 1984. **81**(12): p. 3751-3755.

195. Rosso, J., A. Zachowski, and P.F. Devaux, *Influence of chlorpromazine on the transverse mobility of phospholipids in the human erythrocyte membrane; relation to shape changes.* Biochimica et Biophysica Acta (BBA)-Biomembranes, 1988. **942**(2): p. 271-279.

196. Schrier, S., A. Zachowski, and P. Devaux, *Mechanisms of amphipath-induced stomatocytosis in human erythrocytes.* Blood, 1992. **79**(3): p. 782-786.

197. Chen, J.Y. and W.H. Huestis, *Role of membrane lipid distribution in chlorpromazine-induced shape change of human erythrocytes.* Biochimica et Biophysica Acta (BBA)-Biomembranes, 1997. **1323**(2): p. 299-309.

198. Helenius, A. and K. Simons, *Solubilization of membranes by detergents.* Biochimica et Biophysica Acta (BBA)-Reviews on Biomembranes, 1975. **415**(1): p. 29-79.

199. Wójtowicz, K., *Comparison of the effect of 4-hydroxycoumarin and umbelliferone on the phase transition of dipalmitoylphosphatidylcholine (DPPC) bilayers.* Pharmacological Reports, 2008. **60**(4): p. 555.

200. *National Diabetes Statistics Report: Estimates of Diabetes and Its Burden in the United States, 2014*. 2014, Centers for Disease Control and Prevention. US Department of Health and Human Services: Atlanta, GA.

201. Fowler, M.J., *Microvascular and macrovascular complications of diabetes.* Clinical Diabetes, 2011. **29**(3): p. 116-122.

202. Mitz, M., M. Di Benedetto, G. Klingbeil, J. Melvin, and W. Piering, *Neuropathy in end-stage renal disease secondary to primary renal disease and diabetes.* Archives of physical medicine and rehabilitation, 1984. **65**(5): p. 235-238.

203. Weng, Y., T.T. Hsu, J. Zhao, S. Nishimura, G.G. Fuller, and J.M. Sonner, *Isovaleric, methylmalonic, and propionic acid decrease anesthetic EC50 in tadpoles, modulate glycine receptor function, and interact with the lipid 1, 2-dipalmitoyl-Sn-glycero-3-phosphocholine.* Anesthesia and analgesia, 2009. **108**(5): p. 1538.

204. Landaas, S., *Accumulation of 3-hydroxyisobutyric acid, 2-methyl-3-hydroxybutyric acid and 3-hydroxyisovaleric acid in ketoacidosis.* Clinica Chimica Acta, 1975. **64**(2): p. 143-154.

205. Ramin, K.D., *Diabetic ketoacidosis in pregnancy.* Obstetrics and gynecology clinics of North America, 1999. **26**(3): p. 481-488.

206. Laffel, L., *Ketone bodies: a review of physiology, pathophysiology and application of monitoring to diabetes.* Diabetes/metabolism research and reviews, 1999. **15**(6): p. 412-426.

207. Yang, L. and J.M. Sonner, *Anesthetic-like modulation of receptor function by surfactants: a test of the interfacial theory of anesthesia.* Anesthesia and analgesia, 2008. **107**(3): p. 868.

208. Gilbert, D.L., P.L. Pyzik, and J.M. Freeman, *The ketogenic diet: seizure control correlates better with serum β-hydroxybutyrate than with urine ketones.* Journal of child neurology, 2000. **15**(12): p. 787-790.

209. Berger, W. and U. Keller, *1 Treatment of diabetic ketoacidosis and non-ketotic hyperosmolar diabetic coma.* Baillière's Clinical Endocrinology and Metabolism, 1992. **6**(1): p. 1-22.

210. Tomoaia-Cotisel, M. and A. Mocanu, *Phase Transitions in Phospholipid Monolayers Studied by Atomic Force Microscopy and Langmuir-Blodgett Technique.* Revista De Chimie, 2008. **59**(11): p. 1230-1233.

211. Alam, T.M. and G.P. Drobny, *Solid-State Nmr-Studies of DNA-Structure and Dynamics.* Chemical Reviews, 1991. **91**(7): p. 1545-1590.

212. Huffman, J. and E.H. Kossoff, *State of the ketogenic diet (s) in epilepsy.* Current neurology and neuroscience reports, 2006. **6**(4): p. 332-340.

213. Pan, J., E. Bebin, W. Chu, and H. Hetherington, *Ketosis and epilepsy: 31P spectroscopic imaging at 4.1 T.* Epilepsia, 1999. **40**(6): p. 703-707.

214. *10 Leading Causes of Injury Deaths by Age Group Highlighting Unintentional Injury Deaths, United States - 2013.* National Center for Injury Prevention and Control, CDC. **accessed June 14, 2015**.

215. Howell, B.A. and A. Chauhan, *Current and Emerging Detoxification Therapies for Critical Care.* Materials, 2010. **3**(4): p. 2483-2505.

216. Sirianni, A.J., K.C. Osterhoudt, D.P. Calello, A.A. Muller, M.R. Waterhouse, M.B. Goodkin, G.L. Weinberg, and F.M. Henretig, *Use of lipid emulsion in the resuscitation of a patient with prolonged cardiovascular collapse after overdose of bupropion and lamotrigine.* Annals of Emergency Medicine, 2008. **51**(4): p. 412-415.

217. Finn, S.D.H., D.R. Uncles, J. Willers, and N. Sable, *Early treatment of a quetiapine and sertraline overdose with Intralipid((R)).* Anaesthesia, 2009. **64**(2): p. 191-194.

218. Stiell, I.G., G.A. Wells, B. Field, D.W. Spaite, L.P. Nesbitt, V.J. De Maio, G. Nichol, D. Cousineau, J. Blackburn, D. Munkley, L. Luinstra-Toohey, T. Campeau, E. Dagnone, and M. Lyver, *Advanced cardiac life support in out-of-hospital cardiac arrest.* N Engl J Med, 2004. **351**(7): p. 647-56.

219. Varon, J., J. Robert E. Fromm, and F. Vallejo-Manzur, *Advanced Cardiac Life Support Algorithms: Changes and Current American Heart Association Recommendations.* Hospital Physician, 2002: p. 35-46.

220. Li, J. and K.D. Caldwell, *Structural studies of commercial fat emulsions used in parenteral nutrition.* J Pharm Sci, 1994. **83**(11): p. 1586-92.

221. Litz, R.J., T. Roessel, A.R. Heller, and S.N. Stehr, *Reversal of central nervous system and cardiac toxicity after local anesthetic intoxication by lipid emulsion injection.* Anesth Analg, 2008. **106**(5): p. 1575-7, table of contents.

222. Ludot, H., J.Y. Tharin, M. Belouadah, J.X. Mazoit, and J.M. Malinovsky, *Successful resuscitation after ropivacaine and lidocaine-induced ventricular arrhythmia following posterior lumbar plexus block in a child.* Anesthesia and Analgesia, 2008. **106**(5): p. 1572-1574.

223. Harvey, M. and G. Cave, *Intralipid outperforms sodium bicarbonate in a rabbit model of clomipramine toxicity.* Annals of Emergency Medicine, 2007. **49**(2): p. 178-185.

224. Tebbutt, S., M. Harvey, T. Nicholson, and G. Cave, *Intralipid prolongs survival in a rat model of verapamil toxicity.* Academic Emergency Medicine, 2006. **13**(2): p. 134-139.

225. Harvey, M.G. and G.R. Cave, *Intralipid infusion ameliorates propranolol-induced hypotension in rabbits.* J Med Toxicol, 2008. **4**(2): p. 71-6.

226. Picard, J. and W. Harrop-Griffiths, *Lipid emulsion to treat drug overdose: past, present and future.* Anaesthesia, 2009. **64**(2): p. 119-21.

227. Weinberg, G., *Lipid infusion resuscitation for local anesthetic toxicity - Proof of clinical efficacy.* Anesthesiology, 2006. **105**(1): p. 7-8.

228. Bern, S., B. S Akpa, I. Kuo, and G. Weinberg, *Lipid resuscitation: a life-saving antidote for local anesthetic toxicity.* Current pharmaceutical biotechnology, 2011. **12**(2): p. 313-319.

229. Kuo, I. and B.S. Akpa, *Validity of the lipid sink as a mechanism for the reversal of local anesthetic systemic toxicity: a physiologically based pharmacokinetic model study.* 2013.

230. Fettiplace, M.R., B.S. Akpa, R. Ripper, B. Zider, J. Lang, I. Rubinstein, and G. Weinberg, *Resuscitation with lipid emulsion: dose-dependent recovery from cardiac pharmacotoxicity requires a cardiotonic effect.* Anesthesiology, 2014. **120**(4): p. 915-925.

231. Fettiplace, M.R., K. Lis, R. Ripper, K. Kowal, A. Pichurko, D. Vitello, I. Rubinstein, D. Schwartz, B.S. Akpa, and G. Weinberg, *Multi-modal contributions to detoxification of acute pharmacotoxicity by a triglyceride micro-emulsion.* Journal of Controlled Release, 2015. **198**: p. 62-70.

232. French, D., C. Smollin, W. Ruan, A. Wong, K. Drasner, and A.H. Wu, *Partition constant and volume of distribution as predictors of clinical efficacy of lipid rescue for toxicological emergencies.* Clinical Toxicology, 2011. **49**(9): p. 801-809.

233. Kette, F., M.H. Weil, R.J. Gazmuri, J. Bisera, and E.C. Rackow, *Intramyocardial hypercarbic acidosis during cardiac arrest and resuscitation.* Critical care medicine, 1993. **21**(6): p. 901-906.

234. Chazan, J.A., R. Stenson, and G.S. Kurland, *The acidosis of cardiac arrest.* New England Journal of Medicine, 1968. **278**(7): p. 360-364.

235. Johnson, B.A., M. Weil, W. Tang, M. Noc, D. McKee, and D. McCandless, *Mechanisms of myocardial hypercarbic acidosis during cardiac arrest.* Journal of Applied Physiology, 1995. **78**(4): p. 1579-1584.

236. Von Planta, M., M. Weil, R. Gazmuri, J. Bisera, and E. Rackow, *Myocardial acidosis associated with CO2 production during cardiac arrest and resuscitation.* Circulation, 1989. **80**(3): p. 684-692.

237. Makino, J., S. Uchino, H. Morimatsu, and R. Bellomo, *A quantitative analysis of the acidosis of cardiac arrest: a prospective observational study.* Critical Care, 2005. **9**(4): p. R357.

238. Rotenberg, M., M. Rubin, A. Bor, D. Meyuhas, Y. Talmon, and D. Lichtenberg, *Physicochemical characterization of intralipid emulsions.* Biochimica Et Biophysica Acta, 1991. **1086**(3): p. 265-272.

239. Sotirhos, N., B. Herslöf, and L. Kenne, *Quantitative analysis of phospholipids by 31P-NMR.* Journal of lipid research, 1986. **27**(4): p. 386-392.

240. Harvey, M. and G. Cave, *Case report: successful lipid resuscitation in multi-drug overdose with predominant tricyclic antidepressant toxidrome.* International Journal of Emergency Medicine, 2012. **5**: p. 8-8.

241. de Wolf, F.A., R.W. Staffhorst, H.P. Smits, M.F. Onwezen, and B. de Kruijff, *Role of anionic phospholipids in the interaction of doxorubicin and plasma membrane vesicles: drug binding and structural consequences in bacterial systems.* Biochemistry, 1993. **32**(26): p. 6688-6695.

242. Speelmans, G., R.W. Staffhorst, and B. de Kruijff, *The anionic phospholipid-mediated membrane interaction of the anti-cancer drug doxorubicin is enhanced by*

phosphatidylethanolamine compared to other zwitterionic phospholipids. Biochemistry, 1997. **36**(28): p. 8657-8662.

243. Boya, P. and G. Kroemer, *Lysosomal membrane permeabilization in cell death.* Oncogene, 2008. **27**(50): p. 6434-6451.

244. Brown, R., R.A. Quercia, and R. Sigman, *Total nutrient admixture: a review.* JPEN J Parenter Enteral Nutr, 1986. **10**(6): p. 650-8.

245. Ishii, F., I. Sasaki, and H. Ogata, *Effect of phospholipid emulsifiers on physicochemical properties of intravenous fat emulsions and/or drug carrier emulsions.* Journal of Pharmacy and Pharmacology, 1990. **42**(7): p. 513-515.

246. Li, J. and K.D. Caldwell, *Structural studies of commercial fat emulsions used in parenteral nutrition.* Journal of pharmaceutical sciences, 1994. **83**(11): p. 1586-1592.

247. Crocker, K.S., R. Noga, D.J. Filibeck, S.H. Krey, M. Markovic, and W.P. Steffee, *Microbial Growth Comparisons of Five Commercial Parenteral Lipid Emulsions.* Journal of Parenteral and Enteral Nutrition, 1984. **8**(4): p. 391-395.

248. Van Aerde, J.E., D.R. Duerksen, L. Gramlich, J.B. Meddings, G. Chan, A.B.R. Thomson, and M.T. Clandinin, *Intravenous Fish Oil Emulsion Attenuates Total Parenteral Nutrition-Induced Cholestasis in Newborn Piglets.* Pediatr Res, 1999. **45**(2): p. 202-208.

249. Garcia-de-Lorenzo, A., R. Denia, P. Atlan, S. Martinez-Ratero, A.L. Brun, D. Evard, and G. Bereziat, *Parenteral nutrition providing a restricted amount of linoleic acid in severely burned patients: a randomised double-blind study of an olive oil-based lipid emulsion v. medium/long-chain triacylglycerols.* British Journal of Nutrition, 2005. **94**: p. 221–230.

250. Chambrier, C., M. Lauverjat, and P. Bouletreau, *Structured triglyceride emulsions in parenteral nutrition.* Nutr Clin Pract, 2006. **21**(4): p. 342-50.

251. Litz, R.J., T. Roessel, A.R. Heller, and S.N. Stehr, *Reversal of central nervous system and cardiac toxicity after local anesthetic intoxication by lipid emulsion injection.* Anesthesia & Analgesia, 2008. **106**(5): p. 1575-1577.

252. Ruan, W., D. French, A. Wong, K. Drasner, and A. Wu, *A mixed (long-and medium-chain) triglyceride lipid emulsion extracts local anesthetic from human serum in vitro more effectively than a long-chain emulsion.* Anesthesiology, 2012. **116**(2): p. 334-339.

253. Ascher, J.A., J.O. Cole, J.-N. Colin, J.P. Feighner, R.M. Ferris, H. Fibiger, R.N. Golden, P. Martin, W.Z. Potter, and E. Richelson, *Bupropion: a review of its mechanism of antidepressant activity.* Journal of Clinical Psychiatry, 1995.

254. Jorenby, D.E., S.J. Leischow, M.A. Nides, S.I. Rennard, J.A. Johnston, A.R. Hughes, S.S. Smith, M.L. Muramoto, D.M. Daughton, and K. Doan, *A controlled trial of sustained-release bupropion, a nicotine patch, or both for smoking cessation.* New England Journal of Medicine, 1999. **340**(9): p. 685-691.

255. *National Center for Biotechnology Information.* PubChem Compound Database. https://pubchem.ncbi.nlm.nih.gov/compound/54680676(accessed July 17, 2015).

256. Chiou, C.T., *Partition coefficients of organic compounds in lipid-water systems and correlations with fish bioconcentration factors.* Environmental Science & Technology, 1985. **19**(1): p. 57-62.

257. Ertl, P., B. Rohde, and P. Selzer, *Fast calculation of molecular polar surface area as a sum of fragment-based contributions and its application to the prediction of drug transport properties.* Journal of medicinal chemistry, 2000. **43**(20): p. 3714-3717.

258. Palm, K., P. Stenberg, K. Luthman, and P. Artursson, *Polar molecular surface properties predict the intestinal absorption of drugs in humans.* Pharmaceutical Research, 1997. **14**(5): p. 568-571.

259. Clark, D.E., *Rapid calculation of polar molecular surface area and its application to the prediction of transport phenomena. 1. Prediction of intestinal absorption.* Journal of pharmaceutical sciences, 1999. **88**(8): p. 807-814.

260. Stenberg, P., K. Luthman, H. Ellens, C.P. Lee, P.L. Smith, A. Lago, J.D. Elliott, and P. Artursson, *Prediction of the intestinal absorption of endothelin receptor antagonists using three theoretical methods of increasing complexity.* Pharmaceutical Research, 1999. **16**(10): p. 1520-1526.

261. Palm, K., K. Luthman, A.-L. Ungell, G. Strandlund, and P. Artursson, *Correlation of drug absorption with molecular surface properties.* Journal of pharmaceutical sciences, 1996. **85**(1): p. 32-39.

262. Krarup, L.H., I.T. Christensen, L. Hovgaard, and S. Frokjaer, *Predicting drug absorption from molecular surface properties based on molecular dynamics simulations.* Pharmaceutical Research, 1998. **15**(7): p. 972-978.

263. Shawahna, R. and N.U. Rahman, *Evaluation of the use of partition coefficients and molecular surface properties as predictors of drug absorption: a provisional biopharmaceutical classification of the list of national essential medicines of Pakistan.* DARU : Journal of Faculty of Pharmacy, Tehran University of Medical Sciences, 2011. **19**(2): p. 83-99.

264. Veber, D.F., S.R. Johnson, H.-Y. Cheng, B.R. Smith, K.W. Ward, and K.D. Kopple, *Molecular properties that influence the oral bioavailability of drug candidates.* Journal of medicinal chemistry, 2002. **45**(12): p. 2615-2623.

265. Hildebran, J., J. Goerke, and J. Clements, *Pulmonary surface film stability and composition.* Journal of Applied Physiology, 1979. **47**(3): p. 604-611.

266. Goerke, J. and J. Gonzales, *Temperature dependence of dipalmitoyl phosphatidylcholine monolayer stability.* Journal of Applied Physiology, 1981. **51**(5): p. 1108-1114.

267. Gong, K., S.-S. Feng, M.L. Go, and P.H. Soew, *Effects of pH on the stability and compressibility of DPPC/cholesterol monolayers at the air-water interface.* Colloids and Surfaces A: Physicochemical and Engineering Aspects, 2002. **207**(1): p. 113-125.

268. Lee, K.L., *Applications and Use of Microemulsions.* arXiv preprint arXiv:1108.2794, 2011.

269. Tenjarla, S., *Microemulsions: an overview and pharmaceutical applications.* Critical Reviews™ in Therapeutic Drug Carrier Systems, 1999. **16**(5).

270. Jadhav, K., I. Shaikh, K. Ambade, and V. Kadam, *Applications of microemulsion based drug delivery system.* Current drug delivery, 2006. **3**(3): p. 267-273.

VITA

NAME Manuela Aseye Ayele Ayee

EDUCATION:

Doctor of Philosophy, Chemical Engineering, University of Illinois at Chicago, Chicago, Illinois, 2015
Dissertation Title: Molecular Modeling of Endogenous and Exogenous Toxins at Phospholipid Interfaces

Master of Science, Chemical Engineering, Iowa State University of Science and Technology, Ames, Iowa, 2008
Thesis Title: Luminescent water-soluble quantum dots: Improved stability through surface functionalization

Bachelor of Arts, Engineering Science - Chemistry Emphasis, Dordt College, Sioux Center, Iowa, 2006

PROFESSIONAL EXPERIENCE:

Graduate Research and Teaching Assistant, Department of Chemical Engineering, University of Illinois at Chicago, Chicago, Illinois, 2010 - 2015

Continuous Process Improvement and Quality Supervisor, ITWC Urethane Solutions (acquired by BASF Polyurethanes), Malcom, Iowa, 2009 - 2010

Post-masters Research Assistant, Center for Sustainable Environmental Technologies (CSET), Iowa State University, Ames, Iowa, 2009

Graduate Research and Teaching Assistant, Chemical Engineering Department, Iowa State University, Ames, Iowa, 2006 - 2008

Quality Control, Sioux Biochemical, Ltd., Sioux Center, Iowa, 2005 - 2006

TEACHING EXPERIENCE:

Guest Lecturer, Material and Energy Balances Course (Separators), Department of Chemical Engineering, University of Illinois at Chicago,

2014

Guest Lecturer, Material and Energy Balances Course, Department of Chemical Engineering, University of Illinois at Chicago, 2013

Invited Speaker, Sharma's Soft Matter ODES-lab: Fizzics & Complex Fluids Seminar Series, Department of Chemical Engineering, University of Illinois at Chicago, 2013

Teaching Assistant, Department of Chemical Engineering, University of Illinois at Chicago: Material and Energy Balances Discussion Sessions for Undergraduates, 2010 -2011

Teaching Assistant, Chemical Engineering Department, Iowa State University: Process Control Laboratory Classes and Tutorials for Undergraduates 2007 - 2008

HONORS and AWARDS:

UIC Abraham Lincoln Fellowship, University of Illinois at Chicago, Chicago, Illinois, 2013 - 2014 and 2010 - 2011

Student Presenter Award, Graduate College, University of Illinois at Chicago, Chicago, Illinois, 2014, 2013, and 2012

Janice Lumpkin Award, Minority Affairs Committee, American Institute of Chemical Engineers, 2013

Advancing Science Award, National Organization for the Professional Advancement of Black Chemists and Chemical Engineers, 2013

Represented the University of Illinois at Chicago at “Energy Forward 2011”, University of Chicago Booth School of Business, Gleacher Center, Chicago, Illinois, 2011

Certified Six Sigma Kaizen Process Improvement Orange Belt, Avon Protection Systems, Cadillac, Michigan, 2010

Amoco Fellowship, Iowa State University, Ames, Iowa, 2006 - 2007

Presidential Academic Scholarship, Dordt College, Sioux Center, Iowa, 2002 - 2006

1st Place Principles of Chemistry Achievement Award, CRC Press LLC, Dordt College, Sioux Center, Iowa, 2003

Engineering Design Award, American Society of Mechanical Engineers Region VII-8 Student Design Contest, Minneapolis, Minnesota, 2003

LEADERSHIP and ACTIVITIES:

President (2 terms), Graduate Association of Chemical Engineers, Chemical Engineering Department, University of Illinois at Chicago, Chicago, Illinois, 2012 - 2014

Poster Session Chair, 6th Annual AICHE Midwest Regional Conference, Chicago, Illinois, 2014

Graduate Student Council Representative, Chemical Engineering Department, University of Illinois at Chicago, Chicago, Illinois, 2011 - 2012

Volunteer, World Vision Child Sponsorship Event, Ames, Iowa, 2008

Secretary, Chemical Engineering Graduate Student Organization, Iowa State University, Ames, Iowa, 2007 - 2008

Webmaster, Chemical Engineering Graduate Student Organization, Iowa State University, Ames, Iowa, 2007 - 2008

Constitution Committee, Chemical Engineering Graduate Student Organization, Iowa State University, Ames, Iowa, 2008

CONFERENCE PRESENTATIONS (* - speaker):

Invited Talk. Society for Mathematical Biology Annual Meeting, (June 30 - July 3, 2015)
A biophysical, biochemical, and physiological interrogation of the differential toxicity of hydroxycoumarin anticoagulants.
Bijentimala Keisham, Bernard Hsu, Chuck Roth, **Manuela A. A. Ayee**, Belinda Akpa*

ACS Colloid and Surface Science Symposium, Pittsburgh, PA (June 15 - 17, 2015)
Anticoagulant incorporation in lipid bilayers indicates a biophysical

mechanism for differential toxicity
Manuela A. A. Ayee, Charles Roth, Belinda S. Akpa*

American Institute of Chemical Engineers (AICHE) Annual Meeting, Atlanta, GA (Nov. 18, 2014)
Coarse-Grained Study of Small Molecule Adsorption in a Phospholipid Monolayer: Thermal and Concentration Effects of a Consciousness Impairing Metabolite
Manuela A. A. Ayee * and Belinda S. Akpa

American Institute of Chemical Engineers Annual Meeting, Atlanta, GA (Nov. 18, 2014)
Biodetoxification by Lipid Emulsion Droplets: Coarse Grained Molecular Dynamics at the Oil/Water Interface.
Belinda Akpa* and **Manuela A. A. Ayee**

American Chemical Society (ACS) Colloid and Surface Science Symposium, Philadelphia, PA (June 25, 2014)
Biodetoxification by Lipid Emulsion Droplets: Coarse Grained Molecular Dynamics at the Oil/Water Interface
Manuela A. A. Ayee * and Belinda S. Akpa

Midwest Thermodynamics and Statistical Mechanics Conference, Chicago, IL (May 4, 2014)
Coarse Grained Study of Small Molecule Adsorption in a Phospholipid Monolayer: Thermal and Concentration Effects of a Consciousness Impairing Metabolite
Manuela A. A. Ayee * and Belinda S. Akpa

American Institute of Chemical Engineers (AICHE) Midwest Regional Conference, Chicago, IL (Mar. 10 - 11, 2014)
Coarse Grained Molecular Dynamics Study of Toxin Sequestration by Lipid Emulsions
Manuela A. A. Ayee * and Belinda S. Akpa

American Institute of Chemical Engineers (AICHE) Annual Meeting, San Francisco, CA (Nov. 7, 2013)
Sequestering of toxins for the reversal of drug toxicity: A coarse grained molecular dynamics study
Manuela A. A. Ayee * and Belinda S. Akpa

NOBCChE Annual Meeting, Indianapolis, IN (Oct. 2013)
Coarse Grained Molecular Dynamics Study of Toxin Sequestration by Lipid Emulsions

Manuela A. A. Ayee * and Belinda S. Akpa

BMES Midwest Biomedical Engineering Career Conference, Chicago, IL (Apr. 2013)
Sequestering of toxins for the reversal of drug toxicity: A coarse grained molecular dynamics (MD) study
Manuela A. A. Ayee * and Belinda S. Akpa

Diversifying Higher Education Faculty in Illinois (DFI) Program/IALHEA (Illinois African American and Latino Higher Education Alliance) Conference and Diversity Research Forum (Apr. 2012)
Mesoscale Particulate Model for the Study of Cell Membrane Deformations
Manuela A. A. Ayee *, Richard Minshall, Lewis Wedgewood, Ludwig Nitsche, Irena Levitan, Belinda Akpa

American Chemical Society (ACS) National Meeting, San Diego, CA (Mar. 2012)
Meshless Mesoscale Particulate Model for the Study of Cell Membrane Deformations
Manuela A. A. Ayee *, Richard Minshall, Lewis Wedgewood, Ludwig Nitsche, Irena Levitan, Belinda Akpa

9th Annual Chicago Biomedical Consortium (CBC) Symposium, Chicago, IL (Oct. 2011)
Caveolae-Mediated Endocytosis Mechanisms Studied Using Mesoscale Computer Simulations
Manuela A. A. Ayee *, Richard Minshall, Lewis Wedgewood, Ludwig Nitsche, Irena Levitan, Belinda Akpa

PUBLICATIONS:

Ayee, M.A.A., C. Roth, and B.S. Akpa, *Structural perturbation of a dipalmitoylphosphatidylcholine (DPPC) bilayer by warfarin and its bolaamphiphilic analogue*. Journal of Colloid and Interface Science. (Submitted)

Ayee, M.A.A., and B.S. Akpa, *Coarse-grained study of hydroxycoumarin incorporation into lipid bilayers: a potential mechanism of differential toxicity of anticoagulants*. (In Preparation)

Ayee, M.A.A., N. Barbera, C. Roth, and B.S. Akpa, *Threshold response of a model membrane to beta-hydroxybutyric acid incorporation – a potential mechanism of concentration-dependence in consciousness*

impairment. (In Preparation)

Ayee, M.A.A., K. Corbitt, and B.S. Akpa, *Drug scavenging by a triglyceride emulsion droplet: charge and concentration-dependent effects probed by coarse-grained molecular dynamics*. (In Preparation)